TÉCNICO LISBOA

Analysis of Antennas' Locations on Trains for Mobile Communications

André Gonçalves Ribeiro

Thesis to obtain the Master of Science Degree in

Electrical and Computer Engineering

Supervisor: Prof. Luís Manuel de Jesus Sousa Correia

Examination Committee

Chairperson: Prof. José Eduardo Charters Ribeiro da Cunha Sanguino

Supervisor: Prof. Luís Manuel De Jesus Sousa Correia

Members of Committee: Prof. Custódio José De Oliveira Peixeiro

: Eng. Fernando Manuel Lopes Santana

October 2018

I declare that this document is an original work of my own authorship and that it fulfils all the requirements of the Code of Conduct and Good Practices of the *Universidade de Lisboa*.

To my loved ones

Acknowledgements

First and foremost, I would like to express my thanks to my supervisor, Professor Luís M. Correia, for placing his trust in my competencies to develop this thesis. I am thankful for every weekly meeting, which always provide me something positive to use not only for my academic path, but also to improve my work methodology that will be remembered in my future professional life. I am also grateful for the chance to work directly with a prestigious engineering company that works in several areas, such as aerospace, defence, security or transportation. Moreover, I would like to show my gratitude to be part of the Group of Research On Wireless (GROW), which allowed me to practise my soft skills and provide me a closer look at distinctive projects being developed in telecommunications.

I am grateful to all GROW members for the way I was received and treated during the development of my work, specially to my master thesis colleagues Pedro Delgado, Ismael Belchior, Alexandre Vieira and Anna Agamyrzyansc.

To Thales for allowing me to have a better understanding how the current industry works, by continuing being in touch with experience engineers, particularly to Eng. Fernando Santana, Eng. Nuno Frigolet, and Eng. Sérgio Rodrigues, who not only provided important insights on railways communications, but also contributed with constructive critics and suggestions, providing more value to my work.

To Professor Custódio Peixeiro and the IT manager, Eng. Nuno Silva, for the prompt response and availability concerning the licensing consignment to use the CST software.

To my closest friends and colleagues who accompanied me during all the journey at Instituto Superior Técnico, for the encouragement, compassion and support.

At last, but not least, I would like to thank my family, my mother, Rosa Ribeiro, and my father, Carlos Ribeiro, for the encouragement, support and for allowing me to take my education to the next level, my sister, for her loyalty and companionship, for my grandmother, Lucinda Gonçalves, for all the love and affection and to my grandfather, Manuel Gonçalves, for his role model.

Abstract

The main objective of this thesis was to analyse the performance of antennas for different railway communication systems and the influence of the surrounding environment on them. The work consisted on the analysis of antennas for the current railway communication system in use, GSM-R, working at 900 MHz, the next communication system to be implemented on railways, LTE-R, for 2.6 GHz, and for a system particularly implemented on metro environments at 5.9 GHz, BBRS. One has developed a model based on the CST software, which considers antennas parameters and the physical limitations of the surrounding environment. The results were analysed through the radiation pattern, the half-power beam width, reflection coefficient and the first side lobe level. One has studied the influence of a train rooftop with curve characteristics, which shows a reduction of the maximum gain and an increase of the half-power beamwidth. At last, one has performed the analysis on the presence of obstructions on the train rooftop. For GSM-R, one has established a safety distance to mount the terminals of 1.5 and 2 m, respectively, in the presence of obstructions with 25 and 45 cm of height. In LTE-R, a safety distance of 1 and 1.5 m, considering the same obstructions heights. The study performed for BBRS does not show relevant problems with the use of spatial diversity due to interferences on the train structure, and the finest position to mount the terminal is the highest location on the train's front with a depth of 100 mm.

Keywords

Railway Communications, Antennas Positioning, GSM-R, LTE-R, BBRS.

Resumo

O objetivo desta tese foi o de analisar o desempenho de antenas para diferentes sistemas de comunicações ferroviárias e a influência do ambiente envolvente. O trabalho consistiu na análise de antenas para diferentes sistemas de comunicações ferroviárias, o GSM-R, que trabalha nos 900 MHz, o LTE- R, normalmente utilizado a 2.6 GHz e o BBRS, um sistema particularmente utilizado em ambientes de metro, a 5.9 GHz. Foi desenvolvido um modelo baseado no CST, onde foram considerados os parâmetros das antenas, assim como as limitações físicas do ambiente circundante. Os resultados foram analisados através do diagrama de radiação, da largura de feixe de meia potência, do coeficiente de reflexão e do nível do primeiro lobo lateral. Estudou-se a influência de um tejadilho de comboio com características curvas, que mostrou uma redução do ganho máximo e um aumento da largura do feixe de meia potência. Finalmente, foi realizada uma análise sobre a presença de obstruções no telhado do comboio. No GSM-R, estabeleceu-se uma distância de segurança para instalar os terminais de 1.5 e 2 m, respetivamente, na presença de obstruções com alturas de 25 e 45 cm. No LTE-R, concluiu-se como distâncias de segurança 1 e 1.5 m, considerando as mesmas alturas de obstruções mencionadas anteriormente. O estudo realizado para o BBRS não mostrou problemas relevantes para a utilização de diversidade espacial devido a interferências das estrutura, e a melhor posição para instalar o terminal será na posição mais elevada da parte da frente do comboio com uma profundidade de 100 mm.

Palavras-chave

Comunicações Ferroviárias, Posicionamento de Antenas, GSM-R, LTE-R, BBRS.

Table of Contents

List of Figures

List of Tables

List of Acronyms

1G	1st Generation of Mobile Communications Systems
2G	2nd Generation of Mobile Communications Systems
3G	3rd Generation of Mobile Communications Systems
3GPP	3rd Generation Partnership Project
4G	4th Generation of Mobile Communications Systems
5G	5th Generation of Mobile Communications Systems
ABW	Absolute Bandwidth
AKS	Advanced Krylov Subspace
AP	Access Point
APAC	Asic Pacific
ATP	Automatic Train Protection
AuC	Authentication Centre
BBRS	Broad Band Radio System
BCC	Backup Control Centre
BS	Base Station
BSC	Base Station Controller
BSS	Base Station Subsystem
BTS	Base Transceiver Station
BW	Bandwidth
CCS7	Common Channel Signalling System No.7 from ITU-T
CCTV	Closed-Circuit Television
CEPT	European Conference of Postal and Telecom. Administrations
CER	Central Equipment Room
CSD	Circuit Switch Data
CST	Computer Simulation Technology
D2D	Device-to-Device
DL	Downlink
E-UTRAN	Evolved Universal Terrestrial Radio Access Network
ECC	Electronic Communications Committee
EIR	Equipment Identity Register
EIRENE	European Integrated Railway Radio Enhanced Network
eLDA	Enhanced Location Dependent Addressing
EM	Electromagnetic
eMLPP	Enhanced Multi-Level Precedence and Pre-emption

EPC	Evolved Packet Core
ERTMS	The European Railway Traffic Management System
ETCS	European Train Control System
ETSI	European Telecommunications Standards Institute
FA	Functional Addressing
FBW	Fractional Bandwidth
FDD	Frequency Division Duplex
FDTD	Finite Difference Time Domain
FIT	Finite Integration Technique
FNBW	First Null Beam-Width
FRS	Functional System Requirements
FSS	Frequency Selective Surface
GGSN	Gateway GPRS Support Node
GMSK	Gaussian Minimum Shift Keying
GPRS	General Packet Radio System
GSM-R	Global System for Mobile Communications – Railway
HRL	Home Location Register
HSS	Home Subscriber Service
HVAC	Heating, Ventilating Air-Conditioning
IEEE	Institute of Electrical and Electronics Engineers
IMEI	International Mobile Equipment Identity
IMSI	International Mobile Subscriber Identity
IoT	Internet of Things
ITU-T	International Telecommunication Union
JDM	Jacobi-Davidson method
LAM	Latin America
LCP	Left Circular Polarisation
LDA	Location Dependent Addressing
LEU	Lineside Encoder Unit
LoS	Line of Sight
LTE-R	Long-term Evolution - Railway
M2M	Machine-to-Machine
MLFMM	Multilevel Fast Multipole Method
MME	Mobility Management Entity
MoM	Method of Moments
MORANE	Mobile radio for Railway Networks
MS	Mobile Station
MSC	Mobile service Switching Centre
NAM	North America
NMS	Network Management System

NSS	Network Subsystem
OBU	On-Board Unit
OCC	Operation Control Centre
OFDMA	Orthogonal Frequency Division Multiple Access
OMS	Operation and Maintenance Subsystem
PAMR	Public Access Mobile Radio
PBA	Perfect Boundary Approximation
PBG	Photonic-bandgap
PCRF	Policy and Charging Resource Function
PDN-G	Public Data Network Gateway
PL	Polarisation matching loss
PMC	Perfect Magnetic Conductor
PMR	Private Mobile Radio
PTM-SC	Point-to-Multipoint Service Centre
QoS	Quality of Service
RB	Resource Block
RBC	Radio Block Centre
RCP	Right Circular Polarisation
RSSB	Rail Safety and Standards Board
RSSI	Received Signal Strength Indicator
S-GW	Serving Gateway
SBR	Shooting Bouncing Ray
SC-FDMA	Single Carrier Frequency Division Multiple Access
SGSN	The Serving GPRS Support Node
SLL	Side Lobe Level
TDD	Time Division Duplex
TDMA	Time Division Multiple Access
TETRA	Terrestrial Trunked Radio
TLM	Transmission Line Matrix
TRAU	Transcoding and Rate Adaption Unit
TSR	Temporary Speed Restrictions
UIC	Union Internationale des Chemins de fer
UL	Uplink
UMTS	The Universal Mobile Telecommunications System
USIM	Universal Subscriber Identity Module
VBS	Voice Broadcast Service
VGCS	Voice Group Call Service
VLR	Visitor Location Register
VSWR	Voltage Standing Wave Ratio
WE	Western Europe

WLAN	Wireless Local Area Network

List of Symbols

$\Delta_{\max}$	Maximum mesh step value allowed
$\Delta_{\min}$	Minimum mesh step value allowed
Δx	Mesh dimension for the X axis
Δy	Mesh dimension for the Y axis
Δz	Mesh dimension for the Z axis
ε_r	Relative permittivity
η	Intrinsic impedance
θ	Angle between the positive half of Z-axis and the observation point
λ	Wavelength
φ	Angle between the positive half of X-axis and the observation point projected on XOY plane
α_{3dB}	Half-Power Beam-Width
a_i	Incoming wave
B	Balance parameter related to mismatches losses
b_i	Outcoming wave
D	Antennas' directivity
$\boldsymbol{E}$	Electric field intensity
E_θ^V	Electric field for a vertical dipole at θ direction
E_φ^H	Electric field for a horizontal dipole at φ direction
$E_{máx}$	Maximum electric field of the main lobe
E_{SL}	Maximum value of the lobe adjacent to the major one
G	Gain (IEEE)
$G_{realised}$	Realised gain
$\boldsymbol{H}$	Magnetic field intensity
h	Antenna height
I_0	Maximum current
I_i	Current of port *i*
k	Free space wave number
l	Largest geometrical dimension of the antenna
L_{SLL}	Side lobe level (maximum relative)
M_{LL}	Lower mesh limit applied

M_{LW}	Mesh lines per wavelength
M_{MS}	Maximum mesh step applied
M_{RL}	Mesh line ratio limit
N_L^V	Number of lobes for a vertical dipole
N_L^H	Number of lobes for a horizontal dipole
P_i	Total accepted power
P_{in}	Input power
P_{rad}	Total radiated power
r	Distance between the antenna and the observation point
S_{ij}	S-matrix element
U	Power radiated in a radial direction
V_i	Voltage of port *i*
Z_0	Characteristic impedance
Z_i	Characteristic impedance of port *i*

List of Software

Antenna Magus	Antenna design software
CTS Studio	Electromagnetic simulation software
MathWorks MATLAB R2017a	Numerical computing software
Microsoft Excel 2017	Calculation and graphical chart tool
Microsoft Paint	Image processing
Microsoft Word 2017	Text editor software

Chapter 1

Introduction

The present chapter presents a brief overview of the mobile communications systems evolution, providing an explanation about the technological perspective, as well as the growth in demand for this services. In addition, one presents a brief evolution of railways communications, its corresponding market and a brief reference to the purpose of this work. The entire thesis structure is also given.

1.1 Overview and motivations

In the last few decades, a massive development in Mobile Communications has been witnessed, and it does not show any sign of slowing down. Once seen as a luxury, today there is no arguing that Mobile Communications are fundamental on every developed society, not only for personal use but also for businesses and companies.

It all started during the 1980s with the appearance of the 1st Generation (1G) of mobile wireless communication systems, based only on analogue cellular technology for basic mobile voice interactions. In the early 1990s, the 2nd Generation (2G) was introduced with fundamental concepts that remain on today's mobile communication systems: capacity and coverage. The first digital mobile communication system was designated as the Global System for Mobile communications (GSM), and it was one of the most popular systems providing voice and data services for a more significant number of users, primary through circuit-switched technology usage, then by packet-switching. Packet transmission happened to be an essential progress along with the development of General Packet Radio Services (GPRS) and the radio interface enhancements, called GSM Evolution (EDGE). This evolution brought much attention from operators and telecommunication organisations due to, not only the evidenced potential but also the radio interface and network complexity.

To answer the needs to standardise mobile communications networks, including radio access networks, core transport networks, terminals and services features, the 3rd Generation Partnership Project (3GPP) was created. In 2000, the 3rd Generation (3G) of mobile communication systems was introduced to keep up with user's demands since the Internet has started to expand exponentially. In Europe, the Universal Mobile Telecommunication System (UMTS) was presented as the best system to lead the 3G transition.

With the evolution of services, there was an increasing necessity for higher transmission rates, for example, to watch HD videos or to download apps, hence, in the late 2000s, the Long Term Evolution (LTE) emerges as a 4th Generation (4G) system respecting all 3GPP specifications presented in Releases 7, 8 and 9. LTE specifications show that this system is capable of achieving maximum downlink (DL) peak rates of 300 Mbps and uplink (UL) ones 75 Mbps, thanks to some upgrades on the radio interface and network core performance, like Multiple Input Multiple Output (MIMO) antenna technology, interference control and self-organising networks (SON). This improvements allowed lower latency and opened to the world new possibilities like real-time applications (interactive gaming, virtual reality, etc.).

Without any surprise the next step will be the 5th Generation (5G), which is currently under development, aiming to even higher data rates (peak data rate of 10 Gbps), better coverage, supporting more Device-to-Device (D2D) and Machine-to-Machine (M2M) communications. With 5G, the path is towards a better deployment of Internet of Things (IoT) with lower latency time (<1 ms) and less energy consumption. It will be possible to have a new approach for all type of problems that are based on Mobile

Communications, a proper example being communications on the railway environment, where it is fundamental to have permanent communications between moving trains and control stations at all time.

The purpose of Mobile Communications is to provide mobility between devices without cable connections, and this was a huge step for any kind of transportation method (e.g. trains). With the fast evolution of Mobile Communications, more revolutionary approaches have emerged to optimise the existing solutions concerning time, profit and security. According to a study that gathers data from 30 main markets from 8 world regions [SCIV18], railway transport is an emergent market with an encouraging growth of 4.3%, from 2473 to 3753 billion passengers per km, between 2005 and 2015 and these predictions also show a growth of 3.2% between 2015 to 2025. In another study, the authors presented only the high-speed traffic' growth in the world between 2010 and 2016 dividing data by countries, which revealed a raise of 65.3% of passengers per km for that period, Figure 1.1. These indicators prove a great expansion of railways, and that this transportation method does not only play an important role these days as it will play an even more critical role in the future.

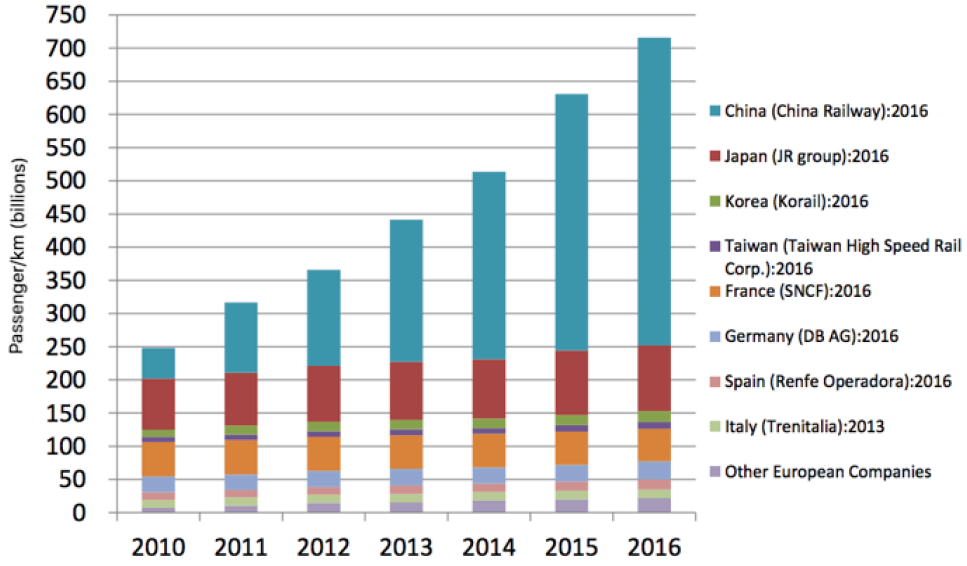

Figure 1.1 High speed traffic in the world (extracted from [IRSt18]).

All this development was well-predicted in 1992, when the UIC – Union Internationale du Chemin-de-Fer launched a European project called EIRENE – European Integrated Radio Enhanced Network [UIC17]. This project was created to answer to some demands, such as the interoperability for railway communication systems. Therefore, EIRENE should be able to have all the specifications of mobile communications requirements for the European railways, which would provide uninterrupted train-services between countries. In 1996, the project entitled MORANE – Mobile radio for Railway Networks was also created in Europe to respond to the obligation of having a valid link that would respect GSM standards and EIRENE specifications, which were attended by ETSI (European Telecommunications Standards Institute) experts. Thanks to EIRENE and MORANE projects, it was possible to take the next step, the development of the European Rail Traffic Management System (ERTMS), which is the combination of the Global System for Mobile Communications – Railways (GSM- R) and the European Train Control System (ECTS).

Currently, the railway industry clearly has justified the bet that has been made over the years. As it may be seen in Figure 1.2 , the railway market still has a lot of space to grow in many areas like in services, infrastructures and signalling. Some of the main reasons why railways will have a major role in the future are due to [Kunz18]:

- Safety: A study revealed that, in Europe, 15 times as many citizens were mortally wounded in car accidents in 2013 and North America the values even are worse, with 304 times more casualties in highways than in railways.
- Energy-efficiency: In Europe, railways only need one-third of the energy used by cars to travel the same distance, but these values change according to different regions of the world. In the United States, high-speed trains are 8 times more efficient than aeroplanes and 4 times more than cars.
- Clean: The railway industry is the least provider of CO_2 emissions in all of the transport sector representing only 1.3%, while road transports contribute 72.2%, the ships 12.7% and the aviation with 12.4%.

Figure 1.2 Accessible railway market by segment (extracted from [Stat18]).

Presently, the trains industry has been developed to provide better services either to passengers or to transport several cargos' type. Whatever the case, carriage systems are more and more complex with the purpose of improving their performance. The issue is that with so many improvements, there is always a convergence of problems that often happen for purely physical limitations. In trains, the antennas placement is done without major concerns and, as it has been mentioned previously, there are several systems that have structures on the rooftop (e.g. air-conditioning systems, pantographs or by the very morphology of the carriage itself). From the antennas' viewpoint, all of these structures are seen as a problem for their best performance, as is illustrated in Figure 1.3.

The thesis' main goal was to analyse the performance of antennas on trains and understand the impact of the different available positions to install the antennas depending on the surrounding environment, in order to optimise and improve services for railway operations and passengers experience. For that, one has chosen a suitable simulation software, the Computer Simulation Technology (CST) Microwave

Studio [CST18]. With this tool, it was possible to import similar 3D model of train antennas of different mobile communication systems and to perform a full analysis of the antenna's parameters.

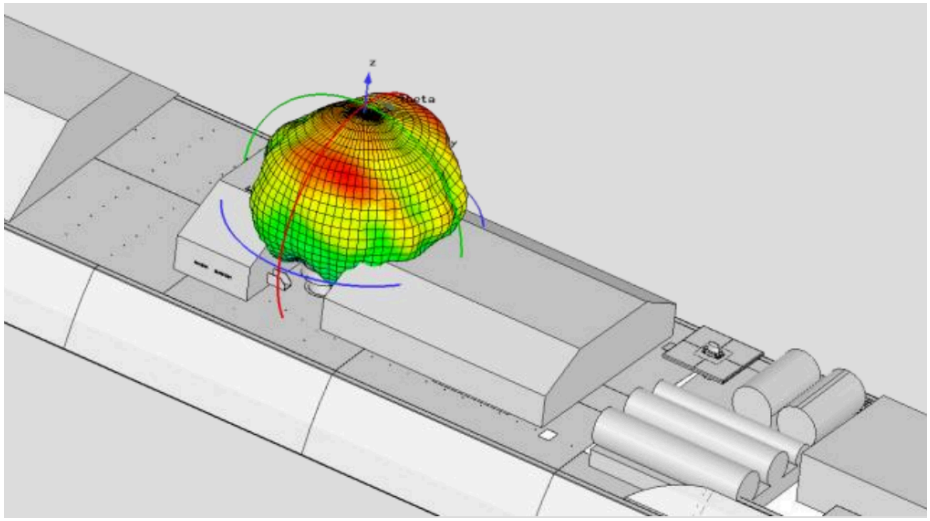

Figure 1.3 Radiation distortion due to train' rooftop structures (extracted from [ANTO18]).

Several studies have already been made concerning on-board antennas' performance for environments related with mobile communications, and a good example is the specific case of terminals on cars' rooftops. However, similar analyses regarding terminals on trains has been poorly explored. Thus, this thesis clearly detaches from what already has been studied until now, since that it clarifies the antennas' working behaviour when they are mounted on rooftops with characteristics of accentuated curvature, and also what happens to them when they are in the presence of standard structures, such as air-conditioning and ventilating units.

1.2 Contents

This thesis is organised into 5 main chapters, followed by 5 annexes to support specific viewpoints. Chapter 1 is the present one, which provides a brief overview of railway communications, as well as, the motivations to investigate the problems when antennas are mounted in a railway environment. The thesis structure is also explained.

In Chapter 2, a description of the most critical aspects of railways communications is introduced, aiming to the clarification of their strict requirements and scenarios. Then, an overview of the railway communications systems to be studied is made (GSM-R, LTE-R and BBRS), providing awareness about their network architectures, radio interfaces and which services they are able to provide. It also contains a description of the most critical parameters to understand antennas' performance. Finally, the chapter is completed with the state of the art where the analysis of the most relevant works regarding the topic of this thesis is presented.

Chapter 3 provides the model developed to achieve the purposes of this work, revealing which are the main parameters to be considered and evaluated. Then, a study is performed to understand the antennas' background concerning their theoretical performance near to PEC grounds. Moreover, the software usage in this work is described, explaining the most appropriate solvers and modelling aspects. Then, the chapter continues by presenting the most critical trains scenarios regarding their antennas' employment. At last, one performed a study focused on the validation of each antenna proper functioning for the three distinct systems frequencies (900 MHz, 2.6 GHz and 5.9 GHz), as well as the maximum boundaries to study the surrounding environment that has an impact on antennas performance.

Chapter 4 contains the analysis of every study performed towards the goals that were established. It starts with the general railways' scenario description, explaining the most important perspectives to consider in the upcoming analysis of the results. The main goal was to mount the monopoles in specific scenarios and understand their influence on the antennas' performance. Firstly, one investigated the effect in the presence of curved grounds, and secondly, one examined the influence of obstructions in the train's rooftop. The last study is about a real situation relating with a BBRS system applied in a subway environment.

Chapter 5 summarises the thesis' main conclusions, clarifying the studies that were accomplished and their results. One also recommends further improvements regarding this work by studying this thesis' work through different approaches.

Additional information to support the decisions made along this work is given in annexes. Annex A presents information about the monopoles developed for the three different systems (GSM- R, LTE-R and BBRS), such as the meshcells view, the S_{11} performances and the farfield patterns for a 2D and 3D views. Annex B shows the antenna's performance according to its ground area, demonstrating the changes in three different perspectives: 2D and 3D farfield gain, as well as, the surface current. Annex C displays the effects on the antennas when they are mounted on curve grounds by presenting the farfield in a 3D view. Annex D provides the specifications of three antennas used as reference for each system, presenting their gain patterns for the vertical and horizontal planes. Annex E is the last one, and it displays the result achieved for the realistic approaches regarding the presence of obstructions and a real case of BBRS system deployed.

Chapter 2

Fundamental Concepts

This chapter provides an overview of the fundamental aspects of railway communications and systems, which provide the necessary conditions for having a proper functioning structure within a brief description of GSM-R, LTE-R and BBRS systems. Then, one mentioned the main parameters required to prepare a thorough analysis of antenna's performance. Finally, a detailed explanation of studies made about the analysis of antenna's location on vehicles is presented at the State of the Art.

2.1 Railway Communications

The current section provides an explanation about the main aspects about railway communications based on [Palu13], [PuTa09], [Thal17], [BFML10], [GSMR15a], [GSMR15b], [FrFC17] and [AGRK15].

2.1.1 Requirements

According to [PuTa09], a railway network may be seen as a set of six sub-systems: Control and Command, Operations, Infrastructure, Energy, Rolling Stock and Maintenance. To have a proper functioning network, it is a must to have proper interoperability among all sub-systems. From the railway's communication point of view, the primary concern is the Control and Command sub-system, where, in Europe, the responsible entity is ERTMS. The adoption of this system brought several advantages, which are presented in [Palu13]:

- Increased safety, due to a constant speed monitoring, panel's standardisation for every European driver, direct surveillance of railway line's intersections and the introduction of the Temporary Speed Restrictions (TSR), among other approaches.
- Reduced cost through the reduction of track magnets with cable connections, the decrease of physical signals and optimisation of traffic management.
- More accessibility thanks to immediate error recovery and, again, to the decrease of track magnets amounts.
- Interoperability because of the standardised screen's data for train drivers and the uniformity of technical and operative interfaces.
- Reduced maintenance costs thanks to the existence of many suppliers on the market and less critical safety interfaces.

The Automatic Train Protection (ATP) system of ERTMS is ETCS, which is the core component of signalling and train control. It works with distinct functional levels with the help of specialised equipment or systems (e.g. Radio Block Centre (RBC), eurobalises, Lineside Encoder Unit (LEU), etc.). These levels may be explained by [Thal17], [Palu13] and [BFML10]:

- Level 0: When a train equipped with ETCS standards uses a non-ETCS route. In this case, the driver has to pay attention to trackside signals, and the train's maximum permitted speed control is performed through the carriage equipment, which is an on-board logic control system with detectors beneath the train.
- ETCS Level 1: With the support of Eurobalises sensors, a control of train's position and movement is given. The Eurobalises are fixed beacons placed between the rails to receive information of a passing train to the nearest LEU where it is stored allowing correct signalling, Figure 2.1 (a). The transmission of information to the train is done by a movement authority, having the permission to cross block sections. With this exchange of information, it is possible to calculate the braking curve

automatically and determine the maximum speed for trains. Occasionally, the data transmission might be interrupted, therefore, to provide continuous transmission of information an additional infill should be added to the system as it is possible to observe in Figure 2.1 (a).

- ETCS Level 2: It is a train protection system supported by GSM-R. At this level, an automatic report about the direction and exact position of all trains is provided to RBC over GSM-R. On the DL perspective, RBC provides information concerning the movement authority, speed restrictions and route data. The eurobalises are also used, but as a passive positioning beacons to have accurate distance measurements. Trackside signals are no longer needed, since all information is sent to the cab driver's interface as is possible to see in Figure 2.1(b).
- ETCS Level 3: It offers a complete train spacing control system based on the same specifications of ETCS Level 2 where the eurobalises have the purpose of determining the train position, and GSM-R is used to control the train's movements. The track is no longer divided into fixed blocks since the train's position information is based on the distance of the next train, Figure 2.1 (c). Such approach has the name of "absolute braking distance spacing" or "moving block" with the primary goal of optimising the distance and speed between trains. Because of the extremely dependence on GSM-R some operational rules are listed to reduce the impact in case of failure, providing some redundancy to the system.

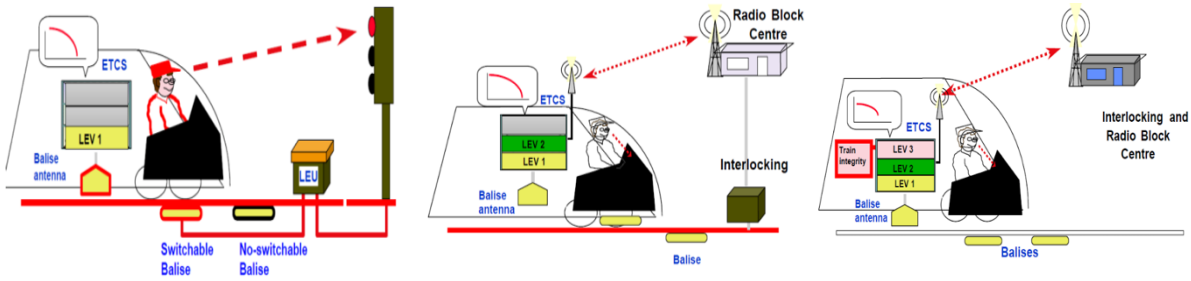

(a) ETCS Level 1. (b) ETCS Level 2. (c) ETCS Level 3.

Figure 2.1. ETCS Levels (adapted from [Palu13]).

All mandatory services are entirely guaranteed through GSM-R. To have a proper functioning and reliable communications system prepared to answer to every need for which it was created, a Quality of Service (QoS) requirement list had to be shaped. It is not enough having a QoS' guarantees for the end-to-end bearer service. The requirements were made for an access point level and the equipment installed in railways has to support a wireless bidirectional data communication service between the train and the trackside at speeds up to 500 km/h for every circumstance (e.g. cuttings, tunnels, bridges, stations, etc.). An overview of ETCS QoS parameters is shown in Table 2.1.

According to [GSMR15b], all specifications can be allocated under four categories: Mandatory for Interoperability (MI), Mandatory for the System (M), Optional (O) or Not Applicable (NA). The answer to all requirements and specifications is based on GSM-R system and the mandatory services created are ([PuTa09]):

- Fast Call Set Up: Essential to support EIRENE FRS requirements, which imply having railways emergency calls in less than 2 s in 95% of cases.

- Location Dependent Addressing (LDA): Offers a particular driver-controller communication system characterised by the simplicity and fast interaction between driver and controller, typically by the press of a single button or entering a short code. These specific communications happen to be addressed based on the location of the train as the train moves through different Base Stations (BSs) without any concerns from the driver.
- Functional Addressing (FA): Allows each train to be addressed by a number identifying the function or application for which it is being used.
- Voice Group Call Service (VGCS): Enables group calls between trains and BSs or among trackside workers, station staff and related groups.
- Voice Broadcast Service (VBS): Allows BSs to broadcast messages to a group of trains. It is also possible to broadcast messages from trains. This feature is mostly used to make train operation announcements or to broadcast record messages.
- Enhanced multi-level precedence and pre-emption (eMLPP): Associates each user's call to a well-defined priority level to optimise the emergency calls performance. In extreme situations, it has a feature (pre-emption) that involves the disconnection of an on-going call of lower precedence to accept an incoming call of higher precedence. The UIC priority order is railway emergencies, control-command (safety), public emergencies and group calls between drivers in the same area, railway operations and at last railway information along with all other calls.
- Emergency calls: Focus on notifying all the personnel (drivers, controllers, etc.) about any dangerous situation involving or not shunting operations, and it is divided into three phases, which are warning (Stage 1), information (Stage 2) and terminate railway emergency call (Stage 3).
- Cell reselect: Handover is continuously happening in railways, hence, it is fundamental to have re-selection of cells for the moving trains. The EIRENE establishes that the speech loss has to be less than 8 s in 95% of case and 12 s for 99% of cases.

Table 2.1 ETCS QoS requirements (based on [FrFC17]).

Requirements	**Value**
Maximum connection establishment delay [s]	< 8.5@95%; < 10@100%
Connection establishment error ratio	$< 10^{-2}$@100%
Connection loss rate [h^{-1}]	$< 10^{-2}$@100%
End-to-end transfer delay [s]	≤ 0.5@99%
Transmission interference period [s]	< 0.8@95%; < 1@99%
Error-free period [s]	> 20@95%; > 7@99%
Network registration delay [s]	≤ 30@95%; ≤ 35@99%; ≤ 40@100%

Regarding optional services, it is strongly recommended to have in the railway services such as the shunting mode, which offers an efficient way to communicate with the personnel responsible for shunting operations. Additionally, more optional and future features are presented in [PuTa09], like eLDA, Direct Mode, General Packet Radio Service (GPRS), on-board applications, among others. The most relevant services are given in Table 2.2 for the different radio types.

Table 2.2 Categorisation of the principal services (based on [GSMR15b]).

Service Group	Type of Service	Cab	ETCS Data	General Purpose	Operational	Shunting
Voice	Point-to-point	MI	NA	M	M	M
	Public emergency	M	NA	M	M	M
	VBS	M	NA	M	M	M
	VGCS	MI	NA	M	M	M
	Multi-party	MI	NA	O	O	M
Data	Text message	MI	NA	M	M	M
	General data applications	M	O	O	O	O
	Automatic fax	O	NA	O	O	O
	ETCS train control	NA	MI	NA	NA	NA
Specific features	FA	MI	NA	M	M	M
	LDA	MI	M	O	O	O
	Direct mode	NA	NA	NA	NA	NA
	Shunting mode	MI	NA	NA	NA	M
	Multiple driver communications within the same train	MI	NA	NA	NA	NA
	Railway emergency calls	MI	NA	O	M	M

Another crucial requirement is related to the call set-up time. It is mandatory for interoperability to have an achievement in 95% of cases and for 99% of cases it cannot overcome 1.5 times of the set-up time for specific call type, which are presented in Table 2.3.

Table 2.3 Call set-up time requirements (based on [GSMR15b]).

Call type	Call set-up time [s]
Railway emergency calls	4 (M)
High priority group calls	5 (M)
All operational and high priority mobile-to-fixed calls not covered by the above	5 (O)
All operational and high priority fixed-to-mobile calls not covered by the above	7 (O)
All operational mobile-to-mobile calls not covered by the above	10 (O)
All other calls	10 (O)

According to [GSMR15a], the handover for voice calls is obliged to be executed in less than 350 ms in 95% and 500 ms in 99% of cases. The decision of using synchronisms among the Base Transceiver Stations (BTSs) is up to each authority, providing the chance of reducing the handover break to 150 ms.

The main problems for high-speed trains concerning handover are the high switching failure rate due to the correlation between the small overlap area and the Doppler frequency shift. The frequent switching

occurs because of the train's high speed and the group switching (there will be several users requesting to switch BSs at the same time). On the other hand, and contrary to standard cases of mobile communications, trains do not have numberless orders of freedom; for this reason, it is achievable to develop smart algorithms to understand which way the trains go and predict the future user's needs offering a good QoS. The Doppler shift effect, mentioned before, occurs due to the separation of received signals in frequency and it has a direct influence on the signal power spectrum. Despite this, according to [XZAZ16], if it could be provided precise information about train's velocity and location, it would be possible to compensate for the Doppler shift, which is easily reachable for trains.

An additional characteristic to recognise in mobile communications is the coverage and interference aspects. Table 2.4 shows the specific coverage probabilities for the minimum received power values in each location interval, with a length of 100 m, taking into account a maximum total loss of 6 dB, 3 dB between antenna and receiver, and an extra margin of 3 dB for other factors (e.g. ageing). Interference has to be carefully analysed in tracks since there are many dependencies. For instance, the frequency reuse alongside tracks has to be planned in order to have acceptable limits of co and adjacent-channel interferences. A different type of interference happens between the direct and reflected signals, and it may vary according to antennas directivity and height, path length and soil characteristics. According to [3GPP05] recommendations, the co-channel interference has to be less than 9 dB and the adjacent interference depending on the bandwidth shall be -9 dB for 200 kHz, -41 dB for 400 kHz and -49 dB for 600 kHz.

Table 2.4 Coverage requirements (based on [GSMR15a]).

Services	Coverage [%]	Receiver sensibility [dBm]	Velocity [km/h]
Voice and non-safety critical data	95	-98	--
ETCS levels 2/3	95	-95	≤ 220
ETCS levels 2/3	95	[-95 ; -92]	[220 ; 280]
ETCS levels 2/3	95	-92	≥ 280

2.1.2 Railway scenarios

Typically, the study of radio propagation signals is supported by the types of environment classification (e.g. rural, suburban, urban, etc.), since there are similar physic behaviours for specific scenarios taking in consideration parameters like terrain undulation, building density and height, vegetation density, etc. The dominant scenarios in railways are: viaducts/bridges, water, suburban, cuttings (regions lower than the normal tracks at least 2 m) or embankments (regions higher, at least 2 m, than the average tracks), mountains, rural, railway stations, urban and tunnels, where the reflection and scattering components have a strong influence.

According to Table 2.5, the railway tracks may be classified into four different groups regarding some railway characteristics such as "urban" for lower traveller speed and smaller line length which do not allow the passengers to use numerous services since its usage time is very short, up until "high-speed"

with trains operating with higher speeds for long journeys offering customers the opportunity to explore several services during the trip.

To understand how mobile communications work in a railway atmosphere it is a must to have a clear understating about each connection between terminals as it is shown in Figure 2.2.

Table 2.5. Characteristics of line types (based on [FrFC17]).

Characteristics	Urban	Urban/inter-City	Inter-City	High-Speed
Maximum speed [km/h]	≤ 70	] 70 ;160]	]160 ; 250 [	≥250
Line length [km]	≤ 20	] 20 ; 100 [	[100 ; 250 [	≥ 250
Parallel tracks	1	2	3	4
Train stations	1-5	6-20	21-50	51+
Range of services	Single	Small diversity	Multiple variance	Very varied

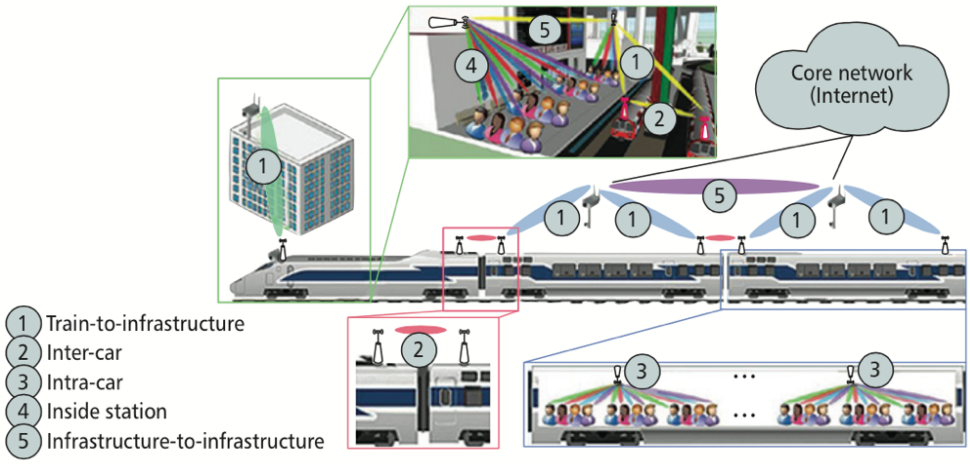

Figure 2.2. Connectivity scenarios for railways (extracted from [AGRK15]).

1. Train-to-infrastructure: A bidirectional link between the nearest BS and a transceiver installed on the train. When trains are travelling at speeds up to 350 km/h, the link has to provide high data rates and latencies lower than 100 ms and always respecting specific requirements related to reliability, availability, maintainability and safety, which request availability of 99%.
2. Inter-car: A connection between adjacent carriages that can be done by two different ways, through optical fibres or by wireless communication. The first approach should be the best option regarding the data transmission, but it is much more expensive to install. For the second method, the access points (APs) are used as an AP for all mobile terminals inside each carriage, while for the next carriage APs are seen as a client station. For this reason, the APs demand a connection with high data rate and low latency.
3. Intra-car: A wireless connection between the AP and the user's terminals is established offering several on-board railway applications.

4. Inside station: Usually is a crowded environment where a link is created between the user's equipment and APs on the stations. The best solution for these scenarios is the installation of massive MIMO technology, providing higher data rates, better spectral efficiency and more capacity.
5. Infrastructure-to-infrastructure: It is a bidirectional link between infrastructures in real time transmitting security camera's data or other relevant information about the railway atmosphere (e.g. trains, platforms, stations and wayside along rail tracks).

2.2 GSM-R

In this section, an overview of GSM-R is presented, based on [GSMR15a], [3GPP05], [PuTa09], [Corr17] and [HAWG16].

2.2.1 Network architecture

GSM-R is identical to GSM, but with specific extra functionalities regarding railways' needs, the primary network elements are presented in Figure 2.3: the Base Station Subsystem (BSS), the Network Subsystem (NSS) and the Operations and Maintenance Subsystem (OMS).

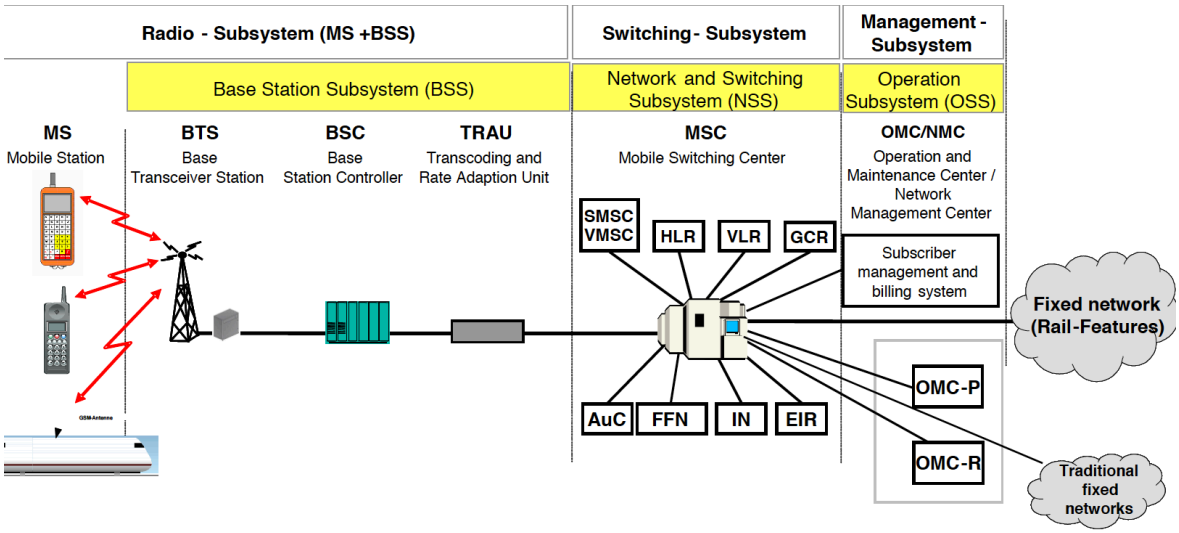

Figure 2.3. GSM-R architecture (extracted from [Dan08]).

In one edge of the architecture, one has the Mobile Station (MS), the only equipment of the GSM/GSM- R architecture the users have in their possession. Subscribers are allowed to choose the operator which they think that will provide a better service for their needs, but all of them work equally. The identification of the subscriber is acquired through a Universal Subscriber Identity Module (USIM) card, which has to be into the MS and possess the International Mobile Subscriber Identity (IMSI) to identify the subscriber in the network. Each MS is identified by the International Mobile Equipment Identity (IMEI), and without the USIM card, it is only possible to perform emergency calls.

The BBS contains all the radio-related functions of a regular GSM system, the BTS, the Base Station Controllers (BSC) and the Transcoding and Rate Adaption Unit (TRAU). It covers several functionalities, like power control, handover decisions, coding, encryption, channel assignment and maintenance of link quality.

The BTS hosts all the radio frequency hardware (transceivers and antennas), and it is responsible for establishing and maintain the connection with the MS. Typically, several transceivers are working at different frequencies regarding the standards for GSM-R, for this particular case, to optimise the capacity of a cell. It is the BSC that manages the BTSs, and controls the signalling traffic, the power levels of each BTS and handovers. Handovers allow calls to be transferred between cells without interrupting communications, which happen to be an essential procedure for a high-quality call experience in railways. The TRAU has the purpose of control the speech coding and decoding as well as the adaption to the user data transmission rate. Physically speaking it resides on the BSC or the Mobile-services Switching Centre (MSC).

The importance of the NSS is related to the necessity to control the traffic of several BSCs. It is constituted by the MSC, the Home Location Register (HLR) and the Visitor Location Register (VLR). The MSC is a high-performance digital switching centre needed to carry out switching tasks between mobile radio users and others Public Land Mobile Networks. It forms the links between MSCs, BSCs as well as the connection between GSM-R network and other wireline ones. The MSC handles all the signalling required for setting up, maintaining and terminating connections regarding the ITU-T Common Channel Signalling System No.7 (CCS7), which covers all aspects of control signalling for digital networks. The HLR is the database where it is stored the most relevant static information relating to each mobile subscriber containing the MS identification number, equipment type and supplementary services. To increase the subscriber's security, the HLR is merged to the Authentication Centre (AuC) to safeguard identity and data transmission. The VLR manage the temporary information about subscribers who are, at the moment of the call, roaming under an area controlled by a specific MSC. Each VLR is integrated with a respective MSC and every time that a new MS enters a specific location area, all the critical information it is copied from the HLR. The purpose is preventing frequent HLR updates and decrease the processing power needed. Similar to the HLR's case, the VLR has a supplementary security measure, which is the equipment identity register (EIR), a database with lists of valid and invalid IMEIs since MSs might be stolen.

The OMC is responsible for manage all the others network entities, i.e., traffic monitoring, status report of network entities, subscriber and security management, and accounting and billing.

According to [PuTa09], one of the several optional features of GSM-R is the implementation of GPRS. It is a data service that allows end-to-end packet-switched data connections which is a more efficient way to use the available bandwidth. GPRS becomes mandatory when railway communications demand better characteristics, like higher data rates. To implement this service, it is necessary to add more three infrastructure elements: the Serving GPRS Support Node (SGSN), the gateway GPRS Support Node (GGSN) and a Point-to-Multipoint Service Centre (PTM-SC).

2.2.2 Radio interface

The radio interface concerns about how the connection between the MS and the BTS is done regarding radio propagation. GSM-R uses a bandwidth of 4 MHz allocated between 876-880 MHz for UP and 921-925 MHz for DL. It has to be noted that some countries have available an additional band of railways called the E-GSM-R, with an additional 200 kHz band guard at the higher end to protect from the interference of the adjacent E-GSM band. On the lower border of frequencies, it is recommended a 400-600 kHz guard-band to prevent interference problems due to Private Mobile Radio(PMR)/Public Access Mobile Radio (PAMR) services (e.g. the Terrestrial Trunked Radio (TETRA)). From this guard-band, 100 kHz belongs to the UIC band, which is also reserved to allow communications over short distances without using the mobile network infrastructure called UIC Direct mode. A summary of the frequencies organisation is given in Figure 2.4.

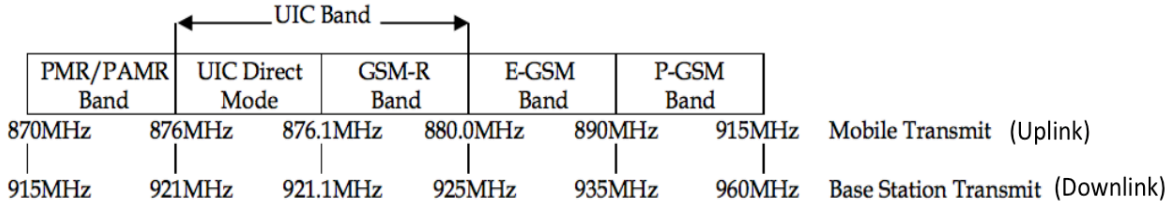

Figure 2.4. Frequency bands for GSM-R (adapted from[PuTa09]).

It is considered narrowband in comparison with other systems, like Long-term Evolution – Railway (LTE- R), and this provides a very long range and a high spectrum efficiency which results in excellent power efficiency, but a narrowband signal has a low data rate. Data are transmitted using the Gaussian Minimum Shift Keying (GMSK) modulation with periodical Time Division Multiple Access (TDMA) frames of 4.615 ms. The system has a bandwidth of 200 kHz, and one TDMA frame is constituted by 8 time slots (logical channels) with 148 bits of information each. This system is capable of providing voice services with 22.8 kbps within a standard transmission rate of 9.6 kbps per time slot. Despite the use of some techniques to have better performances, GSM may use adaptive modulation with 8-PSK through EDGE technology, however it is not the case of GSM-R.

2.3 LTE-R

This section addresses the network architecture of future mobile radio system for railways, LTE-R, based on [HoTo11], [CMAF13], [Cisc16] and [HAWG16]. Then, one presents a description of the radio interface, as well as the services provided through the review of [3GPP17], [CMAF13], [BeBe12], [ACKZ14], [ZAZW17] and [FRGC15].

2.3.1 Network architecture

Unlike GSM-R, LTE-R is purely based on an IP-based packet switched solution, since both voice and data services are carried by the IP protocol. It includes a radio access network of Evolved Universal Terrestrial Radio Access Network (E-UTRAN) and a core network of evolved packet core (EPC). As it was mentioned, for reasons of backwards compatibility with the GSM-R, it was fundamental the evolution of GSM network to be capable of working with GPRS, offering much interoperability as possible to the railway communication system. This development allows LTE-R architecture to have GSM-R working in a parallel level without any problems of coexistence, providing proper conditions for a migration strategy aiming to LTE-R as the worthy successor of GSM-R.

As presented in Figure 2.5, the first block represents the group of all on-board units (OBU) with the technical features needed to be capable of making a connection in this communication system (e.g. cab radio, ETCS Data Only Radio and shunting radio). Identically to GSM-R regarding MSs, OBUs contains USIM responsible for the identification and authentication of users.

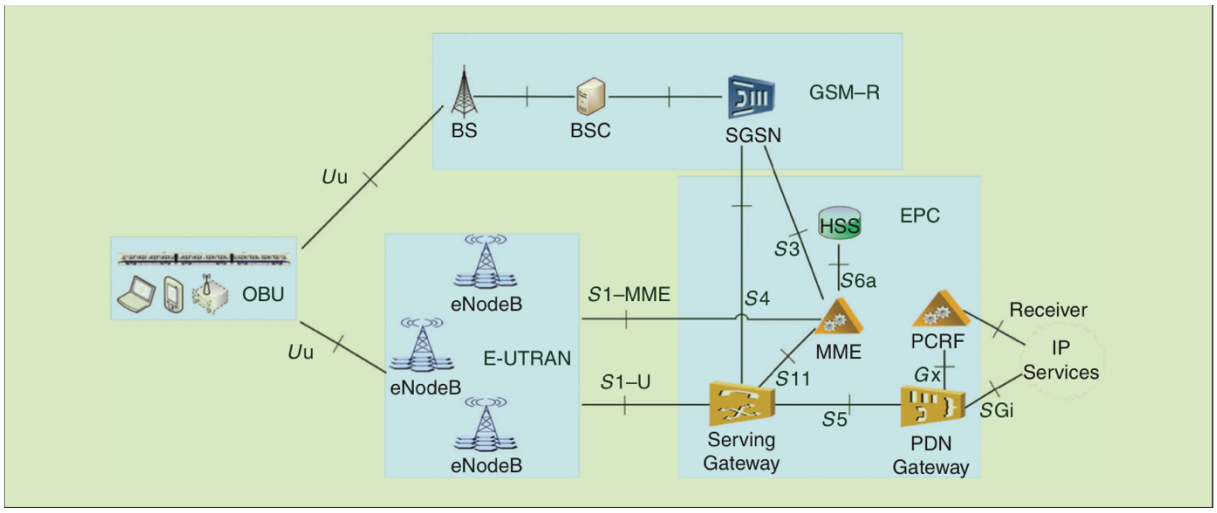

Figure 2.5. LTE architecture (adapted from [HAWG16]).

The E-UTRAN block is comprised of several E-UTRAN Nodes B (eNode B or eNB) where there is no centralised controller, thus leading to a flat architecture. Usually, the eNodeBs are intelligent BSs connected with each other by the X2 interface and towards core network by the S1 interface establishing a connection with the EPC. For additional improvement, an extra feature of the S1 interface was created, being called S1-flex, where multiple Mobility Management Entities (MMEs) / Serving Gateways (S-GWs) can be connected to allow the possibility of load sharing and to increase redundancy (constructing virtual pools). The purpose of E-UTRAN's architecture is to reduce the number of nodes involving the path to improve the real-time behaviour or in other words to reduce the latency of the radio interface operations reducing the time of connection's set-up and the time needed for a handover. To have an efficient network architecture, it is critical to identify which block is responsible for what. Therefore, the E-UTRAN has to ensure the Radio Resource Management (e.g. radio bearer control, radio admission control, radio mobility control, scheduling, dynamic allocation of resources to OBU in UP and DL, etc.), security (through encryption of radio interface data), positioning (detect the accurate OBU's position),

connectivity to the EPC (carrying and delivering signalling towards MME and the beard path towards the Serving Gateway (S-GW)) and to provide header compression (compressing IP packet headers to ensure the effectiveness of radio interface).

The EPC is the last sector of LTE-R core network. It is known for using an all-IP based, even for voice, and for having a multi-access network that enables the outspread and operation of a shared network for different access networks. The radio access to 3GPP networks, such as GSM, UMTS and LTE, are secured by S-GW, while P-GW is the gateway to non-3GPP radio access networks, like WLAN or for fixed access (e.g. Ethernet, Digital Subscriber Line [DSL], etc.). The main logical nodes of EPC are:

- Serving Gateway (S-GW): It is the node where all users' data, based on IP packets, travels through, which is used as a local reference for the data bearers when handovers occur and the OBU moves among eNodeBs. Furthermore, it preserves bearers' information when the OBU is in an idle state, it executes administrative jobs, such as collecting billings' data, and it works as the mobility bases for interoperability with other networks like GSM and UMTS.
- PDN Gateway (P-GW): It is responsible for providing stable IP access as an input and output point between the EPC and the external IP networks entitled Packet Data Network (PDN). It also executes functions as IP address allocation, QoS guarantees, policy enforcement, charging according to PCRF's instructions, as well as working as the anchor for mobility between non-3GPP technologies.
- Mobility Management Entity (MME): It has a physical connection with eNodeBs, S-GW, HSS, SGSN and MMEs from others EPCs, hence it has a critical managing role in the network. The protocols between the core network and the OBU, which are mandatory, are identified as the Non-Access Stratum protocols. MNE is responsible for choosing the appropriate S-GW for a respective OBU, authenticating the user through the HSS, generating and allocating temporary identities for OBUs among other important functions.
- Home Subscriber Service (HSS): It holds users' subscription and authentication data, roaming restrictions as well as information concerning which PDNs the user can establish a connection with.
- Policy and Charging Resource Function (PCRF): It is responsible for controlling and making decisions regarding policies and charging functionalities. It manages, in real-time, how data flow must be treated in the Policy Control Enforcement Function which belongs to P-GW, accordingly QoS' standards and user' subscription profile.

2.3.2 Radio interface

Since LTE-R specifications have not been standardised yet, there are several aspects to be analysed regarding the allocation of spectrum for LTE-R. It is known [3GPP17], that the LTE may operate in 70 different frequency bands, each one standardised to work in one of two different duplex systems to the transmission of bidirectional information: the Time Division Duplex (TDD) or the Frequency Division Duplex (FDD). The range of the working frequency bands is between 450 MHz to 3.8 GHz.

Currently, the majority of LTE network use bands as 1.8 GHz and 2.6 GHz where larger bandwidths are available, resulting in a higher data rate despite the substantial path loss. However, these bands alone

are not the most suitable solutions for railway communications. Assuming the typical transmitting power levels working at 2.6 GHz leads to a cell radius below 500 m, which, in practical terms, results in a considerable investment to have a dense layout of BSs. Therefore, a suitable solution might be using a dual-band mode where the higher priority services should work in a lower frequency band, such as 800 MHz, and the other services should be allocated to a higher working frequency band, like 1.8 GHz or 2.6 GHz.

From the access point of view, LTE uses a multiple access technique called Orthogonal Frequency Division Multiple Access (OFDMA). The OFDMA is a technique to encode information on multiple carrier frequencies where a specific working band is divided into a set of sub-carriers enabling an overlap of carriers that do not bring any problem, since these sub-carriers are orthogonal to each other in the time and frequency domain. This multiple access technique brought many benefits, like higher data rates, low sensitivity to fast fading and the fact that it does not need to have guard-bands to separate carriers leading to higher spectral efficiency. The idea of OFDMA is to simultaneously assign different subsets of sub-carriers to each user to transmit their specific requested data. However, the high Peak-to-Average Ratio that implies a low power conversion happens to be a critical problem, hence OFDMA is exclusively used for DL due to the power limitations of mobile devices. For UL, in order to optimise battery performance it uses a Single Carrier Frequency Division Multiple Access (SC-FDMA) where, unlike ODFMA, the signal is a linear combination of all data symbols relative to a modulated set of sub-carriers. The available LTE carrier bandwidths go from 1.4 MHz (72 sub-carriers) to 20 MHz (1200 sub-carriers) depending on the number of sub-carriers needed with a 15 kHz separation between them. For this specific system, the physical channels are based on units with a duration of 1 slot (0.5 ms) and 12 subcarriers (180 kHz) named as Resource Block (RB). Figure 2.6 provides a better understanding of how these physical channels work. The maximum amount of RBs allocated to each user depends on the bandwidth: the lowest bandwidth (1.4 MHz) provides 6 RBs and the highest one (20 MHz) can afford 100 RBs.

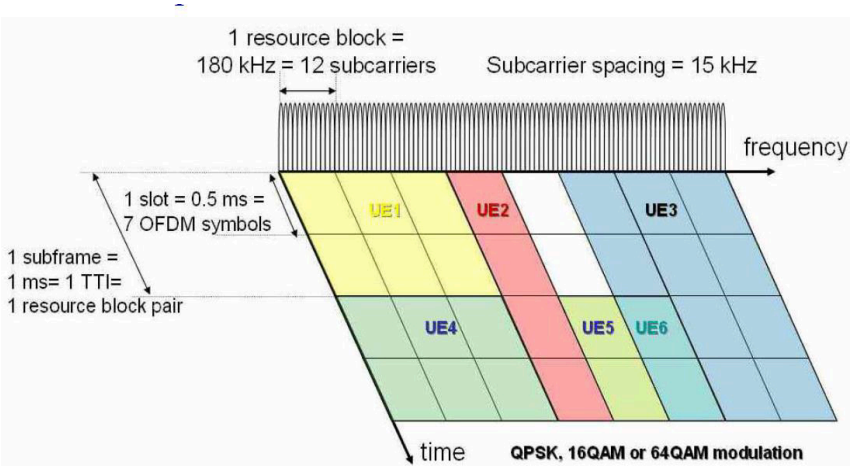

Figure 2.6 Overview of RBs allocation (extracted from [GeRK12]).

2.3.3 LTE-R services

The non-stop pursuit of better conditions is a normal mechanism of progress, and railway mobile

communications are not an exception. It is vital to have a technological evolution to users' experience that does not become obsolete, resulting in a decrease of customers and further ahead to a reduction of income to companies. Although GSM-R is still in implementation phase in several countries, the responsible railway's entities are already working to have a solid answer and disrupt current boundaries created by this technology. The principal limitations are the following:

- Interference: Railway and public operators struggle for the coverage due to the urge of having the best coverage possible.
- Capacity: GSM-R only supports 19 channels of 200 kHz, which is insufficient for the needs of future railway systems, where each train will have continuous data connections.
- Capability: GSM-R is a narrowband system, which implies a low transmission rate (9.6 kbps per connection) and a message delay around 400 ms, which are not acceptable for future services.

To improve the quality, security and safety of the users' travelling experience, LTE-R is going to be the next step towards the future of railway's communication systems, thanks to the flexibility of having several working bands. On the one hand, this flexibility provides a larger bandwidth available in the upper bands (higher data rate), and on the other hand, for low-frequency bands, there are lower propagation losses (an increase of the LTE-R radius cell providing more coverage).

LTE-R will bring many improvements, which will be noticed in railway applications and services. Due to the complexity of future railway services a tree to organise and prioritise the services is presented in Figure 2.7.

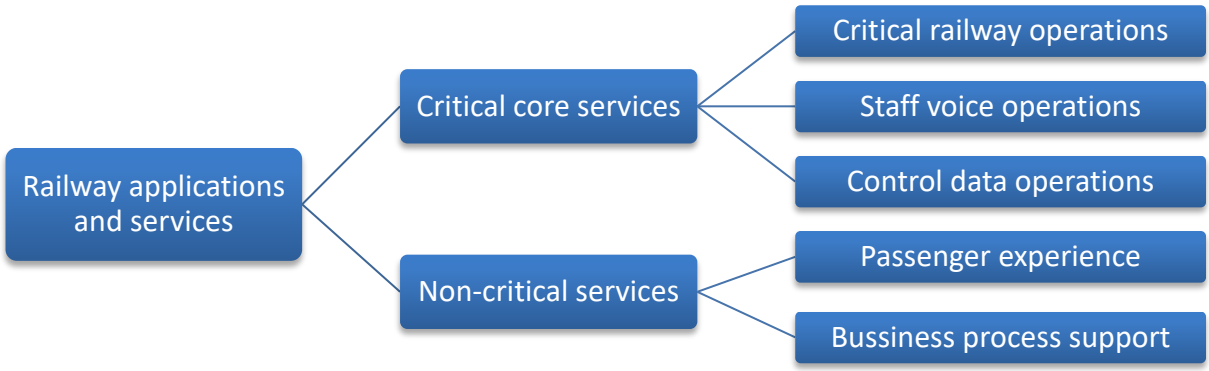

Figure 2.7. Railway services classification (adapted from [CMAF13]).

The same considerations mentioned in the network architecture need to be present in services segment, which means that the GSM-R services migration requires a proper answer from LTE-R. It is mandatory to have a coverage for each service that GSM-R provided. In Table 2.6, one presents the LTE features and mechanisms, which will support GSM-R services.

Always having a well-establish prioritisation order, LTE-R will provide numerous services to improve aspects of security, QoS and network efficiency. A list of some possible services is provided in Figure 2.8.

Table 2.6 Migration from GSM-R services to LTE-R (adapted from [CMAF13] and [FRGC15]).

GSM-R →	LTE-R
Location-dependent addressing (LDA, eLDA)	LTE Positioning Protocol (LPP)
Voice broadcast calls (VBS)	Evolved Multimedia Broadcast Multicast Services (eMBMS)
Voice group call services (VGCS)	Push-to-Talk over Cellular (PoC) system
Railway emergency calls (REC, e-REC)	IMS emergency calls
Priority and pre-emption (eMLPP)	Allocation and Retention Priority (ARP)+ policy control rules + QoS mechanisms
Functional addressing (FN)	Session Initiation Protocol (SIP) addressing
Fast call set up	Very low latency of LTE to support fast exchange of signalling (e.g. IMS-based PoC) + Access class barring
Data exchange (SMS, shunting)	IMS-based SMS service

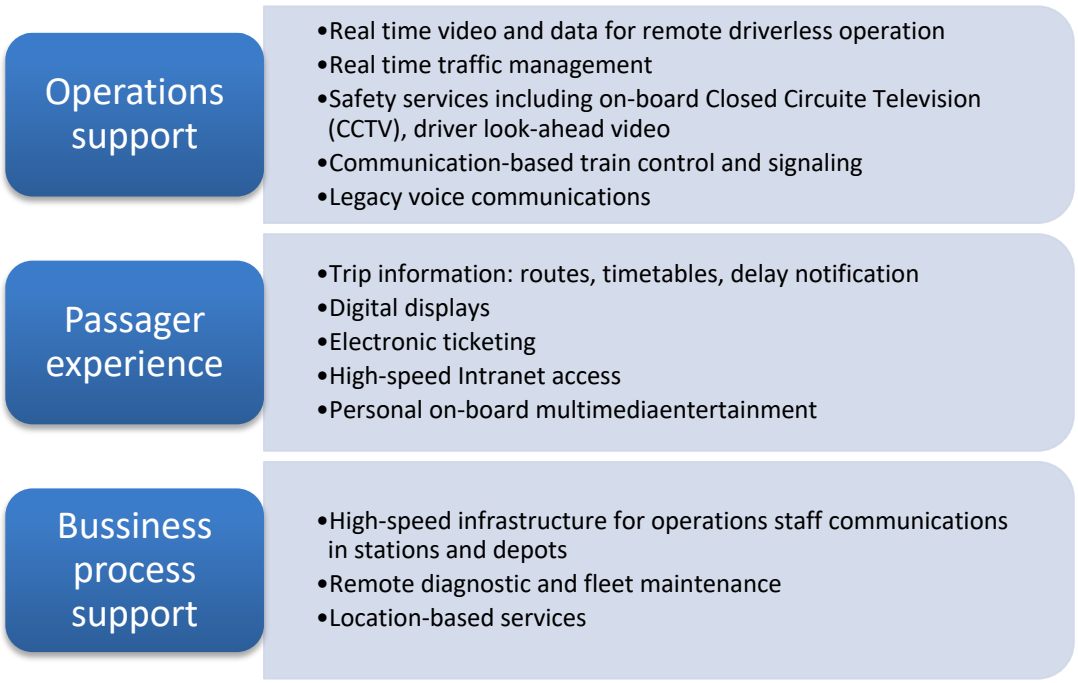

Figure 2.8. Future railway services (adapted from [CMAF13]).

2.4 BBRS (Broad Band Radio System)

In this section, an overview of the BBRS architecture, radio interface and corresponding services are provided based on [Mend10], [Gonç13], [Maso13], and [BBRS17].Maso13

2.4.1 Network architecture

BBRS is a solution integrated and installed by Thales using technical solutions from different vendors to provide a bidirectional data transmission in real time based on Wi-Fi.

One shows in Figure 2.9 the global picture of BBRS architecture, where it is easy to identify the principal components: Network Management System (NMS), S-GW, Mobility Controller, Static Mesh Nodes (on-track radios) and Mobile Mesh Nodes (on-board radios).

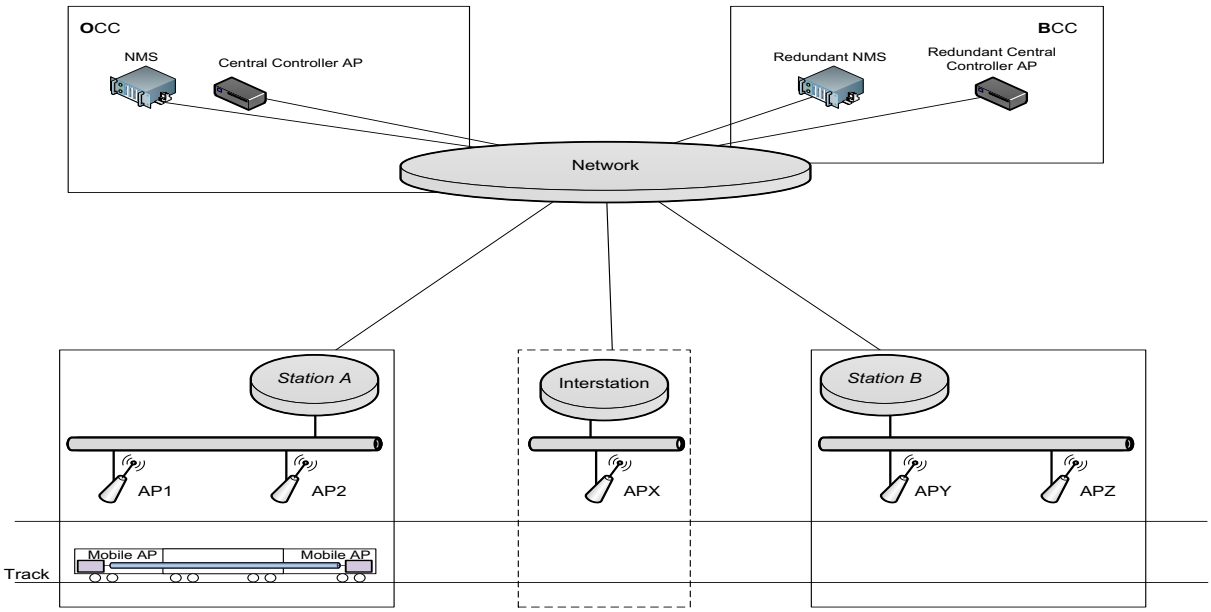

Figure 2.9. BBRS architecture (extracted from [BBRS17]).

The NMS does not execute vital tasks on the network operation level, however this element provides real-time monitoring and configuration of the entire network, which can be used to identify roaming and handover, detect errors or faults that may occur, perform centralised access to the mesh configurations, regulate traffic prioritisation according to the network needs, adjust the radio power controls, and execute security measures, among other assignments. Due to redundancy reasons, it is installed at the same time in the Operation Control Centre (OCC) and Backup Control Centre (BCC).´

S-GWs are located at the BCC inside the Central Equipment Room (CER), hence it has a direct connection to the node responsible for the links to the Static Mesh Nodes. Besides that, they are also placed on OCC for redundancy purpose. The primary goal of S-GW is to manage mobility and traffic that comes from all the static nodes belonging to a particular mesh.

The Mobility Controller can be found at the Central Equipment Room (CER) of OCC, and also on BBC for redundancy, controlling the mobility of all system meshes, in order to reduce future problems of handover.

The Static Mesh Nodes are constituted by sets of two directional antennas positioned along the track, providing proper signalling coverage. Each mesh is constituted several nodes depending on vendor specifications.

The Mobile Mesh Nodes are installed on trains to provide a wireless connection with the Static Mesh Nodes. Typically, the link between the Static Mesh Nodes and the mobile terminals is done in a two-hop communication system (train-to-infrastructure and intra-car) to avoid high penetration losses created by carriages (about 25 dB).

The handover between on-track terminals is done through an autonomous system based on constant evaluation of several parameters, such as RSSI (Received Signal Strength Indicator), throughput and QoS.

2.4.2 Radio Interface

Concerning the radio interface, BBRS is based on the IEEE (Institute of Electrical and Electronics Engineers) 802.11n 2x2 standard, using a multiple-input and multiple-output (MIMO) technology, more precisely two transmitting antennas and two receiving antennas. Usually, it uses OFDM as the transmitting data method. It may use several types of modulation like BPSK, QPSK, 16-QAM or 64-QAM with coding rates varying between 1/2 to 5/6. The IEEE 802.11n uses 2.4 GHz and 5 GHz frequency bands. This wireless network standard uses channels with a bandwidth of 20 MHz or 40 MHz depending on system specifications. Thanks to OFDM a single 20 MHz channel has 48 subcarriers carrying data from a total of 52 subcarriers, allowing to provide data rate of 65 Mbps. For 40 MHz the number of subcarriers used to transmit data increases to 114, meaning that for a single spatial data stream is possible to have throughputs of 135 Mbps [Maso13]. The specific working frequency bands for the BBRS are presented in Table 2.7. Although there are three distinct categories, it is recommended to use the non-standard with license category due to security issues, and because the licensed spectrum has 10 to 100 times more signalling power than the unlicensed one, which provides a link without significant interferences [Reed18].

Table 2.7 BBRS working frequencies (based on [BBRS17]).

Wi-Fi Type	**Frequency [GHz]**
Standard without license	2.405 – 2.495
	5.150 – 5.825
Non-Standard without license	5.825 - 5.875
Non-Standard with license (recommended)	5.875 – 5.925

BBRS allows bidirectional transmission of data packets providing the possibility of transmitting or receiving any data through IP standards and Table 2.8 shows the improved characteristics provided by Thales.

Table 2.8 BBRS performance (based on [BBRS17]).

Requirements	Values
Speed [km/h]	≤250
Rate [Mbps]	70 ≤ x ≤ 125
Handover [ms]	< 100
Range [m]	< 1000 (300 for urban environment)

2.4.3 BBRS services

The range of services provided by BBRS is very large thanks to the constant technologic improvement, pointing towards the Internet of Trains. For more details, it is recommended to read [FrFC17].
According to [BBRS17], the principal services provided by BBRS are the following:

- Train Maintenance System: It offers real-time notifications (alarms, warnings or other type of information) automatically of all on-board systems with instantaneous warnings if any problem occurs in a specific system.
- On-board live CCTV: It provides real-time footages or video streams of every camera connected to the railway environment and also offers the possibility to visualise specific events that have occurred (e.g. Namma Metro project offers a camera stream, 25 fps at 4 CIF, which corresponds to a 2 Mbps Bandwidth).
- Platform cameras visualisation: Train's drivers have access to real-time footages of the railway platform.
- Passenger Information System: It increases interactivity with the passenger by sending text and audio messages and also sending video content to the train.
- Internet for passengers: The BBRS was created to provide the best QoS possible and nowadays, in this environment, a fundamental feature is a stable connection to the Internet, which is provided with excellent rates.

The services mentioned above are those that are seen from a user's perception, but from the network one other features show up as is the case of the seamless mobility for the entire track thanks to the handover between adjacent APs, an integrated remote graphical network management and encrypted links.

2.5 Performance parameters

In this section, a description of the principal parameters of mobile communications and antennas is based on [Viss12], [SAUH14], [WaZG12], [Corr17] and [More17].

2.5.1 System parameters

To have a system capable of providing the best services, it is necessary to measure the QoS that is analysed through many parameters, the essential ones being: coverage, interference between BSs and system's capacity. These parameters are inter-correlated, hence one needs a trade-off that must be analysed depending on system requirements. To have a system with good performance, cellular planning needs to take them into account, not only the morphology of the area but also signal estimation. These considerations provide a proper decision of which propagation model may be used to optimise BSs location, in other words, to establish the right coverage and minimise interference.

The determination of which is the best model for propagation in mobile communications is supported by a proper knowledge of signal estimation behaviour. The signal may be affected by slow (long-term) and fast (short-term) fadings. Slow fading depends mostly on distance through a log-normal distribution, and the fast one is related to terminal mobility, with a Rice distribution [Corr17]. To perform a QoS evaluation it is essential to have an estimation of the percentage of BSs coverage area. With that purpose, it is possible to know the percentage of locations with a specific receiving power and distance by only taking slow fading into account, neglecting fast one.

To establish the coverage of a particular region, one performs cellular planning. In normal circumstances, hexagonal shapes are used to approach the theoretical coverage of omnidirectional antennas. However, in railway communications, the frequency reuse cluster is done for linear coverage with directional a1ntennas, since it is well-known where trains travel. As it is shown in Figure 2.10, there is an increase of performance for this specific coverage. To have an accurate understanding of frequency allocation, it is recommended to read [SAUH14] and [WaZG12] where the "moving cell" concept is presented for railways, a technique to avoid handover problems in highway communications, using remote access units.

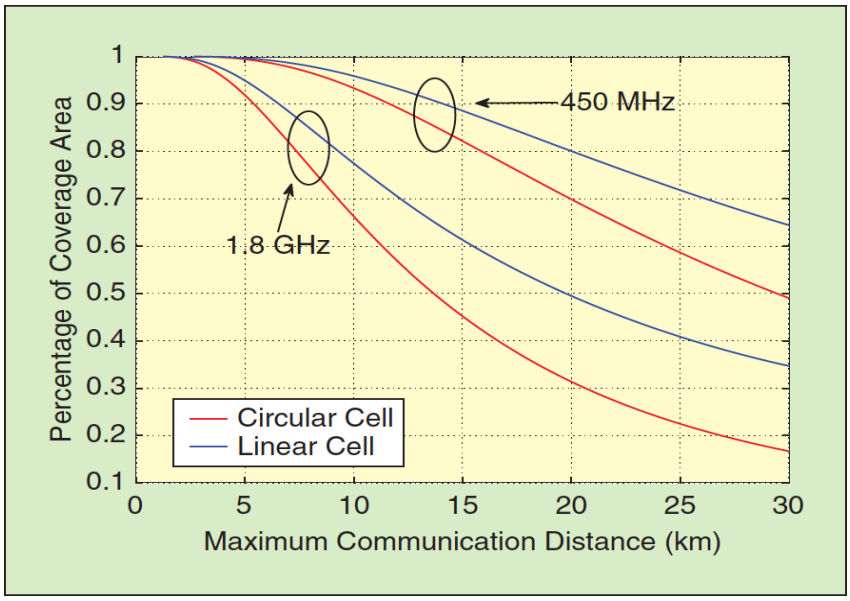

Figure 2.10. Coverage area regarding circular and linear cells (extracted from [HAWG16]).

2.5.2 Antennas' parameters

To have a proper connection between terminals, one needs to analyse all the losses and gains that exist. One of the main aspects is path loss, which depends on several parameters, and there are several propagation models to have the best estimation possible like the free space model, the "Flat Earth" model for short distances, the Knife-Edge model when there are obstacles with dimensions much larger than the wavelength, COST 231 – Okumura-Hata model for more considerable distances and COST 231 – Walfish-Ikegami model for small distances as well as for urban environments [Corr17]. For the majority of the models, the parameters required are the frequency, the distance between terminals and the height of antennas. Additionally, some correction factors are considered due to specific characteristics of the environment under study.

The frequency bandwidth (BW) of an antenna is associated with the range of frequencies where the antennas characteristics are working according to the specifications. It may be expressed as the absolute bandwidth (ABW) or as the fractional bandwidth (FBW). The ABW expresses the difference between the upper and lower edges of the antenna's working frequencies. The FBW is defined as the percentage of the frequency difference over the centre frequency.

A proper understanding of how the electromagnetic field behaves is fundamental to be able to make a detailed analysis of antennas performance. The antenna's radiated field may be separated into three regions, depending on distance. The reactive (non-radiative) near-field region is the nearest area to the antenna, where the EM field behaviour is way too complicated to predict due to the reactive oscillation and the non-radiating energy strength. Further away, there is a transition region so-called of radiating near-field region or the Fresnel region; in this specific zone, there is a dependence of the angular distribution of the EM field with distance, and for this reason, it is possible to make some approximations. The farthest region from the transmitting antenna is the far-field (Fraunhoffer) one, where the radiating field prevails, and the angular field distribution no longer depends on the distance from the antenna; this region is the most important to study since, in normal circumstances, the separation between terminals happens in the far-field region.

To have a better understanding of antenna's radiation properties, one defines a set of space coordinates (r, θ and φ) centred on the antenna to represent the field patterns, which displays the spatial variation of the power density or the field intensity along a constant radius. Since a three-dimensional representation is too complex, there are also two-dimensional graphics as a more straightforward way to understand antennas main characteristics, where is possible to rapidly identify lobes and beam-widths (e.g. Polar and rectangular radiation patterns).

The lobe beam-widths are an essential characteristic of the radiation pattern, being the angular separations between two identical points on opposite sides of the most influential pattern. As shown in Figure 2.11, there are the major lobe, minor lobes, side lobes and the back lobe. The major lobe is simply the radiation lobe containing the direction of maximum radiation. The remaining lobes, so-called the minor lobes, represent radiation in undesired directions, typically the side lobes are larger ones. The back lobe is defined as the radiation lobe that makes roughly 180º with the main lobe.

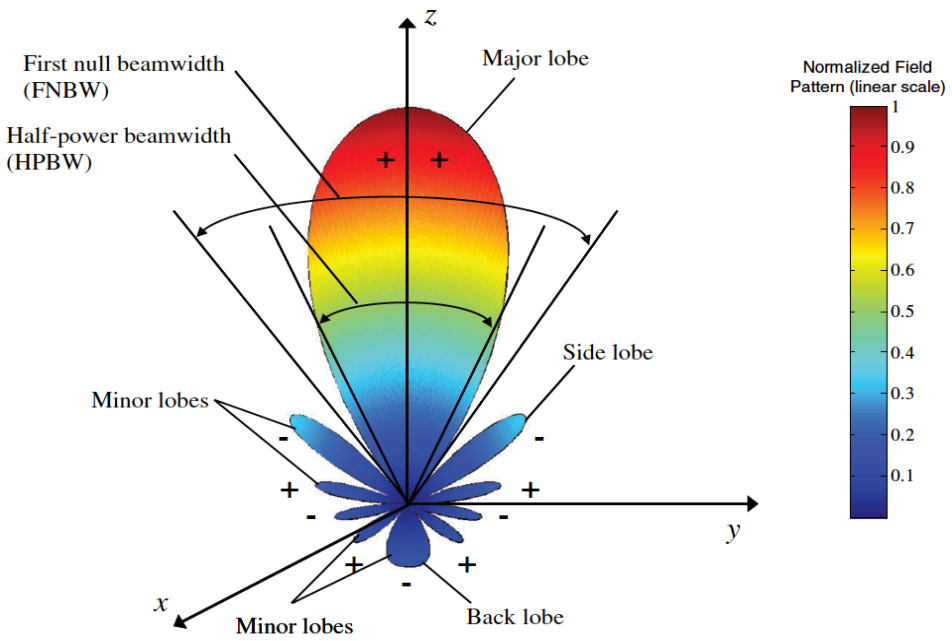

Figure 2.11. Type of lobes (adapted from [Bala16]).

The Half-Power Beam-Width (α_{3dB}) refers to the angle between the two directions in which the radiation intensity is half of the maximum radiation intensity, i.e., 3 dB difference. The angular separation between the first nulls enclosing the major beam corresponds to the First Null Beam-Width (FNBW). The radiation patterns are classified through three groups: the isotropic radiation pattern described by a uniform radiation configuration in all directions, the omnidirectional radiation pattern defined by a uniform signal in all directions for a given plane, and the directional radiation pattern that has a clear main lobe.

The analysis of antenna's radiation performance may be completed through several parameters, to have an insight of how much transmitting power losses exists. The Side Lobe Level (SLL) is one of these parameters, providing the difference between the maximum value of the main beam and the side lobe peak value. The Front-to-Back Ratio describes the magnitude of backward radiation; it may be estimated through the ratio between the value of back and forward radiations associated to the primary lobe.

Regarding the radiation fields' intensity, the directivity is set as the ratio between the specific radiation intensity direction under study and the radiation intensity averaged over all directions. This specific parameter attached to the antennas gain provides an indicator of the antenna's radiation efficiency.

On the receiving signal perspective, antennas are defined by the maximum equivalent area or antenna effective aperture, where the maximum directivity direction is assumed, without dielectric and ohmic losses that could be provided by the polarisation conditions, providing the relation between the power delivered to the antenna and the power density of the incident wave.

The antennas are only one of several elements that make communications possible. From the viewpoint of a system, one also needs to understand the impedance characteristics. The antenna terminals may be seen as a complex impedance, where the resistive part characterises the ohmic and radiation losses, and the reactive part shows the energy stored in the reactive near-field. During the process of a particular transmission, the EM wave has some attenuation or reflection. To avoid reflections the radiation

resistance needs to be equal to the generator resistance that is connected to the antenna. To measure that reflected power, one uses the Voltage Standing Wave Ratio (VSWR).

Regarding the fundamental characteristics of antennas, one should also mention the polarisation of the radiated fields created by an antenna, since, according to the reciprocity theorem, if both terminals are not set with the same polarisation the signal will not be received. Thanks to this parameter the antenna's transmission or reception waves may be described in the spatial orientation of electric field through the time evolution. There are two particular states of polarisation: circular (right or left) or linear (vertical or horizontal). The increase of the spectral efficiency is undoubtedly one of the benefits due to the possibility of using simultaneous two independent communication channels to occupy the same spectral space (e.g. Right Circular Polarisation (RCP) and Left Circular Polarisation (LCP)). To analyse the level of matching polarisation between terminals, there is the polarisation matching loss (PL) parameter, which is the ratio between the received power and the maximum value possible when there is a perfect polarisation match.

2.6 State of the art on railway communication antennas

An overview of relevant research is provided in this subchapter regarding the subject of the thesis, where one presents the work developed in the area of analysis of antennas' signalling for railway communications. Despite the numerous aspects mentioned previously in this chapter, the thesis's main focus is the signal parameters of antennas and its behaviour to understand the optimal location for antennas on trains.

[Will09] presents a thorough analysis of the antennas' installation on the rooftop of trains due to the physical size constraints of trains' rooftops. The study is provided by Siemens Mobility aiming to the Railway Safety and Standards Board (RSSB) with the purpose of finding the best location for antennas on trains. It is considered a priority ranking of Operation Safety, Operational important, Operation useful and Passenger use, the first one being the highest priority. Besides that, it also considers the antennas as a group of several communication systems divided into three groups (Group A: GSM-R voice, Group B: GSM-R CSD (Circuit Switch Data) or GPRS, and group C: GSM-Public and UMTS 900). Besides that, it also considers the effects of radio propagation due to the several types of possible obstructions on the rooftops (e.g. air conditioning units, sunken roofs, longitudinal strengthening bars, curved roofs and pantographs) The results show the necessary spacing between antennas and isolation between transceivers to avoid problems among several systems (e.g. GSM-R, GPS, Wi-Fi 2.45 GHz/ 5 GHz, GSM-P 1800, etc.)

There are several ways to analyse the receiving and radiating characteristics of antennas, and in [PuWa09] the authors introduced an integrative modelling technique involving a finite-difference-time-domain method and a perfectly matched layer technique, which are used to study wave propagation of mobile communications. The study is done in 900 MHz with a train antenna system of 9 monopoles, the

surrounding environment being an artificial box surface. To take the electromagnetic parameters of materials into account specific values of relative permeability are set, together with relative permittivity and conductivity for the locomotive, the windows, conducting wire, the steel rails and the earth plane. A detailed examination of azimuth, receiving and radiating patterns is presented, where it is possible to see the relation between angles and amplitude. The results show a different zenithal and azimuthal pattern in space due to an “inconsistent surrounding environment”.

In [LXFZ16], the authors approach two different strategies to deploy antennas on top of trains, and a careful analysis is made to understand in which way these methods impact on channel capacity and performance over the time domain. They studied the DL, since it requires much more service amount in a two-hop link. The scenario is constituted by a train in a straight railway line with omnidirectional antennas, constant speed and parallel BSs. On the one hand, an equidistant strategy is deployed, where a set of antennas is placed evenly and longer than half wavelength. On the other hand, a fixed-interval strategy is implemented, where “the antennas are divided into two sets with equal amount and the antennas in the first set is placed one by one from the head to the tail of the train while the antennas in the second set is placed one by one from the tail to the head of the train”. The analyse is made for a frequency of 2 GHz with a bandwidth of 15 kHz, a moving speed of 360 km/h and a train length of 200 m. According to the authors, the fixed-interval strategy performs better when the number of antenna is much larger (“massive antenna case” with 600 antennas).

The study of antennas locations may be seen as a general problem for any vehicle. In [Pals13], the author investigated the influence of conducting environments on the performance of an antenna. The work is based on a 3D car model with the help of CST. Firstly, a finite flat square plane was considered to understand the influence of corners and edges on the antenna radiation pattern, which is minimal over a specific size for a working frequency of 2 GHz. Secondly, a similar analysis was made for a flat structure with circular edges. It was concluded that the radiation pattern is more intense due to caustics effects. Then a more realistic approach was studied with a curved structure similar to a car’s rooftop, where the influence of the distance between the plane and the antenna was examined. Lastly, in order to have accurate results, a full car structure was included in the simulations, and it is possible the see in Figure 2.12 the 3D radiation pattern for a vertical dipole antenna on the car rooftop.

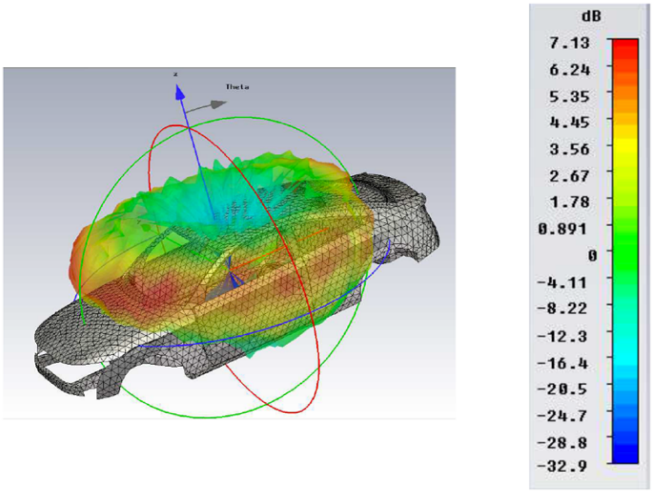

Figure 2.12 The 3D radiation pattern for a CST simulation (extracted from [Pals13]).

In [PRRB11], the authors analyse distributed microstrip patch antennas mounted on a vehicle. The antennas performance is evaluated between 0.8 to 1 GHz and 1.7 to 2.5 GHz with six and eight aperture field sources instead of real antennas to reduce the complexity and computational time. Through the variation of several aspects of antennas, as their locations, quantity and orientation, for both frequency bands, it is concluded where is the optimised location for mounting antennas in that specific vehicle.

Another thorough study regarding different deployments of antennas is done in [Mana16]. The purpose is to create a reliable vehicular communication system for trucks with specific conditions of mining environments. It evaluates antennas performance, firstly, using CST, Figure 2.13, and, secondly, through measurements. The report is evaluated for a microstrip patch antenna working for two distinctive frequencies (5.9 GHz and 2.4 GHz) and for a λ/4 dipole in 5.9 GHz. Two configurations for the optimal deployment of antennas are determined: using an omnidirectional antenna with similar properties of the tested dipole at a central position under the chassis, but there is some probability to damage the antenna due to the ground morphology; alternatively, two patch antennas could be considered for each lower flank of the truck.

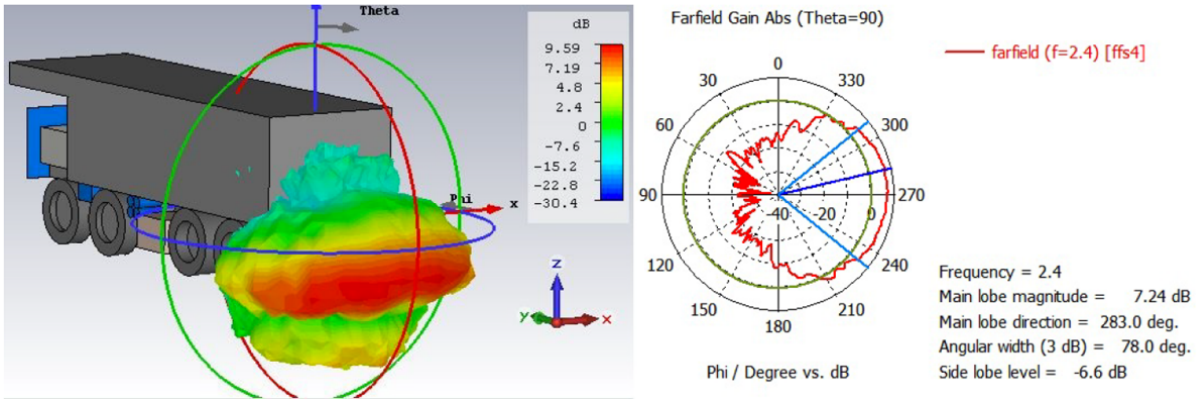

Figure 2.13 Antenna performance in a truck using CST (extracted from [Mana16]).

Chapter 3

Models and Simulator

This chapter contains the problem methodology and the most relevant aspects that will have a direct effect on simulations. One also explains, in detail, the software together with the implementation of the antenna's models and scenarios.

3.1 Model overview

This section shows a high-level perspective of the approach taken for the analysis of antennas' performance and the corresponding model. In Figure 3.1, one displays the model overview, where the path to reach results is shown to have better performance from antennas through the improvement of the antennas' locations on trains.

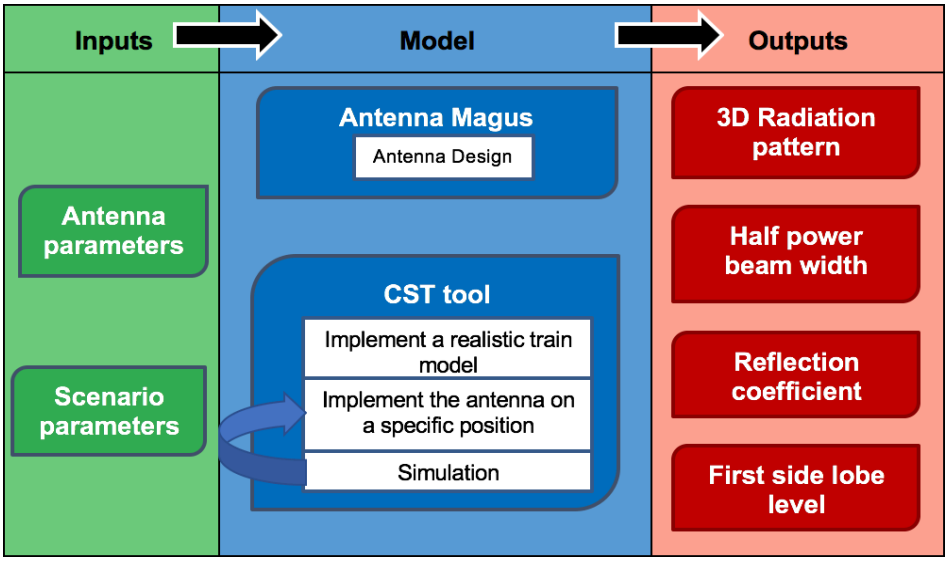

Figure 3.1 Model configuration.

First of all, the model considers several input factors regarding the antennas' technical aspects, as well as the surrounding environment that may affect the expected behaviour of the radiation pattern. For this thesis, the major antennas' input parameters are the working bandwidth, which depends on the system (GSM-R, LTE-R, BBRS, etc.), keeping in mind that there are dual-band antennas, the gain and the polarisation type. Besides these electrical properties, also has to consider the mechanical properties, more precisely, the dimensions. Regarding the scenario parameters, one needs to have a well-defined surrounding environment where the antennas will be mounted. According to [Pals13], it is considered as a good approximation to analyse the surrounding environment up to 20λ of distance from the antenna, which means that for GSM-R with a minimum working frequency of 876 MHz ($\lambda \cong 0.34\ m$), the maximum distance between the antenna and the surrounding critical scenario that will directly influence the antennas' performance corresponds approximately to 6.8 m.

After having all the input parameters well-defined, the proposed model consists of exploiting the CST features to understand which are the more significant interferences regarding specific antennas' locations. For that, one has created a representative 3D model of the trains' rooftop and its side borders, with particular attention to structures with extra height, having the regular train height as the reference. Finally, CST provides the necessary outputs to do a rigorous study through the 3D or 2D views of radiation patterns, the α_{3dB}, the S_{11} reflection coefficients, as well as the SLL properties.

3.2 Analytical models

This section explains in detail all the technical aspects that may influence antennas' performance, mentioning the image theory, and the vertical and the horizontal dipole cases under specific circumstances.

3.2.1 Image theory

Antennas are often operating in the presence of other structures or obstacles, which have a direct effect on their radiation characteristics. One of the most common circumstances is the presence of a ground plane near to the radiating element, which is exactly what happens for antennas on the rooftop of trains. Transmitted or received energy of a radiating element directed toward the ground experiences a reflection that has different behaviours depending on the particular geometry of the problem, on the grounds' characteristics and radiopropagation parameters, as frequency or antennas' specifications. To simplify the analysis of this particular case, it is considered that the flat ground is an ideal situation being infinite and a Perfect Electric Conductor (PEC). A material can be considered a PEC when it has an electric conductivity around 10^7 and 10^8 S/m.

Image theory is the best method to have a proper understanding of how the reflected electric field behaves near a PEC, taking into account that the field underneath the boundary is null. This behaviour is important to consider, since the received electric field will be different depending on the way that antennas are installed. In Figure 3.2, it is possible to see the electric behaviour of the reflected sources. For the vertical source, the reflection has the same direction, but for the horizontal one, the reflected source has a 180º phase shift; this suggests that for the receiving element the electric field is going to have constructive or destructive effects leading to better or worst performances.

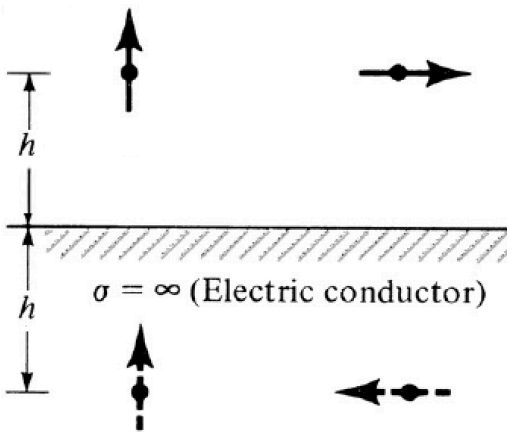

Figure 3.2 Electric sources behaviour near to a PEC ground (adapted from [Bala16]).

The analysis of the radiated fields is often limited to the far-field region due to mathematical difficulties, and the three well-defined region restrictions are given, as [Bala16]:

- Reactive near-field:

$$0.62\sqrt{\frac{l^3{}_{[\mathrm{m}]}}{\lambda_{[\mathrm{m}]}}} > r_{[\mathrm{m}]} > 0 \tag{3.1}$$

- Radiating near-field:

$$\frac{2l^2{}_{[\mathrm{m}]}}{\lambda_{[\mathrm{m}]}} > r_{[\mathrm{m}]} \geq 0.62\sqrt{\frac{l^3{}_{[\mathrm{m}]}}{\lambda_{[\mathrm{m}]}}} \tag{3.2}$$

- Far-field region:

$$r_{[m]} > \frac{2l^2{}_{[m]}}{\lambda_{[m]}} \tag{3.3}$$

where:

- l: Largest geometrical dimension of the antenna;
- λ: Wavelength;
- r : Distance between the antenna and the observation point.

3.2.2 Vertical electric dipole

According to [Bala16], with $\varphi = \frac{\pi}{2}$, the total field for a vertical dipole is given by:

$$E_{\theta\,[\mathrm{V/m}]}^{V} \cong j\eta_{[\Omega]}\frac{k_{[\mathrm{m}^{-1}]}I_{0\,[\mathrm{A}]}e^{-jk_{[\mathrm{m}^{-1}]}r_{[\mathrm{m}]}}}{4\pi\, r_{[\mathrm{m}]}}\sin\theta\left[2\,\cos\left(k_{[\mathrm{m}^{-1}]}h_{[\mathrm{m}]}\cos\theta\right)\right], \qquad z \geq 0 \tag{3.4}$$

where:

- η: intrinsic impedance (120π [Ω] for free-space);
- $k = \frac{2\pi}{\lambda_{[\mathrm{m}]}}$: the free space wave number;
- I_0: maximum current;
- θ: Angle between the positive half of Z-axis and the observation point;
- h: antenna height.

The total electric field of an antenna may be seen as the product of the element factor by the array factor which is often called as the pattern multiplication, being used for antenna arrays. The former is the pattern produced by a single element at the origin, and it will depend on the current direction. The array factor may be observed in (3.4) as the part within the brackets and provides a relation between the radiation pattern and the antenna height, which also has a direct effect on the electric field form and amplitude. Figure 3.3 shows that when the antenna starts to move away from the ground, the number of lobes (N_L^V) increases:

$$N_L^V \cong \frac{2h_{[\mathrm{m}]}}{\lambda_{[\mathrm{m}]}} + 1 \tag{3.5}$$

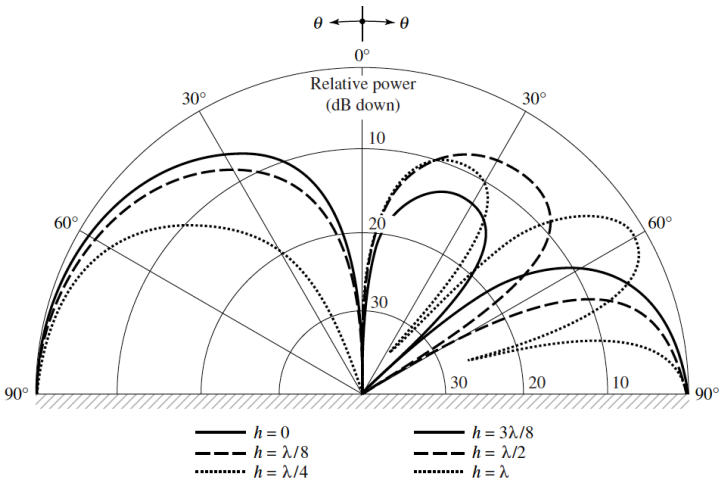

Figure 3.3 Performance of a vertical dipole for different heights (extracted from [Bala16]).

3.2.3 Horizontal electric dipole

The same approach is used for horizontal dipoles, with a geometric boundary of $z \geq h\,;\ 0 \leq \theta \leq \frac{\pi}{2}; 0 \leq \varphi \leq 2\pi$. The radiation pattern behaviour of a horizontal dipole for different antenna heights is presented in Figure 3.4, the total electric field being:

$$E_{\varphi\,[\mathrm{V/m}]}^{H} = j\eta_{[\Omega]}\frac{k_{[\mathrm{m}^{-1}]}I_{0[\mathrm{A}]}e^{-jk_{[\mathrm{m}^{-1}]}r_{[\mathrm{m}]}}}{4\pi\, r_{[\mathrm{m}]}}\sqrt{1-\sin^2\theta\,\sin^2\varphi}\left[2j\,\sin\left(k_{[\mathrm{m}^{-1}]}h_{[\mathrm{m}]}\cos\theta\right)\right], \quad (3.6)$$

$$z \geq h;\ 0 \leq \theta \leq \frac{\pi}{2}\,; 0 \leq \varphi \leq 2\pi.$$

where:

- φ: Angle between the positive half of X-axis and the observation point projected on XOY plane.

For this particular case the number of lobes is estimated by:

$$N_L^H \cong \frac{2h_{[\mathrm{m}]}}{\lambda_{[\mathrm{m}]}} \quad (3.7)$$

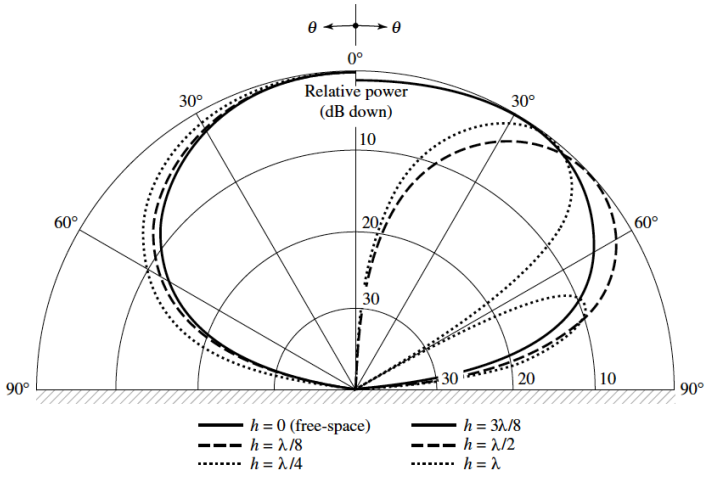

Figure 3.4 Performance of a horizontal dipole for different heights (extracted from [Bala16]).

3.3 The CST simulation tool

Nowadays, there are vast options to approach electromagnetic problems based on the development and application of computational methods. It is possible to divide the computational electromagnetic methods into two big groups: the numeric methods and analytical methods for high frequencies. For this thesis, the best option is the former, which allows an exhaustive analyses of electromagnetic fields behaviour. The Method of Moments (MoM) is based on the resolution of integrals in the frequency domain, but it has some efficiency problems compared with volume discretisation methods, which is the particular case of the Finite Integration Technique (FIT). FIT is a technique that is established through a full-wave model, which is the best approach to analyse antennas' parameters, like the radiation pattern, gain, S-parameters, etc. This technique is applied in CST Microwave Studio [CST18], being a time-domain process similar to the Finite Difference Time Domain (FDTD). It is a reliable discretisation arrangement of Maxwell equations from their integral form to a discrete reformulation, providing the proper settings to simulate real electromagnetic problems.

CST 2017 [CST18] owns a very cooperative system, named Project Wizard, to help users adopting the best project settings available to achieve accurate performances when a specific simulation is requested. The first step is to create a project template, where one can choose one of five different application areas: Statistics and low frequencies, MW & RF & Optical, EDA / Electronics, EMC/EMI or Charged particles Dynamics. The MW & RF & Optical is the best option for the purpose of antennas' analysis. For this specific application area, it also has to be selected a specific workflow where there are six possibilities: antennas, circuits & components, radar cross section, biomedical/exposure/Specific Absorption Rate (SAR), optical applications and periodic structures. When the option of antennas is selected an additional and more specific workflow appears with all antennas types: waveguide, planar, wire phased array / Unit cell, mobile phone / integrated, reflector, dielectric resonator and RFID. After selecting the proper conditions for the problem under analysis, it is time to select the best solver available. All of this stages can be seen in Figure 3.5.

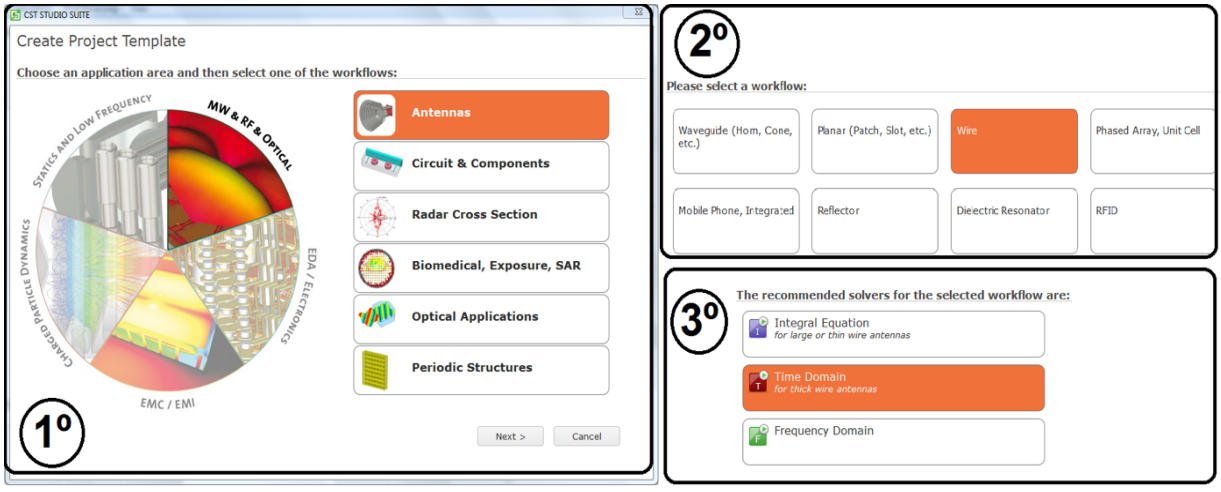

Figure 3.5 CST Project Wizard template (adapted from [CSTH17]).

Although it is given the manual choice of selecting six different solvers (Time domain solver(), frequency domain solver(), eigenmode solver(), integral equation solver (), asymptotic solver ( ) and multilayer solver()), according to the steps mentioned before, and through Figure 3.5, it is possible to identify only three different solvers to approach the problem ([CSTH17] and [CST18]), which are explained to understand the most suitable solver:

- Time domain solver: There are two types of time domain solvers equally based on hexahedral meshes: Transient and Transmission-Line Matrix (TLM). The former simulates, in a flexible way, problems to study the electromagnetic field behaviour, being capable of showing the broadband frequency domain effects through S-parameters, which are essential for understanding the performance of any antenna problem. It also simulates the radiation pattern at a decent spectrum resolution, making possible to analyse resonances inside the simulated spectrum. One of the most significant advantages is that this solver performs the electromagnetic results in a single calculation run for several wanted frequencies. The latter benefit is the fact that it is appropriate to understand the performance deviation due to the presence of small objects like slots, vents and shielded cables, which is very helpful for things such as design broadband antennas.
- Frequency domain solver: It is a full resolution tool similar to the transient solver. The main features of this solver are to display the near and far fields electromagnetic performance and the S-parameters. The frequency domain solver is the best solution for periodic structures like PBGs (Photonic-bandgap), FFSs (frequency-selective surfaces) or phased arrays, since each frequency sample requires a new simulation run, in other words, the required simulation time is linear to the needed frequency step. For this reason, the solver should only be executed for a small range of frequencies and, in this case, results have better accuracy and smaller simulation time.
- Integral Equation solver: The primary focus of this solver goes to electrically large structures which are mainly constituted by metals, such as aeroplanes, cars or trains. It provides data about the S-parameters as well as the far field pattern. The solver is based on the MoM discretisation with an integral formulation of the object. Based on the Multilevel Fast Multipole Method (MLFMM), this solver is able to decrease the calculation area through the object margins avoiding the extra computation of structures' volume.

According to the different characteristics of each solver, the most suitable option happens to be the transient solver, which is based on the FIT. CST produces an appropriate hexahedral mesh constituted by small variable size cuboids (Δx, Δy and $\Delta \mathrm{z}$), named grid cells, to discretise the problem with a specific electric and magnetic field behaviour for each cell, hence two orthogonal meshes being required. They are based on Yee cells, which have the electric field, **E**, and the magnetic field, **H**, spatial organised where there each element of **E** is surrounded by four elements of **H** and each element of **E** also is surrounded by four elements of **H**. As seen in Figure 3.6, the elements of **E** are always positioned on the central points of Yee cells edges of the facet, and the elements of **H** are always located on the central points of each Yee cell facet. One of the concerns of computational methods is the border conditions, which can be solved through several approximations; CST applies the Perfect Boundary

Approximation (PBA) technique, which takes sub-cellular data into account, being an algorithm of second-order accuracy for arbitrary shaped limits [KSTW98].

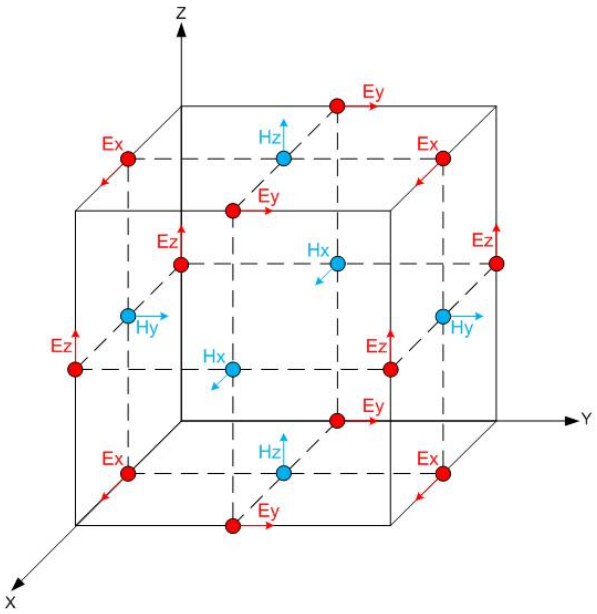

Figure 3.6 Yee cell with the electric and magnetic components (extracted from [CSTH17]).

Another fundamental decision is the definition of the best mesh type for the problem, which has a direct influence on accuracy and simulation time. There are two ways to define a hexahedral mesh without considering the option of creating a manual meshing, which is time-consuming, since it requires a complete understanding of each variable of CST, and it is not recommended due to the complexity level of the software. One possible option is the “Automatic Mesh Generation with an Expert System”, which is an automatic mesh generator capable of creating a proper mesh through the identification of the relevant features of each structure. The uses method is straightforward: firstly the structure is analysed, then a redefinition of critical regions is done, and it set to simulate. The other option would be the “Adaptive Mesh Refinement” that discovers the mesh by a loop, where an initial mesh is created, then with a local error estimation the mesh is refined. If the results start to diverge below a certain accuracy level, the process stops. To optimise the mesh generation, some settings may be arranged. The main properties to take into account are:

- Lines per wavelength (M_{LW}): It is directly linked to the wavelength of the upper frequency set for simulation and expresses the minimum number of mesh lines in each coordinate vector. To have an indication, a suitable value for an acceptable compromise between computation time and accuracy is about 10.
- Lower mesh limit (M_{LL}): It defines the maximum mesh step (M_{MS}) to be applied for the mesh formation. The relation between the M_{LL} and the M_{MS} is given by:

$$M_{MS} = \frac{D_{SBF} \cdot \sqrt{3}}{M_{LL}} \tag{3.8}$$

where:

- D_{SBF}: Smallest box face diagonal.

- Mesh line ratio limit (M_{RL}): This provides a relation between the maximum (Δ_{max}) and the minimum (Δ_{min}) allowed values of meshes steps, as shown in Figure 3.7.

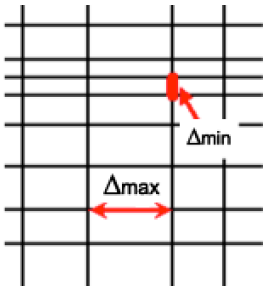

Figure 3.7 Different mesh step widths (adapted from [CSTH17]).

Another approach that directly affects the simulation time, and therefore the simulation accuracy, goes by changing the cells per wavelength in the mesh properties. As the term indicates, it defines the maximum number of cells for the smallest wavelength, which is established by the highest frequency of the working band. Space discretisation must be taken into account when these properties are modified, hence to minimise this effect, a minimum of 10 cells per wavelength is recommended, at least near to the model bounding box ("near to model" setting).

To have a realistic approach of the simulated models, it is also important to understand how CST takes in consideration the boundaries conditions, since, in the computational perspective, all simulations require a finite expansion. A rectangular grid system is used, which may be defined through the minimum and maximum positions (X_{min}, X_{max}, Y_{min}, Y_{max}, Z_{min}, Z_{max}) in each coordinate direction to identify the six boundary surfaces. For the high-frequency properties, there are seven available conditions, and they are displayed in the models with a specific bounding colour representing the type of condition selected, represented by the icons of Figure 3.8:

- Electric: It has the performance of a PEC, in others words it fixes to zero each tangential electric fields and normal magnetic fluxes.
- Magnetic: It behaves like a perfect magnetic conductor (PMC), setting all tangential magnetic fields and normal electric fluxes to zero.
- Open (PLM): It works as free space allowing waves to pass the boundary with minimal reflections. The structures that touch this boundary have their geometry virtual extended to infinite through the use of a perfectly matched layer (PLM) boundary.
- Open (add space): Similar to the previous one, however, it is added extra space for farfield calculations. This option is recommended for antenna analysis, since it will automatically adapt to the centre frequency of the working bandwidth.
- Periodic: It links two opposite boundaries so that the calculation domain is simulated as a periodical wave expansion in that direction, hence changing one boundary to this type will automatically change the opposite one.
- Conducting Wall: This boundary acts as a lossy conducting wall.
- Unit Cell: It is identical to the periodic boundary, where a two-dimensional periodicity other than the direction of the coordinates axes may be set.

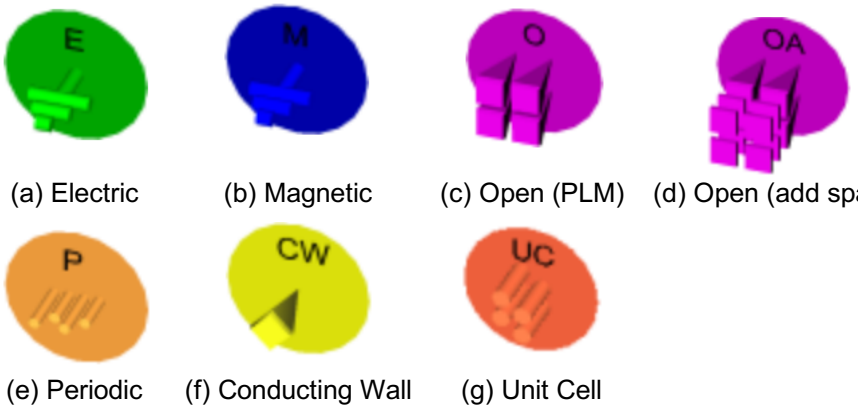

(a) Electric (b) Magnetic (c) Open (PLM) (d) Open (add space)

(e) Periodic (f) Conducting Wall (g) Unit Cell

Figure 3.8 Icons representing the types of boundaries conditions (extracted from [CSTH17]).

Regarding some important farfield properties of CST, a clear understanding of a few options to analyse the antennas' performance is required: Directivity, Gain (IEEE) and the Realised Gain. Firstly, it is required to understand that the radiated power of an antenna is directly related to its far-field region of through:

$$U(\theta,\varphi)_{[\mathrm{W}]} = \frac{r^2_{[\mathrm{m}]}}{2\eta_{[\Omega]}}\left|\boldsymbol{E}(r,\theta,\varphi)_{[\mathrm{V/m}]}\right|^2 \cong \frac{1}{2\eta_{[\Omega]}}\left[\left|E^V_\theta(\theta,\varphi)_{[\mathrm{V/m}]}\right|^2 + \left|E^H_\varphi(\theta,\varphi)_{[\mathrm{V/m}]}\right|^2\right] \tag{3.9}$$

The directivity is easily interpreted as "the ratio between the radiation intensity in a given direction from the antenna to the radiation intensity averaged over all directions" [CSTH17]:

$$D(\theta,\varphi)_{[\mathrm{dBi}]} = 10log_{10}\left(4\pi\cdot\frac{U(\theta,\varphi)_{[\mathrm{W}]}}{P_{rad\,[\mathrm{W}]}}\right) \tag{3.10}$$

where:

- P_{rad}: Total radiated power.

The Gain (IEEE) is also a ratio, but this time between a specific radiated power direction and the input or accepted power of the antenna. For an antenna perfectly adapted without any kind of conduction or dielectric losses, the Gain (IEEE) should have exactly the same value of its directivity, being:

$$G(\theta,\varphi)_{[\mathrm{dBi}]} = 10log_{10}\left(4\pi\cdot\frac{U(\theta,\varphi)_{[\mathrm{W}]}}{P_{in\,[\mathrm{W}]}}\right) \tag{3.11}$$

where:

- P_{in}: Input or accepted power.

Another possibility is to evaluate the realised gain, which includes impedance mismatches (reflection losses) within the information of the "S-Parameters Balance" graph. Through (3.11), the expression of the realised gain may be expressed as:

$$G_{realized\,[\mathrm{dBi}]} = G(\theta,\varphi)_{[\mathrm{dBi}]}\cdot(1-B^2)\,, \qquad 0\le B\le 1 \tag{3.12}$$

where:

- B: S-parameter balance given by the square root of the summed power leaving the structure through all ports. The balance should be one for structures that do not have any losses and closed (without open or lossy boundary conditions).

For this work, the scenario nearby the antenna on the rooftop does not change over time, as is the case of an antenna in a standard mobile phone. For this reason, it is not necessary to take impedance and polarisation losses into account. If an antenna is well matched when mounted on the trains' rooftop, the impedance losses will remain the same, hence the Gain (IEEE) is the parameter chosen to study the antennas' performance.

To have a clear knowledge of which are the most significant directions that have a stronger signal regarding the antenna's radiation pattern, the α_{3dB} is a fundamental parameter to study. As [IEEE13] describes, "in a radiation-pattern cut containing the direction of the maximum of a lobe, the angle between the two directions in which the radiation intensity is one-half the maximum value". Considering θ=0º the maximum lobe direction, α_{3dB} is given by:

$$E\left(\theta = \frac{\alpha_{3dB}}{2}\right)_{[\mathrm{V/m}]} = \frac{E_{máx[\mathrm{V/m}]}}{\sqrt{2}} \tag{3.13}$$

where:

- $E_{máx}$:Maximum electric field of the main lobe.

To measure how well the power is concentrated into the main lobe, usually the L_{SLL} is used:

$$L_{SLL\,[\mathrm{dB}]} = 20\log_{10}\left(\frac{E_{SL[\mathrm{V/m}]}}{E_{máx[\mathrm{V/m}]}}\right) \tag{3.14}$$

- E_{SL}:Maximum value of the second major lobe.

Before performing an analysis of any type of antenna's parameter, it is mandatory to recognise if the antennas are well-matched. To do so, it is needed to understand the S_{11} reflection coefficient of the specific antenna under evaluation. In general terms, for a network with n-ports, there are incoming (a_i) and outgoing waves (b_i) associated to each port given by:

$$a_{i_{[\mathrm{V}]}} = \frac{1}{2}\left(\frac{V_{i_{[\mathrm{V}]}}}{\sqrt{Z_{i_{[\Omega]}}}} + \sqrt{Z_{i_{[\Omega]}}}I_{i_{[\mathrm{A}]}}\right) \tag{3.15}$$

$$b_{i_{[\mathrm{V}]}} = \frac{1}{2}\left(\frac{V_{i_{[\mathrm{V}]}}}{\sqrt{Z_{i_{[\Omega]}}}} - \sqrt{Z_{i_{[\Omega]}}}I_{i_{[\mathrm{A}]}}\right) \tag{3.16}$$

where:

- V_i: Voltage of port i.
- I_i: Current of port i.
- Z_i: Characteristic impedance of port i.

The relationship between these outgoing and incoming waves of a particular n-port network leads to the following S-matrix:

$$\begin{pmatrix} b_1 \\ b_2 \\ b_3 \\ \vdots \\ b_n \end{pmatrix} = \begin{pmatrix} S_{11} & S_{12} & S_{13} & & S_{1n} \\ S_{21} & S_{22} & S_{23} & \cdots & S_{2n} \\ S_{31} & S_{32} & S_{33} & & S_{3n} \\ & \vdots & & \ddots & \vdots \\ S_{n1} & S_{n2} & S_{n3} & \cdots & S_{nn} \end{pmatrix} \begin{pmatrix} a_1 \\ a_2 \\ a_3 \\ \vdots \\ a_n \end{pmatrix} \quad (3.17)$$

The main diagonal elements (S_{11}, S_{22}, …, S_{nn}) express the reflection coefficient of that particular port and the other elements are transmission factors between two specific ports considered in that network. When the element holds only reciprocal materials, and if the characteristic impedances are real, the S-matrix is symmetric: $S_{ij}=S_{ji}$.

Another way to acknowledge the efficiency of a certain port *i* is through the total accepted power provided by:

$$P_i = |a_i|^2 - |b_i|^2 \quad (3.18)$$

3.4 Surrounding environments for the antennas' deployment

Towards a realistic approach to the simulation environment, it is mandatory to recognise the limitations and potential problems regarding antenna's radiation pattern. Nowadays, there are a vast number of different train models, which makes it not possible to specify the details about each type of carriage and which are the most prominent problems for transmitting or receiving data in the antennas' perspective. Nevertheless, it is possible to summarise them through a more carefully analysis and gather different models with joint problems.

First of all, it should be mentioned the fact that many carriage types may reasonably be approximated as a very smooth roof with a few curvature degrees between sides. For this specify cases, it is expected from the antennas to have an almost ideal performance with an omnidirectional behaviour in the horizontal plane, without any obstruction between terminals.

The slight **rooftop curvature** due to aerodynamics reasons does not bring significant concerns, but when this curvature is too exaggerated, it will have a direct effect on antenna performance, as seen in Figure 3.9 (a). The most significant conclusion to be drawn from this type of roofs is the fact that if an antenna is placed farther from the centre line (higher part of the roof), it will have a worse performance due to roof obstructions. Regarding the antenna installation on the centre line, an interesting performance may be expected than the flat roof setting for the lower angles in the directions where the roof is sloped down.

Currently, the well-being and comfort of passengers is a priority, which explains the existence of **heating, ventilating and air-conditioning (HVAC) units** on trains' rooftop. These units have structures with 0.3 m or more above the roof level, being a frequent type of barrier to antennas, Figure 3.9 (b). The presence of these units has a significant impact on antennas' performance, which is studied later on.

Other types of structures frequently seen on trains are the **longitudinal strengthening bars**, Figure 3.10 (a). For this particular case, two distinctive approaches must be considered. The standard method is to install the antenna on a plane supported for several strengthening bars, and so its functioning will be very similar to what is theoretically expected. On the other hand, if the antenna is positioned between bars, its performance may suffer some changes that will also be related to the working frequency. For obvious reasons, the higher the working frequency is, the higher the influence of these bars will be.

(a) Class 59 with an exaggerated curvature. (adapted from [Wiki18b]).

(b) Train with air-conditioning units. (extract from [Wiki18a]).

Figure 3.9 Two different type of rooftop problems.

(a) Strengthening bars (adapted from [Wiki18c]).

(b) Pantograph structure (extracted from [EngM18]).

Figure 3.10 Others types of rooftop problems.

There are several types of carriages, and the physical obstructions explained above are the most frequent. Still, it does not mean that others may not have a greater impact on the antenna radiation pattern, like the example of **sunken roofs** or the presence of **pantographs**, Figure 3.10 (b), which provides energy to the trains. However, in cases like this, it is common-sense that antennas should not

be placed near or on these structures. It is not necessary to make a complex study to realise that sunken roofs obstruct the LoS between terminals, leading to an extra attenuation of several dBs, which is not reasonable from the antenna's performance optimisation point of view. For the pantograph case, it is also easily understandable that it is not suitable to position an antenna near to this structures, since, in addition to the extra attenuation due to the structure itself, it will disturb the normal functioning of antennas thanks to the electromagnetic interference provided by the energy transfer within the train and the higher wires. According to [DFHR13], sometimes it may occur a "High-Speed Circuit Breaker", when there is a disconnection between the pantograph and the catenary, henceforward, the GSM-R antenna will be affected by a propagation delay; it presents a time-frequency analysis, which shows only one transient event for an antenna placed at 1 m, 2 m and 3 m, but for higher distances, such as 10 m, 15 m or 20 m, it appears more transient events, demonstrating the existence of reflected signals. This type of EM events must be taken into consideration when an antenna on a train is installed, even though, it will not be considered in this study.

3.5 Monopoles' performance

3.5.1 Simulation Approach

To understand the behaviour of the main antennas' parameters under study, one has chosen a λ/4 resonant monopole due to the rooftop trains' morphology, and because a monopole operating above an infinite ground plane is equivalent to a conventional λ/2 resonant dipole. This decision that may be considered as a suitable approach to reality, since monopoles are typically installed inside an aerodynamic structure entitled by blades. In several situations, blades are nothing more than a monopole encapsulated in a shell, to have better aerodynamic characteristics [Macn10]. It is possible to observe a design sketch in Figure 3.11, as well as the corresponding dimensions exported to CST for different communication systems on Table 3.1. One considered a 900 MHz working frequency for GSM-R, 2.6 GHz for LTE-R and 5.9 GHz for BBRS.

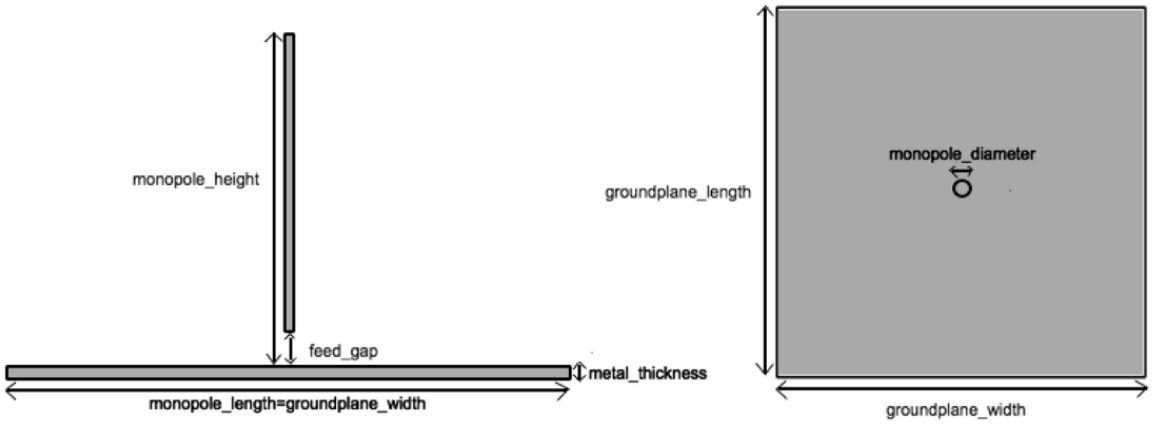

Figure 3.11 Sketch of a λ/4 monopole above a square conducting plane.

With the support of Antenna Magus 2017 [CSTH17], antennas' design is a much lesser problematic task. The interface is very friendly, allowing the user to choose from more than 300 different types of antennas. One has chosen a custom monopole antenna with a circular ground plane, which may be modified for a rectangular ground plane in the "Export Mode". Regarding antennas specifications, it may be set specific parameters, such as the centre working frequency, the minimum and maximum frequencies, the bandwidth percentage associated to them, the directivity or the realised gain and the port impedance characteristics, such as S_{11} parameter and characteristic impedance (Z_0). For the particular case of a $\lambda/4$ resonant monopole, the impedance is merely resistive (36.5 Ω), without any inductance or capacitance contributions, therefore, the reactive impedance is zero.

Table 3.1 Monopole dimensions for the different systems (GSM-R, LTE-R, BBRS).

Parameters	Dimensions [mm]		
	900 MHz	2.6 GHz	5.9 GHz
Wavelength centre	333.(3)	115.38	50.85
Monopole height	79.92	27.48	12.11
Metal thickness (λ/100)	3.33	1.15	0.51
Ground plane width (1.5λ)	499.65	172.96	76.22
Ground plane length (1.5λ)	499.65	172.96	76.22
Feed gap (monopole height/100)	0.80	0.27	0.12
Monopole diameter	0.31	0.23	0.10

First of all, the three antennas were imported to CST and simulated to understand if their performance was the expected one, closest to the theoretical performance. All simulations in this work were based on the Time Domain Solver and the global properties set at "Hexahedral", because compared to the Integral Equation solver, it seems to be the better option for problems with big structures, such as trains; this solver needs to perform an automatic surface mesh generation every time that the structure under analysis changes, and it may take a lot of time. Regarding mesh settings, these simulations were made within the standards options, 20 cells per wavelength near and far from the model, since the models are elementary and the bounding box surrounding the antennas is relatively small. Besides, two local mesh groups were created for the Port 1, easily identified in Figure 3.12 within a red marker, and for the antenna itself. The goal of these local mesh groups is to increase the number of cells, leading to a better simulation accuracy, as seen in the zoomed part of Figure 3.12. Regarding simulation time, the most critical case is the 5.9 GHz, due to the smallest wavelength, creating 251,464 meshcells. The simulation took less than 6 minutes, which is quite acceptable. The boundaries, as recommended, were fixed to "open (add space)" for all the limits, excepted the Z_{min}, which was settled at "conducting wall" to have the theoretical characteristics of a $\lambda/4$ monopole at an infinite ground plane.

All simulations performed in this work were executed using a laptop equipped with an Intel Core i7-2630QM CPU with 2 GHz of clock speed and with 4 GB of RAM. Despite the complexity of specific scenarios, there was no usage of additional features such as acceleration tokens.

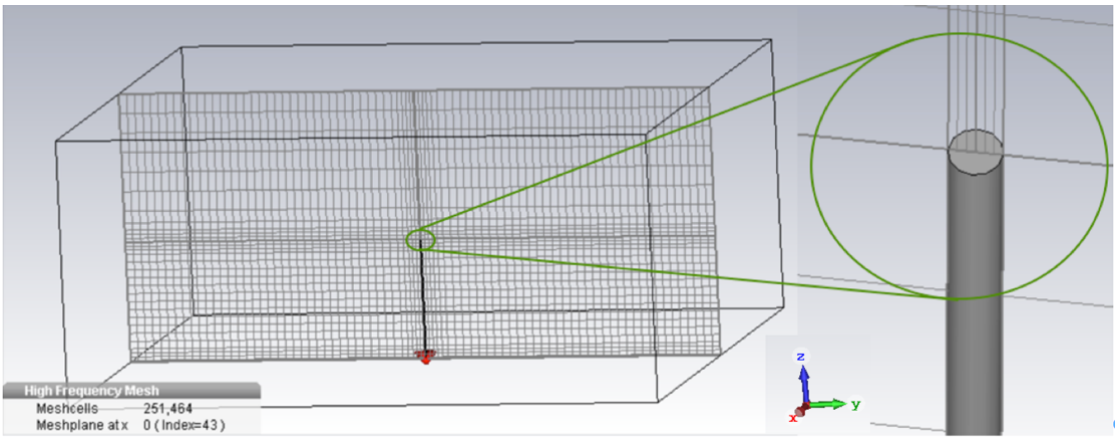

Figure 3.12 Mesh view of a λ/4 monopole working at 5.9 GHz.

The theoretical directivity value of a λ/4 monopole is twice the one of a λ/2 dipole, 5.16 dBi. The radiation pattern of the former can be seen at Figure 3.13 and the remaining are shown in Annex A. In every situation, the directivity is equal to the gain (IEEE), which implies that there are no losses from the accepted power of the structure. At the worst case, the antenna has a slight difference of 0.12 dBi, which can be explained by some technical aspects of antennas' design.

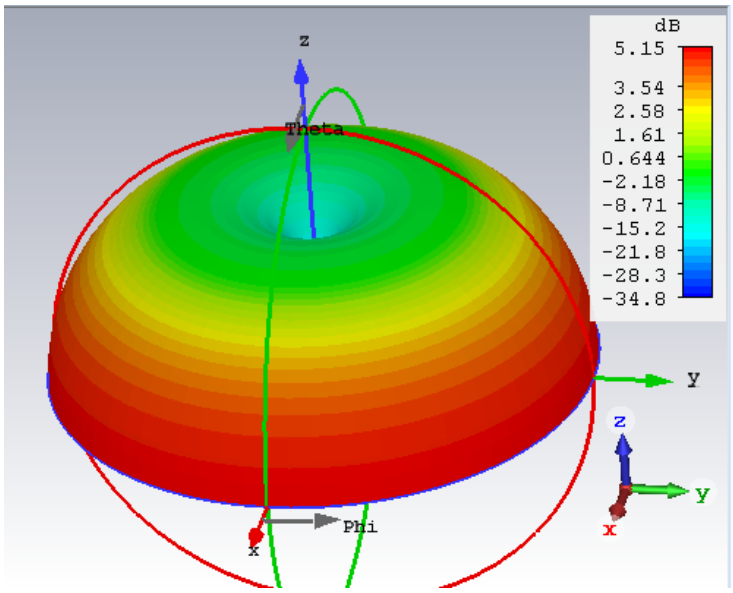

Figure 3.13 3D farfield view of a λ/4 monopole working at 5.9 GHz.

Figure 3.14 displays the reflection coefficient S_{11} of each working frequency to verify that a proper impedance matching is reached. It is considered as fair values the ones that are below -10 dB, meaning that, in the worst case scenario, 10% of the power provided to the antenna is reflected. For the chosen frequencies, it is possible to see that S_{11} is, approximately, - 20 dB, which means only 1% of the power delivered to the antenna is reflected, and for this reason, the antennas are well-matched.

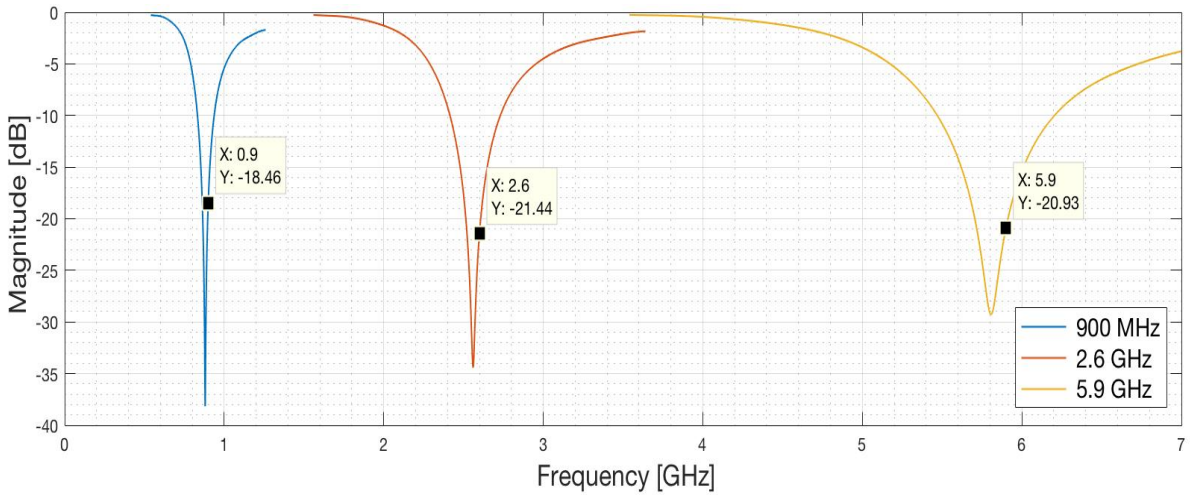

Figure 3.14 S_{11} parameters of the theoretical monopoles at different frequencies.

3.5.2 Modelling Analysis

The second step goes by the pursuit of achieving a good compromise between the results' accuracy (mesh density) and the simulation time required to analyse the maximum distance of the surrounding train environment that has a strong influence on the antenna performance. In other words, it is essential to reduce the problem boundaries to guarantee appropriate simulation results for an acceptable period.

A performance analysis, at 900 MHz, is completed with a gradual flat ground growth concerning its wavelength, to have a direct correlation with all the frequencies that are under study. The square ground is composed of PEC material, and was studied with the length dimensions of 1.5λ, 5λ, 15λ, 25λ and 40λ. Simulations were executed with 15 cells per wavelength near and 8 cells per wavelength far from the model and with additional local mesh groups. Regarding the boundaries properties, similar to the previous case, all borders were fixed at “open (add space)”, excepted the Z_{min}, which was set as an open border, with the purpose of minimising the number of meshcells. This issue needs to be extremely well-defined, since it may have a big influence on all the results that are made after these considerations.

At first, one has studied a lateral perspective with φ = 0º. It must be recognised that this problem has geometrical similarities, therefore, studying this angle is the exact same as studying φ at 90º, 180º or 270º. The simulated results are presented in Table 3.2, where one can compared important parameters of the monopole with the theoretical performance, named as “Reference”. By comparing the values, it is verified that with the increase of the ground area, the gain also increases, as well as the main lobe direction, θ, which tends to approach the reference value. α_{3dB} starts with a very high value, almost suggesting an omnidirectional behaviour if it was not the existence of side lobes. However, when the ground area increases, α_{3dB} begins to decrease creating a primary lobe with more directional properties. The performance of each case may be inspected in Annex B, where one shows the 2D and 3D farfield outputs, as well as the surface current on the ground. This annex provides a better understanding of the antenna’s performance, facilitating the perception of how the parameters presented in Table 3.2 change.

Table 3.2 Performance parameters of a λ/4 Monopole for φ =0º at 900 MHz.

Ground	Gain [dBi]	Direction (θ [º])	α_{3dB} [º]	L_{SLL} [dB]
Reference	**5.28**	**90**	**38.8**	**-----**
$1.5\lambda \times 1.5\lambda$	2.19	54	74.8	-8.0
$5\lambda \times 5\lambda$	5.85	64	27.5	-5.2
$15\lambda \times 15\lambda$	6.70	73	17.6	-3.5
$25\lambda \times 25\lambda$	7.37	75	14.3	-4.1
$40\lambda \times 40\lambda$	7.92	76	11.6	-4.0

In order to perform a thorough analysis and understand the variations of each case relatively to the reference one, in Figure 3.15 it is possible to recognise that, in the first two situations ("1.5 λ x 1.5 λ" and "5λ x 5 λ") there is a perceptible deviation of the farfield behaviour regarding the data from gain and θ direction. For the remaining cases, the differences are no longer perceptible to a visual evaluation, therefore, another approach is required to perceive the differences.

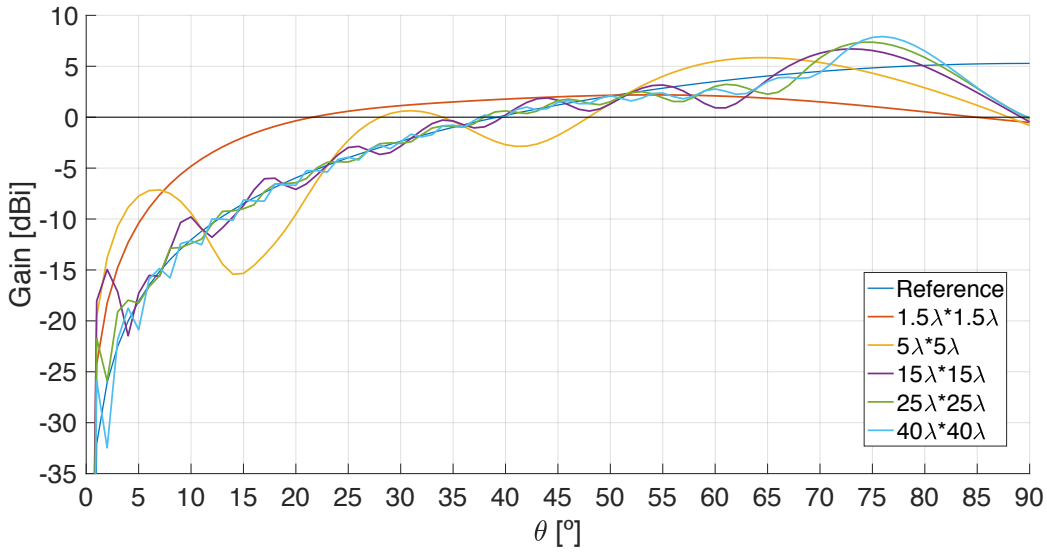

Figure 3.15 Farfield gain for different values of θ with φ =0º at 900 MHz.

In Figure 3.16, one presents the absolute errors concerning the theoretical performance. The calculation of these values only considered the range between 10º and 90º, since having lower values of θ, means that on-board and on-track terminals are close, and for these cases the connection between them is strong enough, hence the monopole gain does not have a critical impact on the proper functioning of the system.

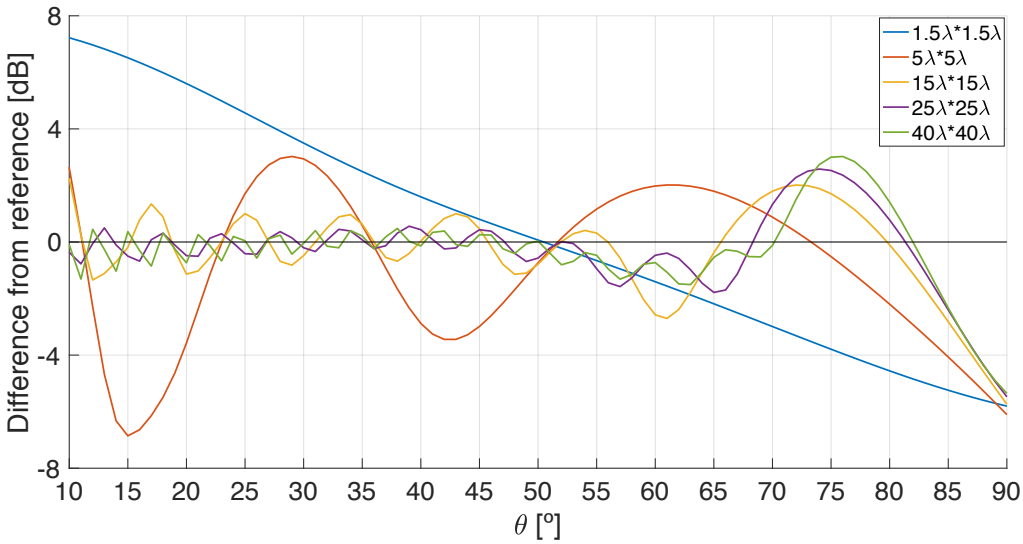

Figure 3.16 Absolute error for different ground sizes with φ =0º at 900 MHz.

The next step is to implement the same analysis but with φ pointing to one of the ground vertexes, φ = 45º, hence, the number of meshcells and the simulation time are exactly the same as in the previous study. The problem geometry suggests that the antenna performance will be identical for every direction of φ contemplating the other vertexes (135º, 225º and 315º). In Annex B, this assumption is confirmed. The corresponding λ/4 monopole performance is shown in Table 3.3, for φ = 45º. Despite small variations in comparison with Table 3.2, the trends are equal. With the increase of the ground's region: the gain growths, as well as the main lobe direction and the shrinking of α_{3dB} providing a more directional main lobe.

Table 3.3 Performance parameters of a λ/4 monopole for φ =45º at 900 MHz.

Ground	Gain [dBi]	Direction (θ [º])	α_{3dB} [º]	L_{SLL} [dB]
Reference	**5.28**	**90**	**38.8**	**-----**
$1.5\lambda \times 1.5\lambda$	4.29	45	58.1	-7.5
$5\lambda \times 5\lambda$	5.45	65	25.5	-5.5
$15\lambda \times 15\lambda$	7.29	73	14.5	-3.9
$25\lambda \times 25\lambda$	7.66	75	11.8	-4.2
$40\lambda \times 40\lambda$	7.86	76	11.2	-5.1

Figure 3.17 shows the farfield viewpoint of the reference antenna and the differences with the ground expansion. Undoubtedly, for 1.5λ x 1.5λ and 5λ x 5λ, the performance remains very different from the reference and these boundaries limits cannot be considered as suitable conditions to implement in future

simulations. Figure 3.18 represents the related differences regarding the farfield performance, also between 10º and 90º, with φ = 45º.

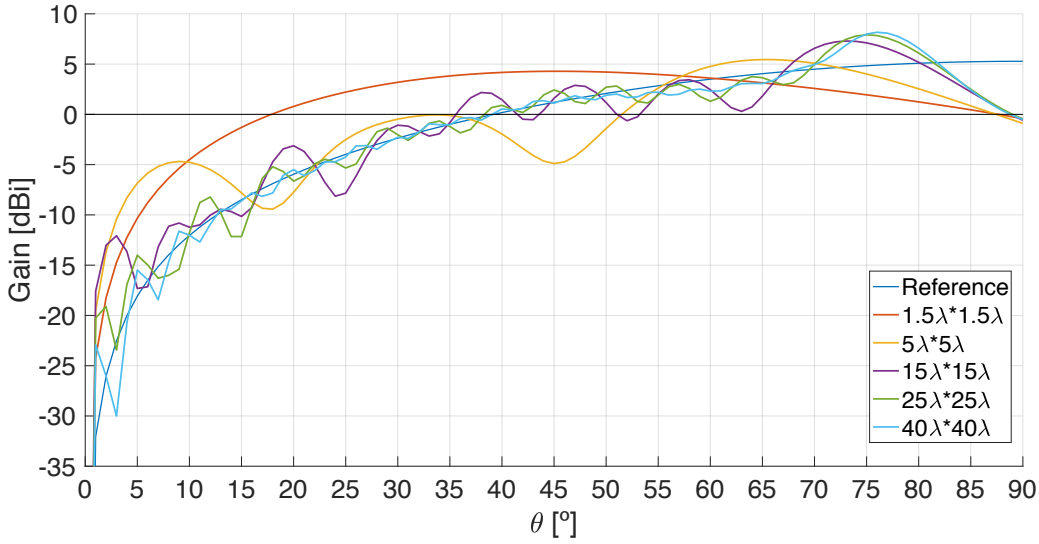

Figure 3.17 Farfield gain for different values of θ with φ =45º at 900 MHz.

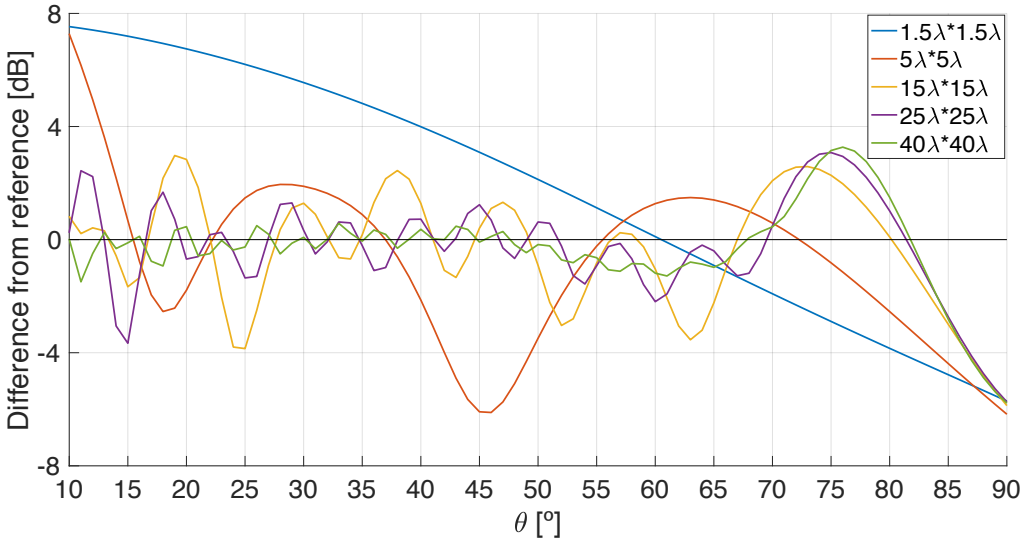

Figure 3.18 Absolute error for different ground sizes with φ =45º at 900 MHz.

Table 3.4 presents the most relevant information regarding the root-mean-square errors (RMSEs) of both perspectives analysed (φ = 0º and φ = 45º) based on Figure 3.16 and Figure 3.18, as well as the number of meshcells and respective simulation time of each ground area. It is clear that for a larger ground area average errors are smaller, and, as expected, there are a direct relation between the simulation time and the number of meshcells, which is a crucial aspect to consider when one has to decide on the best compromise among these parameters.

In addition to these studies, an analysis of the surface current propagation in the monopole ground was also performed, Annex B.3. The comparison between the five different situations can be made since all of them were carefully placed with the same units' limits (0.12 A/m). For 1.5λ x1.5 λ and 5λ x 5λ, the

boundaries are small, hence, the first case shows high values of current arriving to the limits and the second case displays a clear deformation that is also triggered by the boundaries settings. Such problems cease to happen in the remaining cases.

Table 3.4 RMSE for different ground areas of a λ/4 monopole and their simulation times.

Ground	RMSE (φ = 0º) [dB]	RMSE (φ = 45º) [dB]	Nº of mesh cells	Simulation time
$1.5\lambda \times 1.5\lambda$	3.92	3.95	77,372	1m 51s
$5\lambda \times 5\lambda$	2.91	2.35	388,700	8m 7s
$15\lambda \times 15\lambda$	1.64	1.68	2,658,800	1h 0m 36s
$25\lambda \times 25\lambda$	1.49	1.32	6,957,500	2h 52m 1s
$40\lambda \times 40\lambda$	1.50	1.02	17,248,988	9h 6m 20s

Therefore, taking in consideration each perspective, the most reasonable decision to make is to accept some reduction in accuracy, in favour of less computation effort. A decent compromise between simulation time and problem accuracy seems to be with a ground area of 15λ x 15λ, and the surface current behaviour for this case may be seen in Figure 3.19.

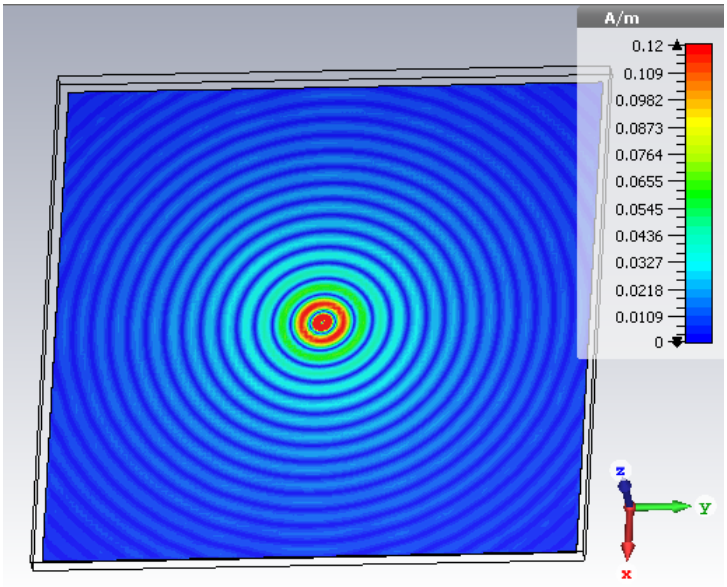

Figure 3.19 Surface current of λ/4 monopole with 15λx15λ ground area.

Regarding the monopole design, it is known that some parameters may change the antenna working frequency. For this reason, one has analysed the S_{11} parameter for each situation, Figure 3.20. It is seen that the frequency with lower reflected power tends to decrease with the ground's area enlargement. Nonetheless, all cases keep an S_{11} value lower than –10 dB, for 900 MHz, representing well matched monopoles.

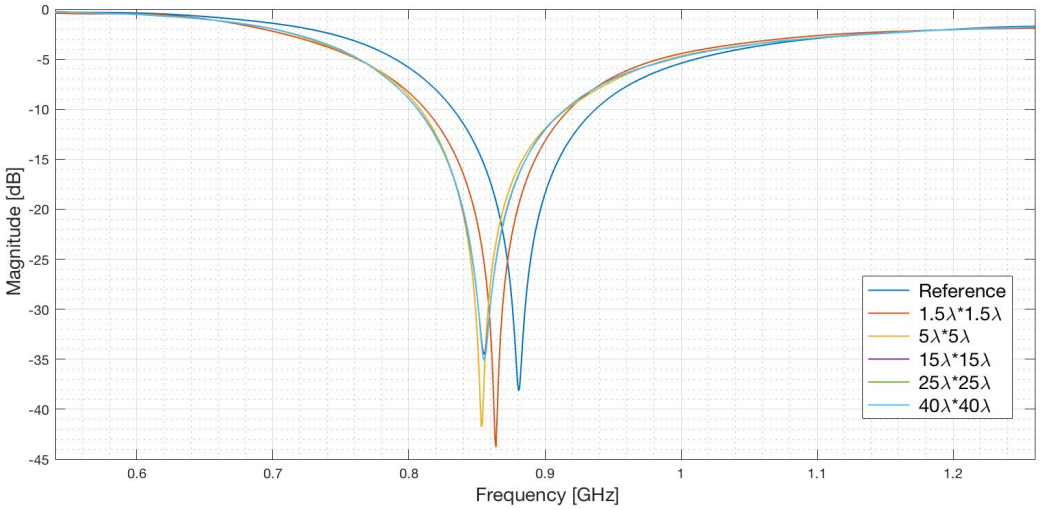

Figure 3.20 S_{11} parameter with the variation of the ground size.

Chapter 4

Results' Analysis

This chapter begins with an explanation about the scenario under evaluation regarding the physical aspects and the most relevant perspectives to understand antennas' performance variations. Then, one explains the monopoles' behaviour for each system (GSM-R, LTE-R and BBRS), from their dimensions to their performance. Finally, one implemented the antennas into specific scenarios and the corresponding analysis is made.

4.1 Scenarios Description

In this section, a description of the reference scenario for standard railway environments is set. For the particular case of this thesis, the analysis of the signal received at the antennas on trains addresses the BSS part where it is the wireless radio communication equipment. This segment may be summarised in two systems: the on-track and the on-board radios.

The on-track radios are the BTSs or the eNodeBs depending on which system is been investigated. As seen in Figure 4.1, the first system is constituted by two sectorised antennas. To minimise the power losses of the distributed signal, the link between the radio and the antennas is done through a 2-way splitter. The adjacent on-track radios are installed with a maximum distance of 1 km for BBRS, and for GSM-R the typical cell range is about 8 km. All of them are connected via the deployment of optical fibre [ECCa18].

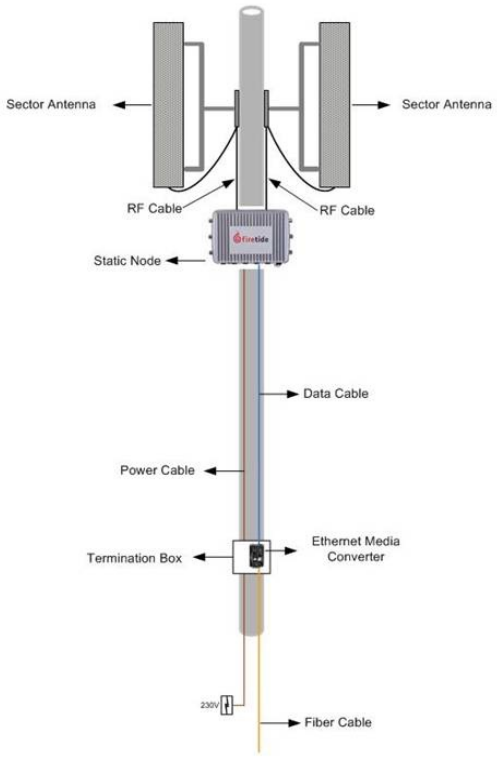

Figure 4.1 On-track antennas (adapted from [IvRS12]).

The on-board radios are the mobile stations present in trains that allow wireless communications. Typically, every train possesses a rooftop antenna in each extremity that is connected with low loss cables to the on-board radios. Generally, the train rooftop is a rectangular metallic structure with a specific width and length at a certain height from the ground. To have an idea of a conventional trains' dimensions, Figure 4.2, shows a height of 4 m (Train_Height), a carriage length of 18 m (Train_Length) and a width of 3.5 m (Train_Width) [Ali16].

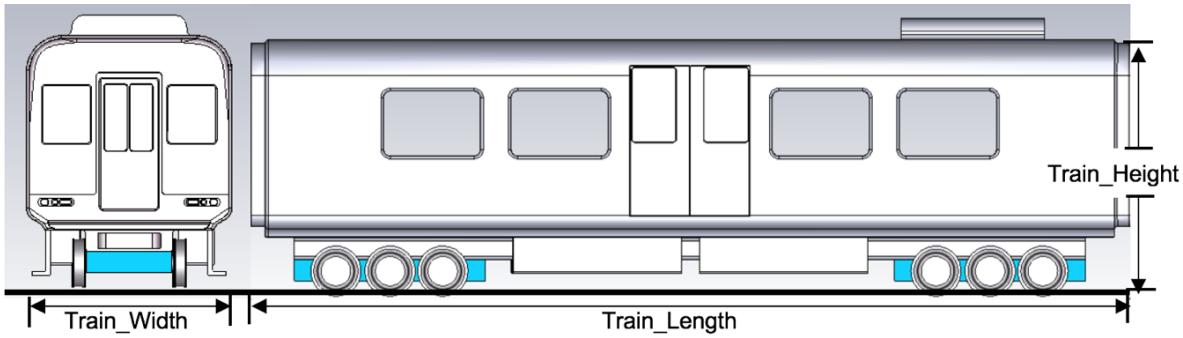

Figure 4.2 Front and side view of a standard train model (adapted from [Ali16]).

Since the BS must be installed periodically along the track, the reference scenario may be simplified to a straight railway track with the BSs positioning at equal distance interval and parallel to the railway as represented in Figure 4.3, along with the most important distances and directions to have a suitable reference scenario:

- d_bs_bs: The distance between the BSs.
- d_bs_ms: The distance between the nearest BS and the MS.
- d_ms_ms: The distance between the rooftop antennas in each extremity of the train.
- d_0: The distance between the BS and the railway track.
- L: the total length of the train.

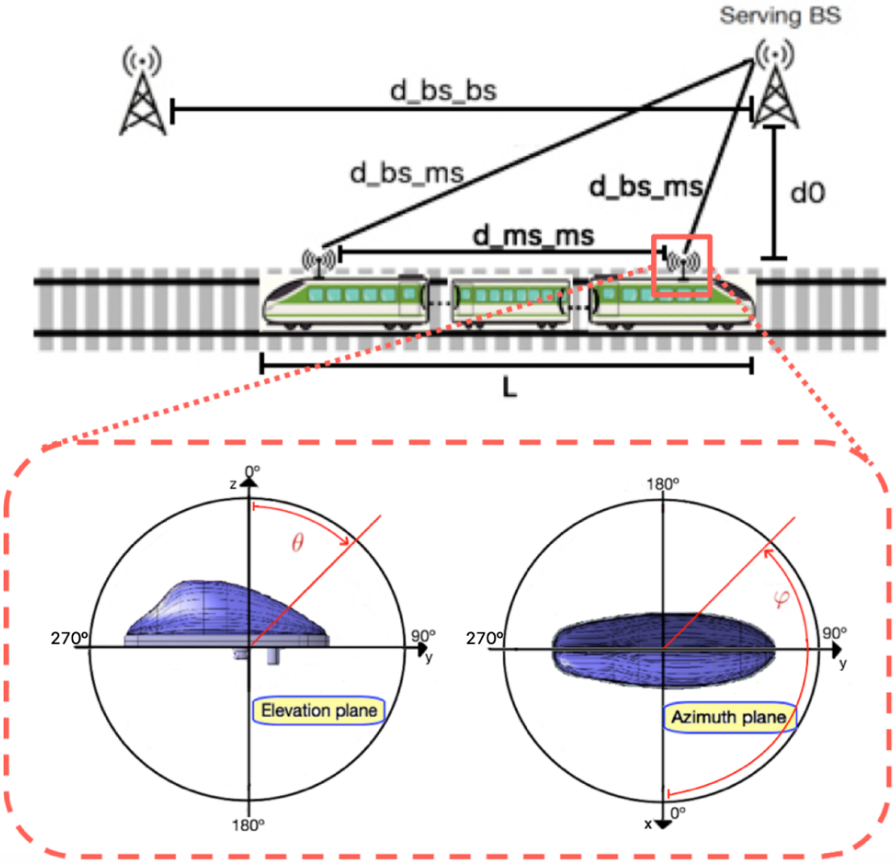

(a) Vertical perspective. (b) Horizontal perspective.

Figure 4.3 Reference scenario with two perspectives of an antenna on the top of a train.

These distances are essential to have a coherent approach to the problem, however, the main focus of antennas' analysis are the two different perspectives between the train rooftop antenna and the BSs. The elevation plane provides the information about the elevation angle (θ) between the train antenna and the BS. This means that with $\theta = 0°$ the train antenna is passing by the BS antenna and for $\theta = 90°$ both antennas have the same height due to the region topology. Thanks to the azimuth plane, it is possible to comprehend the relation between the antenna's direction through the angle φ, for example when $\varphi = 0° \vee \varphi = \pm 180°$ the BS is located exactly at the right or left side of the train, and when $\varphi = 90°$ the BS antenna is located at the same direction of the movement of the train. With these two parameters, it is given the opportunity to identify the most significant performance parameters as the main lobe direction. In the particular case of GSM-R, one has to the possibility of, not only, having a link between the most adjacent BS and the train antenna, but also, having the train antenna receiving signals from distant BSs due to the higher range of lower frequencies.

4.2 Curved ground

Firstly, to analyse how the antenna performance may change when the ground is modified from flat to curved, a simplistic 3D model was created, in CST, considering a segment of real dimensions of a standard train. To reduce the problem dimensions, as well as, the simulation time, the structure was reduced to a width of 3.5 m, a length of 4 m and a height of 0.6 m, in Figure 4.4.

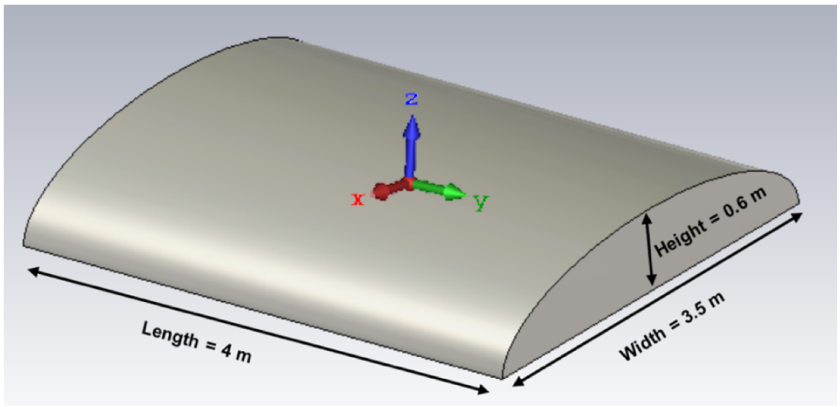

Figure 4.4 Sketch of the curved roof model.

The first simulation concerned the 900 MHz working frequency. In Table 4.1, one compares the antenna performance between the flat and curved grounds. As explained before, the flat ground performance is equal at φ=0º and φ=90º due to geometrical reasons, which does not happen for the curved surface. One observes a clear decrease of 2.77 dB for the side view (φ=0º), along with a large α_{3dB} value, due to the roof curvature morphology that provides a dispersion of the electromagnetic waves. This effect may not be considered a problem, but rather an advantage, depending on system requirements. The α_{3dB} has more than twice the value of the flat ground case, meaning that the values of θ between 49.5º

and 96.5º have a gain higher than 0.93 dBi. Therefore, one detects a compromise concerning the gain and the main lobe width. With an inclusion of curvature in the monopole ground, its gain magnitude drops in favour of losing the strong omnidirectional characteristics. For φ=90º the ground is flat, hence, the gap between the performance of these tested surfaces is much less significant. To have a better understanding of what was explained before, the 2D monopole performance with flat and curved ground concerning the angles of θ and φ is presented, respectively, in Figure 4.5 and Figure 4.6 and a supplementary perspective (3D view) is shown in Annex C.

Table 4.1 Comparison between flat and curved ground performance at 900 MHz.

Ground		Gain [dBi]	Direction (θ [º])	α_{3dB} [º]	L_{SLL} [dB]
Flat	φ=0º	6.70	73	17.6	-3.5
Curved	φ=0º	3.93	73	47.0	-18.4
	φ=90º	5.46	71	24.0	-2.8

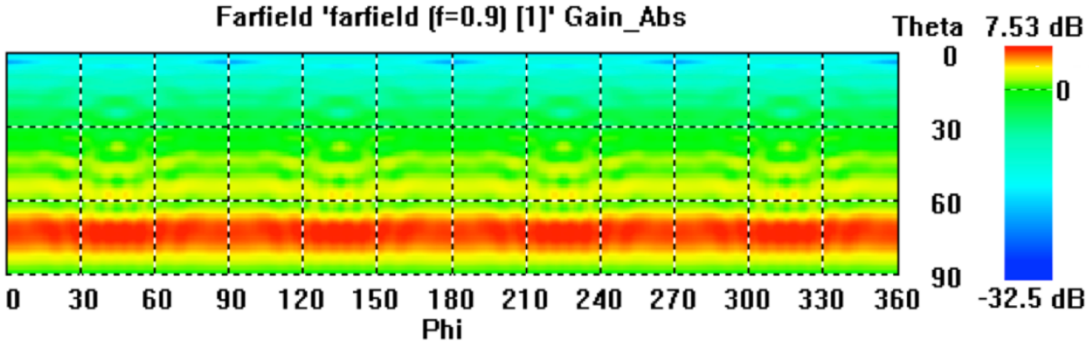

Figure 4.5 Farfield performance of a flat ground for a λ/4 monopole at 900 MHz.

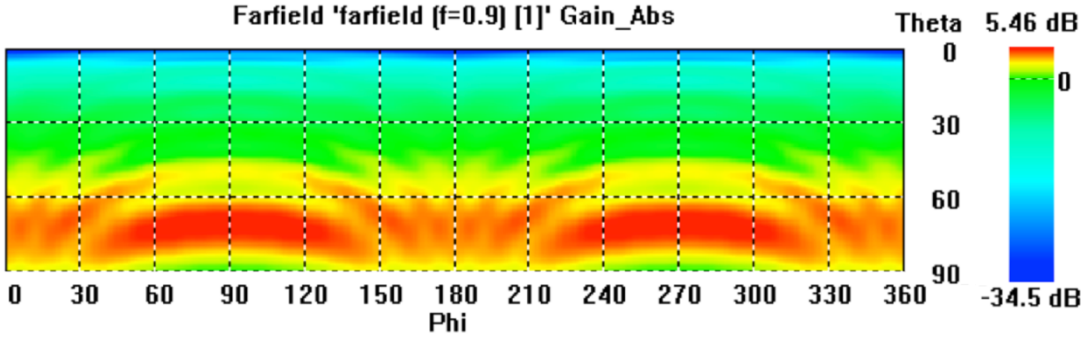

Figure 4.6 Farfield performance of a curved ground for a λ/4 monopole at 900 MHz.

For the exact same scenario, but using different monopole dimensions to study the effects on LTE-R working at 2.6 GHz, one executed the corresponding simulations, and results may be examined in Table 4.2. The gap between the gains, regarding the case of φ=0º, starts to decrease, however the antenna's radiation pattern remains affected by these structure. The main lobe direction increases 6º more than in the flat case, providing a better reception for lower angle situations. From the system viewpoint, this is

not a particularly critical event, since for φ=0º or φ=180º the BS is very close to the train and an exciting result would be having good gain values for 15º <θ< 80º, an issue that is not a priority, because for these distance there are a low attenuation and interference, leading to a steady signal between terminals, as already mentioned before. More important is the performance for φ=90º (front-view) or φ =270º (back-view) and $\theta \in [60° ; 90°[$, since that, in most of the cases, the angles between the on-board terminal and the on-track terminal, regarding this thesis formulation, are in $\varphi \in [60°; 120°]$, and for $\varphi \in [240°; 300°]$ it is considered small variations regarding the travel direction of the train. For φ = 90º, as seen in Table 4.2, Figure 4.7 and Figure 4.8, the same compromise explained before for the 900 MHz exists between a stronger linear omnidirectional characteristic for the flat ground instead of the curved ground where the main lobe gain is weaker but with a larger α_{3dB}. In other words, for the flat ground, a gain higher than 3.63 dBi is provided for an interval of $\theta \in [64.2°; 81.9°]$ and with the curved ground one gets a gain larger than 2.3 dBi for $\theta \in [50.9°; 79.2°]$.

Table 4.2 Comparison between flat and curved ground performance at 2.6 GHz.

Ground		Gain [dBi]	Direction (θ [º])	α_{3dB} [º]	L_{SLL} [dB]
Flat	φ = 0º	6.63	73	17.7	-3.4
Curved	φ = 0º	5.40	79	30.4	-3.3
	φ = 90º	5.30	65	28.3	-4.4

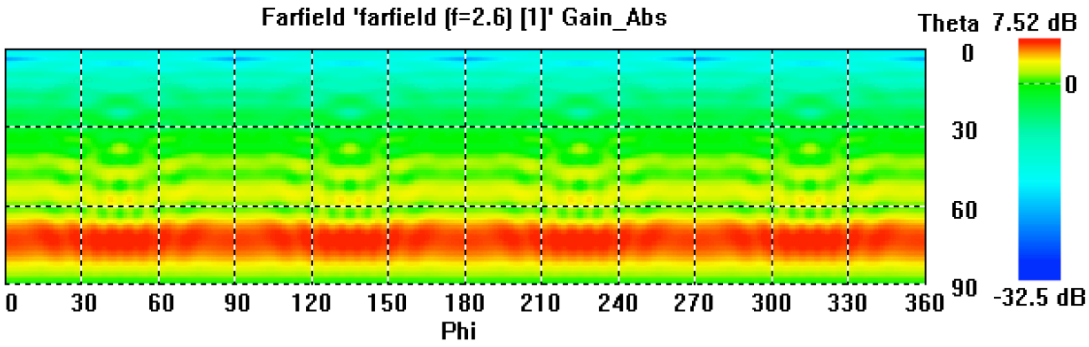

Figure 4.7 Farfield performance of a flat ground for a λ/4 monopole at 2.6 GHz.

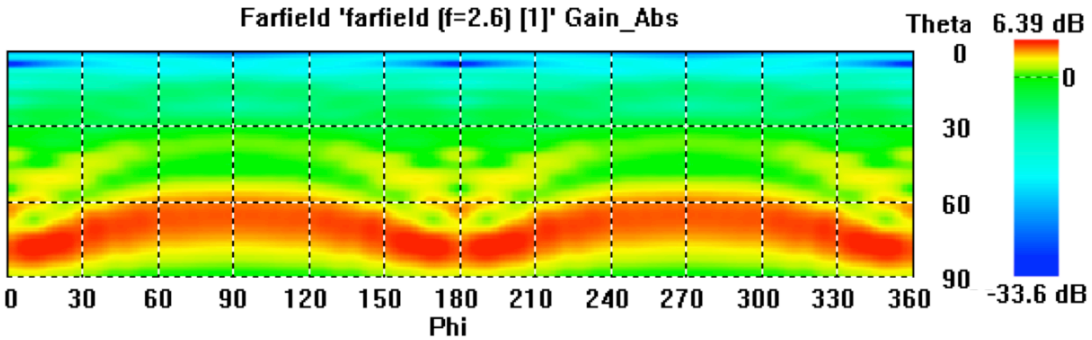

Figure 4.8 Farfield performance of a curved ground for a λ/4 monopole at 2.6 GHz.

For the last system under study, BBRS, the antenna behaviour is similar to the performance shown in LTE-R, as expected. The working frequencies are increasing, and the wavelengths are decreasing, hence the problem boundaries are likewise decreasing, not covering the extremities where the curvature is more evident. Nevertheless, with the wavelength reduction, the sensitivity to the ground curvature is much higher, Figure 4.9 and Figure 4.10. It must be mentioned the fact that, the explanation done before regarding the most important angles starts to be a bit different when the working frequency increases due to higher propagation losses, which leads to smaller cells (more BSs) and some changes regarding the problem geometry. Usually, for frequencies such as 5.9 GHz the BSs are positioned with lower masts, reducing interference problems. Therefore, geometrically speaking, the most important angles under study are similar to the other systems, since the distance between BSs is reduced , as well as their height. The values displayed in Table 4.3 confirm this analysis, showing minor differences in the performance of the monopole for the grounds under study.

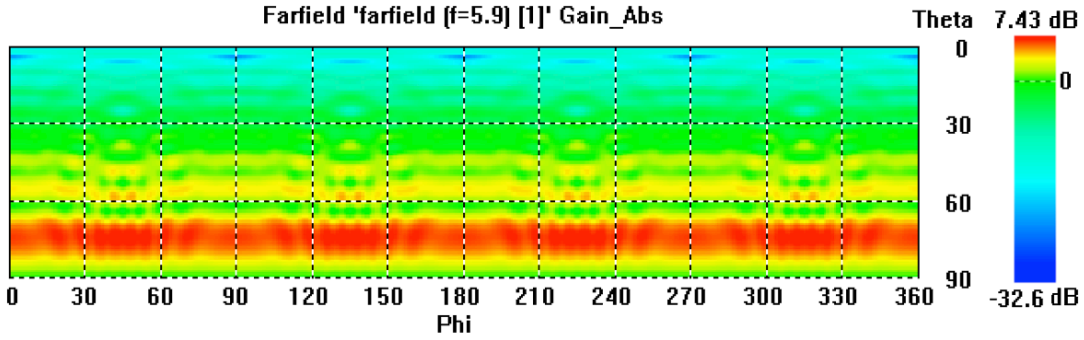

Figure 4.9 Farfield performance of a flat ground for a λ/4 monopole at 5.9 GHz.

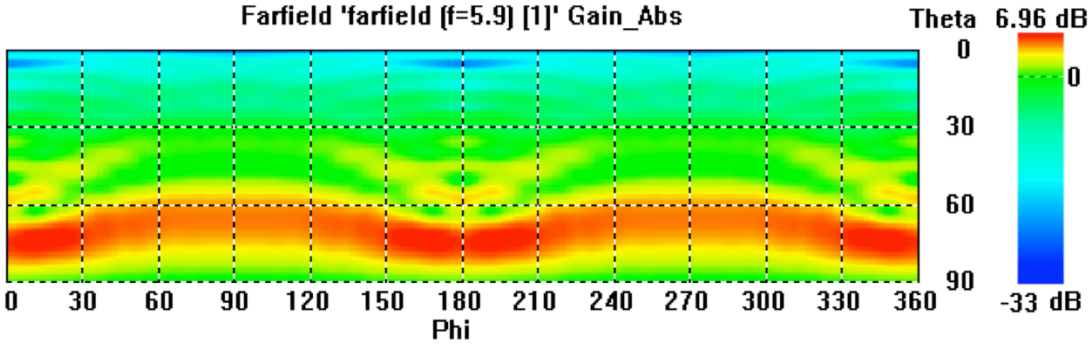

Figure 4.10 Farfield performance of a curved ground for a λ/4 monopole at 5.9 GHz.

Table 4.3 Comparison between flat and curved ground performance at 5.9 GHz.

Ground		Gain [dBi]	Direction (θ [º])	α_{3dB} [º]	L_{SLL} [dB]
Flat	φ = 0º	6.54	74	16.8	-2.6
Curved	φ = 0º	6.30	75	18.1	-2.2
	φ = 90º	5.30	65	28.9	-4.8

4.3 Obstructions on trains' rooftops

4.3.1 GSM-R (900 MHz)

In this section, a thorough analysis is done to determine the effect on antennas' performance from the presence of an obstacle in a nearby region. As noted before, usually, these obstacles are HVAC units with a significant size that will lead to a direct impact on antennas. There are numerous types of HVAC units with different dimensions, however, it was considered reasonable to take a maximum height of 45 cm and, to perceive how the antennas' performance responds in the presence of a less relevant obstacle, a minimum height of 25 cm. Regarding the width and length of these units it is considered the dimensions of 1.4 m and 1.5 m, respectively. The parameters to be modified in this analysis were the obstacle height regarding the antenna installation plane and the longitudinal length between the antenna and the obstacle, as presented in Figure 4.11.

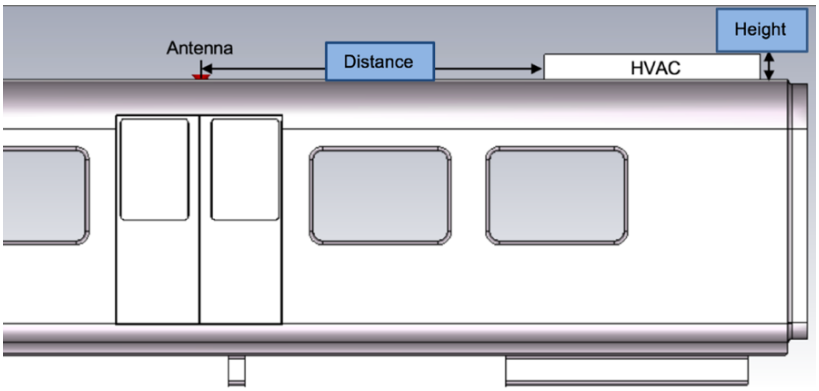

Figure 4.11 Physical parameters to consider in the simulations.

It is much more valuable to have a perspective as close to reality as possible, hence, one has considered a set of technical characteristics used in a real situation. For GSM-R, one considered the antennas implemented on the North-South Railway (NSR) Project across Saudi Arabia [BGLI10]. This particular antenna is named BGLI, being a dual-band one, used for GSM-R and for GPS. A more detailed overview is presented in Annex D.1. Since it was not possible to obtain this specific antenna model to implement on CST, based on its radiation pattern, one has adopted an equivalent 900 MHz monopole to perform simulations, since both, have an omnidirectional behaviour with an identical gain.

Regarding the problem formulation, one has analysed three different perspectives in the azimuth plane: φ = 0º (lateral view), φ = 90º (HVAC obstruction) and φ = 270º (without any obstruction type).

For the first study, CST was ran 14 times within 7 different distances between the antenna and the HVAC (0.5 m, 1 m, 1.5 m, 2 m, 2.5 m, 3 m and 3.5 m) for 2 HVAC heights (25 cm and 45 cm). One also ran a simulation without the presence of any structure at the top of the train to use as a reference performance. The results of these simulations are available in Annex E.1, where one presents the 2D monopole performance for each set of specifications.

For φ = 0º, the antenna performance does not deviate much from the reference scenario. Figure 4.12 shows a maximum gain of 6.76 dBi when the HVAC has the highest height, and it is in the nearest position to the antenna, that one observes a maximum disparity of 1.18 dBi from the reference (5.58 dBi). For the HVAC with 25 cm of height, the maximum gain is also for the nearest position between the antenna and this structure, and then the gain has a slight reduction. After 2 m of distance, the gain reaches an approximate steady value below the reference. Despite the small variation of the gain for φ = 0, the existence of values higher than the reference, near to the HVAC, are due to reflections effects on the structure.

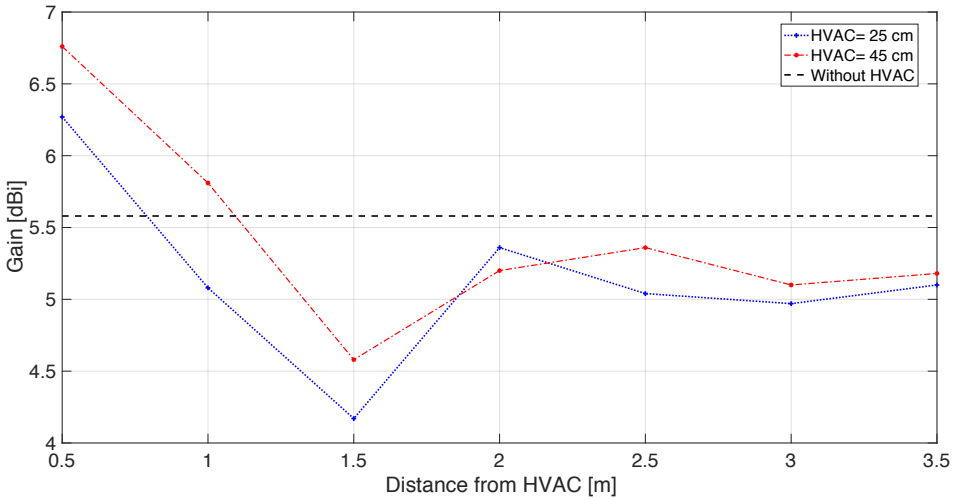

Figure 4.12 Antennas' gain with the presence of HVAC for φ=0º at 900 MHz.

Still for the same perspective, lateral view, it is equally important to analyse the elevation direction of the main lobe with the presence of obstructions, Figure 4.13, via the analysis of angle θ. For φ=0º, the main lobe elevation has a maximum variation of 6º, which is not significant, since the closest BSs usually are located at φ=90º (train's front) and φ=270º (train's back). However, for some cases GSM-R antennas may connect with other parallel BSs at greater distances due to the railways deployment, and for these cases a variation of 6º at larger distance may be critical.

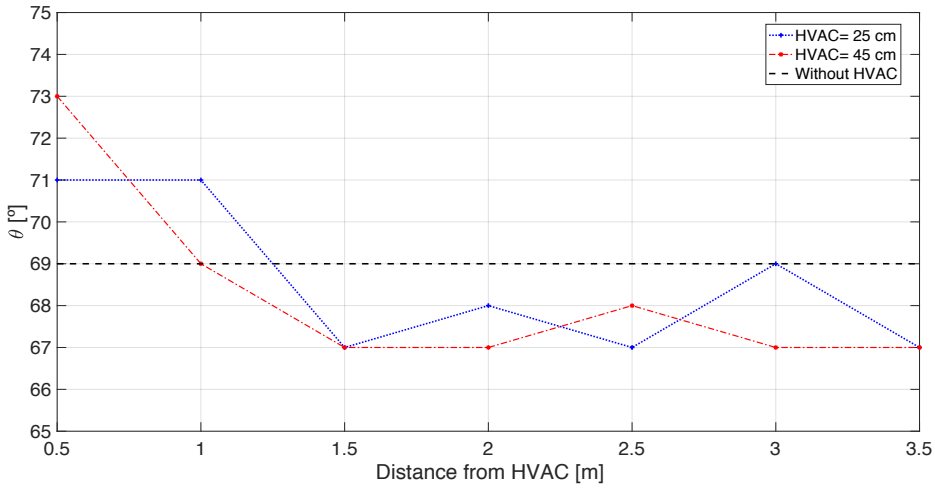

Figure 4.13 Main lobe direction with the presence of HVAC for φ=0º at 900 MHz.

The direction where the HVAC unit is located is for φ = 90º. For this reason, it is the perspective where there are more critical variations in the output parameters to be investigated, which must be analysed more thoroughly. Regarding the antenna's gain, Figure 4.14, in the closest region to the HVAC unit, the antenna shows a vast distortion and a drastic reduction in the primary lobe gain. The highest obstruction, for the HVAC with 45 cm of height, leads to a gain of -3.24 dBi, with a difference of -9.76 dBi compared to the 6.52 dBi of the reference scenario. In a general way, the HVAC with 25 cm has a lower impact on the antenna gain, Figure 4.14. Nevertheless, in its worst-case scenario, for a distance of 0.5 m, it exhibits a negative gain of -0.29 dBi, which means a difference of -6.81 dBi to the reference. The simulations with a distance of 2.5 m show a higher gain for "HVAC = 45 cm" which is illogical. However, it is a disparity of 0.82 dBi between the two cases under study, which may be justified through the minor lobes behaviour that interfere in the main lobe performance. According to the behaviour of both HVAC heights, it is reasonable to say that there is a convergence to a constant gain of 5 dBi, near to the reference gain, and that the variation of the gains is negligible for a distance over 1.5 m.

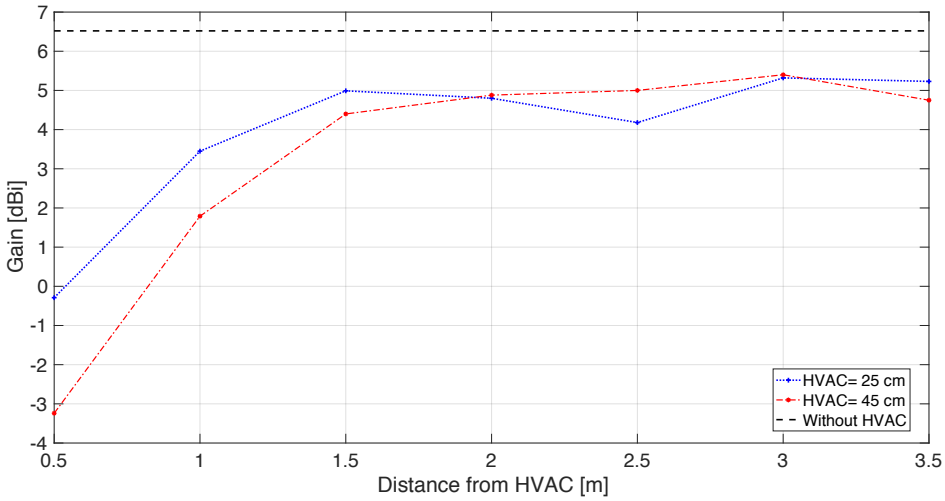

Figure 4.14 Antennas' gain with the presence of HVAC for φ=90º at 900 MHz.

The main lobe direction will also suffer significant variations. One expects worse results for the "HVAC=45 cm" situation, that is, θ angles are much smaller than usual (reference of 70º), and, in fact, it happens for almost all distances, Figure 4.15. The only case where it does not occur is for the nearest position, 0.5 m, which presents an unacceptable outcome of -3.24 dBi for the primary lobe gain, so it does not need to be investigate more thoroughly. On average, α_{3dB} values are around 25º, and taking a safety margin, one can consider as an acceptable performance angles that do not have a difference greater than 10º compared with the reference. On the one hand, for the obstacle with 25 cm of height, the main lobe elevation angles starts to be satisfactory at the distance of 1.5 m, and on the other hand, the 45 cm case only begins to have suitable results for distances larger than 2 m.

At last, one has analysed the case for no obstruction, φ = 270º, Figure 4.16. It would be expected that results are very close to the reference, since there are no obstacles in this viewpoint, as it happens in the reference scenario, nevertheless, the results show an average gain much higher than the reference

one (6.52 dBi), reaching a maximum of 8.48 dBi for “HVAC=45 cm” and 8.29 dBi for “HVAC=25 cm”. These outcomes occur because, added to the fact that there is a clear view for φ = 270º, there is the HVAC unit in the opposite direction, which provides an extra area to reflect the EM signal, providing an additional gain. In fact, performing a more detailed analysis based on the 2D results, Annex E.1, there is a higher gain for both situations for a distance of 0.5 m. For “HVAC=25 cm” the maximum gain is 10.8 dBi and for “HVAC=45 cm” it reaches 11.6 dBi. For example, in the case of “HVAC=25 cm” at 0.5 m, the main lobe has two different directions (φ=240º and φ=300º), and that is the reason for having a gain lower than the reference for φ = 270º. Since these simulations were ran in an ideal environment where structures are a PEC material, without losses, the results will always have a mathematical balance between them. Hence, results are coherent with expectations, tending to stabilise above the reference, near to 7.5 dBi, compensating the values below the reference for the other two cases.

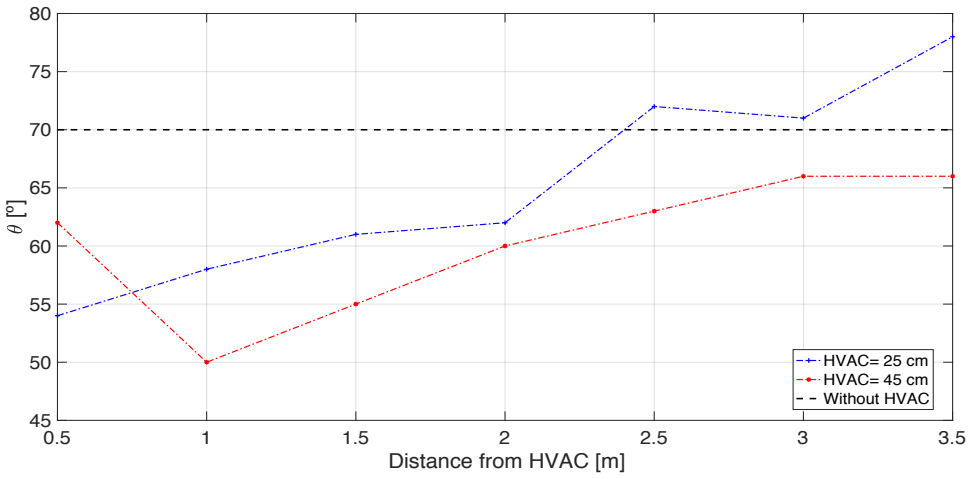

Figure 4.15 Main lobe direction with the presence of HVAC for φ=90º at 900 MHz.

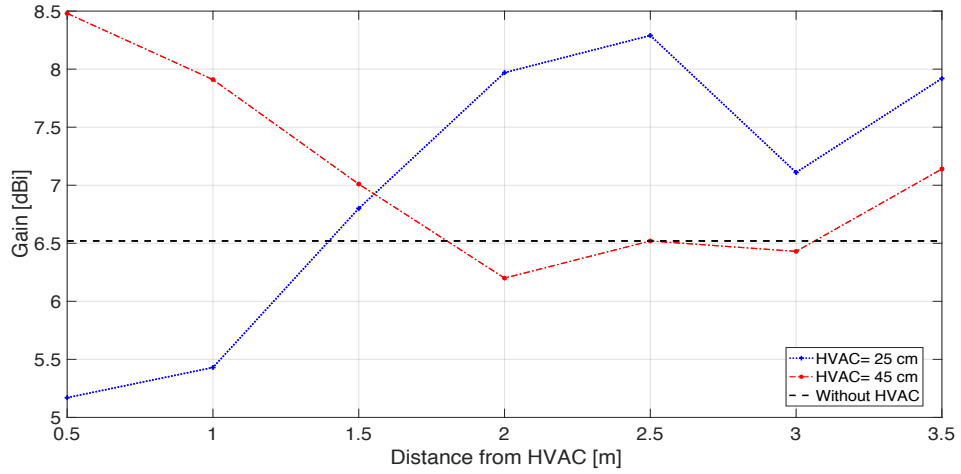

Figure 4.16 Antennas’ gain with the presence of HVAC for φ=270º at 900 MHz.

Figure 4.17 shows the lobe direction behaviour for φ = 270º. For the “HVAC=25 cm” case, θ values are very close to the reference of 70º, excepting for the distance of 0.5 m, where there is a discrepancy of almost 15º, for the same reason of the previous case for gain. For φ = 240º or φ = 300º, the lobe direction

is identical to the reference, θ = 70º. Regarding the remaining setting, “HVAC=45 cm”, there are two results that are not expected due to their divergence, compared with the reference value, at 2 m and 2.5 m. With the visual support of the 2D performances in Annex E.1, it is easily verified that, besides the main lobe considered for the θ values used on the graph, there are also, in both cases, the presence of strong secondary lobes with similar gains that have θ near to the reference value of 70º.

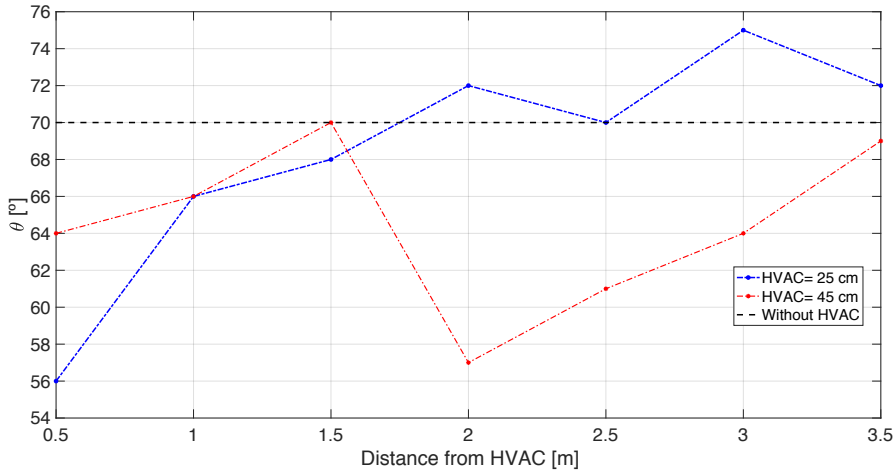

Figure 4.17 Main lobe direction with the presence of HVAC for φ=270º at 900 MHz.

4.3.2 LTE-R (2.6 GHz)

It is also interesting to analyse the problem of potential systems to use in the future, like LTE- R. Although this system is not yet fully standardised, there are already several companies considering the best approach to implement LTE-R, aiming at high-speed networks, wholly dedicated to railways usage, opening a new world of opportunities for the creation of smart trains. The key goal is to migrate the current system, GSM-R, to LTE-R, which will be responsible for all operations currently being done at GSM-R, such as voice and data for train control and safety operations, and offer more services like on-board video surveillance and passenger infotainment services. It is reasonable to assume as having the 2.6 GHz λ/4 monopole as a decent approximation to a real antenna, such as the LTE antenna accessible on Annex D.2.

An identical analysis was performed, prioritising the study of the main lobe gain and direction behaviours for the three more relevant perspectives according to this problem formulation: φ=0º, φ=90º and φ=270º.

Firstly, the results for φ=0º are investigated. In Figure 4.18, it is possible to observe the primary lobe gain behaviour when the distance between the antenna and the HVAC unit is increased and, also, with two different HVAC unit heights. The results suggest a perform very close to the reference without significant variations, less than 1 dBi from the reference of 6.63 dBi. In the beginning, the gain is above the reference due to the reflection on the HVAC unit and then, when the distance increases, the reflections have less weight justifying the gain reduction, but in a smoother way. As expected the “HVAC= 45 cm” shows more significant variations, since the provided reflected area is more extensive.

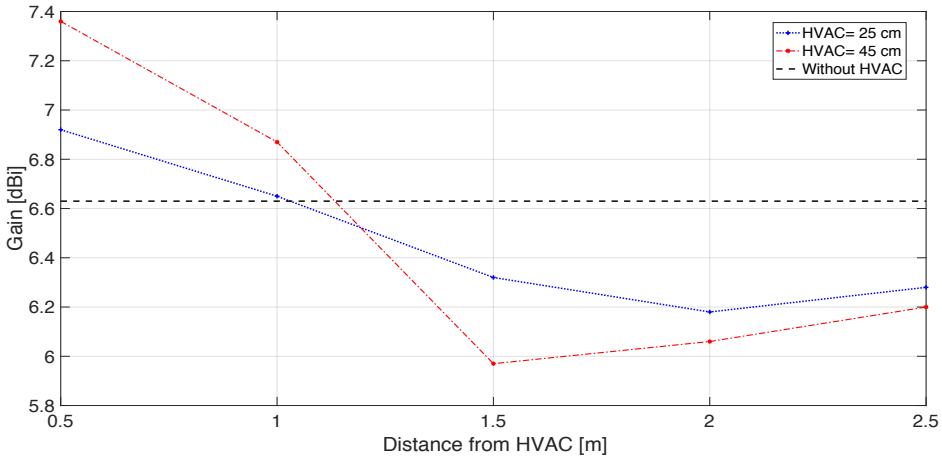

Figure 4.18 Antennas' gain with the presence of HVAC for φ=0º at 2.6 GHz.

Since θ = 90º corresponds to the maximum value possible, representing the circumstance when the on-board antenna and the on-track antenna are at the same elevation level, regarding lobe direction at this particular viewpoint, it is foreseeable to have a direction similar to the reference, θ = 73º. For this perspective, there are no substantial deviations, and the obstacle presence does not show interference with this parameter for φ = 0º. Figure 4.19 reveals an identical performance for both HVAC heights, within a minor difference of 3º above the reference scenario, and this means a lobe slightly closest to the installation plane.

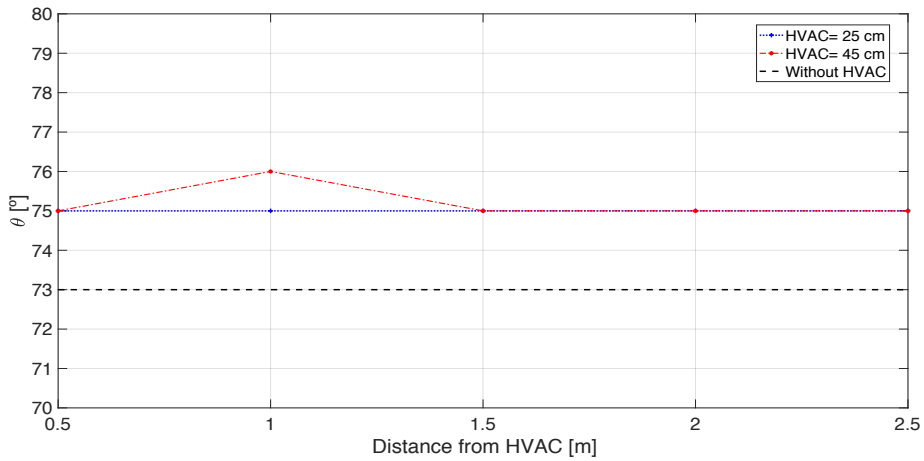

Figure 4.19 Main lobe direction with the presence of HVAC for φ=0º at 2.6 GHz.

Towards the HVAC unit direction, at φ=90º, one sees much more significant variations, meeting the behaviour already seen in GSM-R. In Figure 4.20, one may see that for the "HVAC = 25 cm" case, a minimal gain of 1.69 dBi at 0.5 m is reached, and from then on the gain improves until it reaches a saturation level around 5.25 dBi. As the obstruction height increases, results behave in a similar way, notwithstanding the fact that, when near to the HVAC, there is much more evident losses, at -1.44 dBi. After this, the performance, continuously, improves until it reaches a stability point around 5.50 dBi. Regarding the HVAC with 25 cm, ahead from the distance of 1 m gain variations are no longer relevant.

For the other situation, the “safety” distance is reached at 1.5 m. Both cases will have losses around -1.5 dB regarding the reference value of 6.63 dBi, for the distances considered.

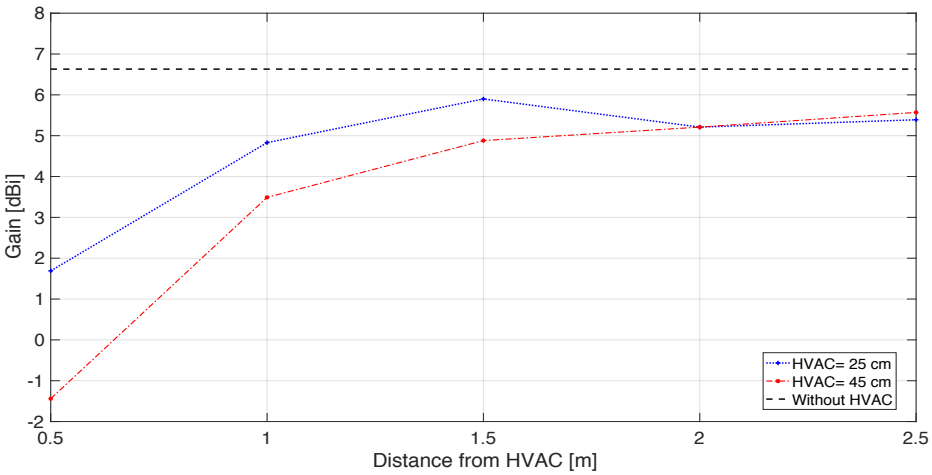

Figure 4.20 Antennas’ gain with the presence of HVAC for φ=90º at 2.6 GHz.

The main lobe elevation for φ = 90º is investigated in Figure 4.21. As before, concerning the gain, the higher HVAC structure has a more significant influence on the main lobe elevation and, for that reason, θ outcomes are always below the smaller HVAC. For the “HVAC = 25 cm”, the main lobe direction starts to be adjoining to the reference of 73º from the distance of 1 m. Still as, in the previous situation, when the λ/4 monopole is standing at a distance of 2.5 m, it appears that the θ performance is even better than without any obstacle due to some constructive and destructive wave interference leading to θ=76º. The analysis is further taken through the evaluation of Figure E.20, which reveals the appearance of a secondary lobe with only an L_{SLL} of -1.9 dB, at θ = 65º. The existence of this second lobe is influencing the primary lobe elevation, and this is the reason for having an elevation performance slightly better than the case without any blockage. For the “HVAC = 45 cm” case, a performance with acceptable angles starts to emerge at the distance of 1.5 m. These decisions were based on the same assumptions explained for the GSM-R, taking the average values of α_{3dB} of 20º, accepting angles that do not have a difference larger than 10º compared with the reference.

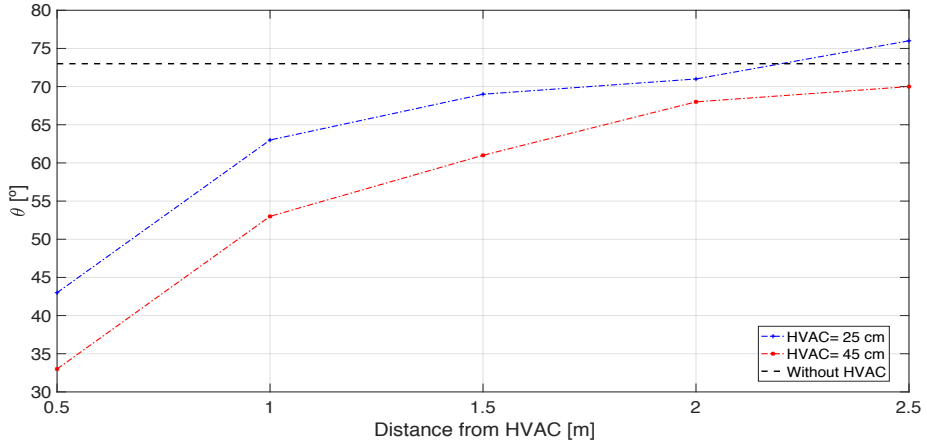

Figure 4.21 Main lobe direction with the presence of HVAC for φ=90º at 2.6 GHz.

The last perspective to consider is the opposite side to the HVAC unit, for φ = 270º, which may be seen in Figure 4.22. Firstly, one analysed how the main lobe gain behaves. Contrary to what happened in GSM-R, there are not unexpected behaviour. For each simulation, a gain larger than the reference of 6.63 dBi is achieved, reaching higher marks in the "HVAC = 45 cm", since it has the advantage of owning a greater area to reflect the EM signal. Even though the graphs do not display an apparent steadiness, it may be reasonable to assume a trend for a gain higher than the reference, roughly, at 8 dBi.

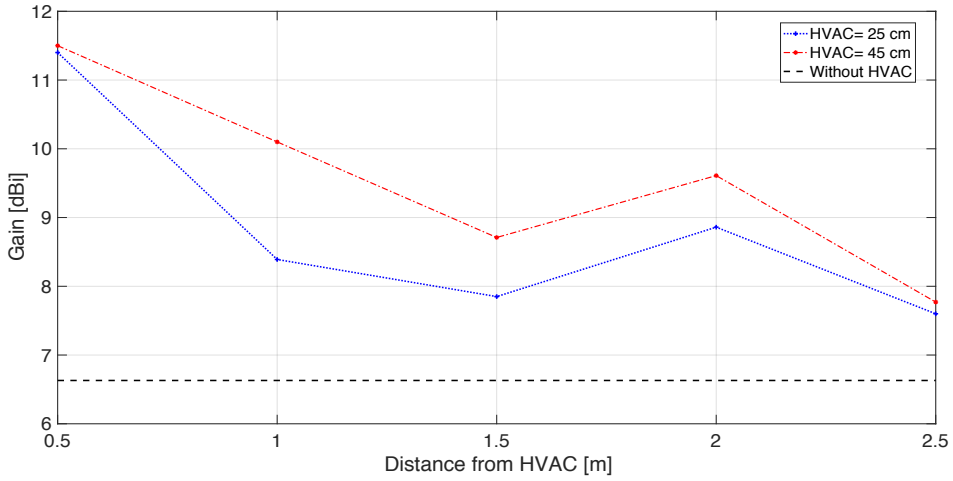

Figure 4.22 Antennas' gain with the presence of HVAC for φ=270º at 2.6 GHz.

Secondly, one evaluated the lobes directions, regarding the elevation plane, supported on the results presented in Figure 4.23. For the HVAC with 25 cm height, there is a consistent performance amongst the reference elevation of 73º. For the other setting, with a height of 45 cm, angle θ appears to diverge from the reference. In Figure E.25, one may observe the presence of several lobes that will push the θ direction to higher values. Nevertheless, the L_{SLL} is -1.2 dB at 71º, below the reference level, and there is even another lobe between the main and the secondary one with 6.51 dBi, at 76º. Everything suggests that the performance does not deviate too much from the reference.

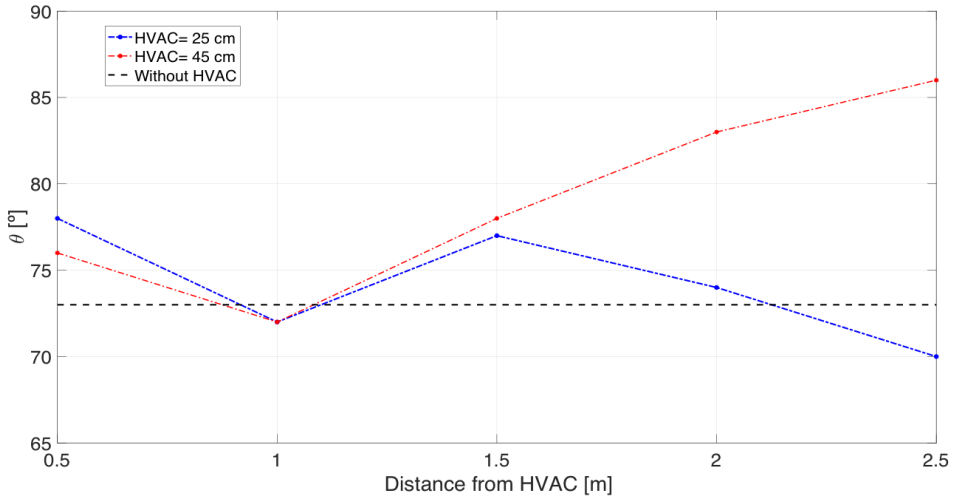

Figure 4.23 Main lobe direction with the presence of HVAC for φ=270º at 2.6 GHz.

4.3.3 BBRS (5.9 GHz)

BBRS is a communication system built to deliver improved services, demanding higher data rates and capacity. Therefore, this system is the one that has the higher working frequency from all systems analysed in this thesis. In terms of cellular planning, several aspects should be considered, namely, the physical limitations of signal propagation when using higher frequencies. The higher the frequency, the higher the signal attenuation, which forces the maximum distance between terminals to be reduced. To have an idea, in free space, signal path loss reaches 107.9 dB considering the maximum range used for BBRS (1 km), and for urban conditions, where the uppermost distance between terminals is 300 m, there are losses of 97.5 dB also contemplating free space settings. For these reasons, and always taking into account the environment where the system is installed, antennas with more directional characteristics may be used to struggle with these losses.

One has considered a different environment from the previous other two systems. The antennas performance was analysed based on the specific case of the “AZUR metro cars” project used by the Sociéte de Transport de Montréal (stm), [Gonç15]. In this subway scenario, the used antennas are the Sencity® Spot-S WiFi that has unidirectional features, a detailed description being given in Annex D.3.

Since it was not possible to have an operational 3D model to implement in CST, it was necessary to resort to Antenna Magus and find an antenna that grants a similar performance to the Sencity® Spot-S WiFi one. The chosen one was a 2-by-2 rectangular microstrip patch array designed to work at 5.9 GHz. It is a complex antenna to design, sketched in Figure 4.24, with dimensions in Table 4.4.

The four co-polarised patches of this antenna are fed from a single feed point, and mitred sections are used on 90º corners as well as on T-junctions to reduce mismatch due to reflections from discontinuities. Patches are composed of PEC material, and its substrate is generated by “Normal” material that exists in CST with relative permittivity of 2 and permeability of 1.

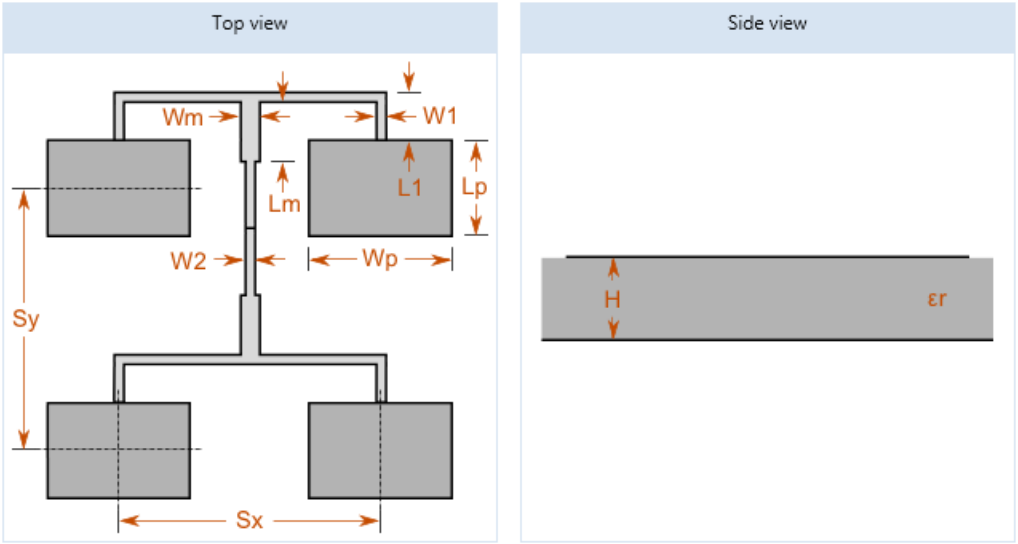

Figure 4.24. The 2-by-2 rectangular microstrip patch sketch (extracted from [AntM17]).

Table 4.4 Antenna dimensions for BBRS system (extracted from [AntM17]).

Name	Variable	Size [mm]
Matching line width	Wm	2.07
Matching line length	Lm	9.92
Line width 1	W1	0.31
Line width 2	W2	1.94
Line length 1	L1	20.40
Patch length	Lp	16.61
Patch width	Wp	20.74
Vertical patch spacing	Sy	40.65
Horizontal patch spacing	Sx	40.65
Substrate height	H	2.00

The first step was to import the 2-by-2 rectangular microstrip patch model to CST and run a simulation to validate its characteristics. Figure 4.25 shows its performance in a 3D view, demonstrating an unidirectional radiation pattern with a gain of 13.5 dBi, close enough to the 14 dBi of the Sencity® Spot- S WiFi antenna, and a vertical α_{3dB} of 32.8º that is also acceptable compared with the 35º from the reference. However, one has detected an S_{11} of -3.8 dB, larger than the acceptable threshold of - 10 dBi, hence one has tested several changes regarding the antenna's physical parameters like substrate height and relative permittivity. The best result is when the relative permittivity is changed from 2 to 1.8, reaching a value of -13.9 dB. This change is important, since when the subway structure is added to simulate its impact, the S_{11} parameter achieves values larger than -10 dB, indicating that the antenna is not well matched, and that reflection losses are too big to be ignored.

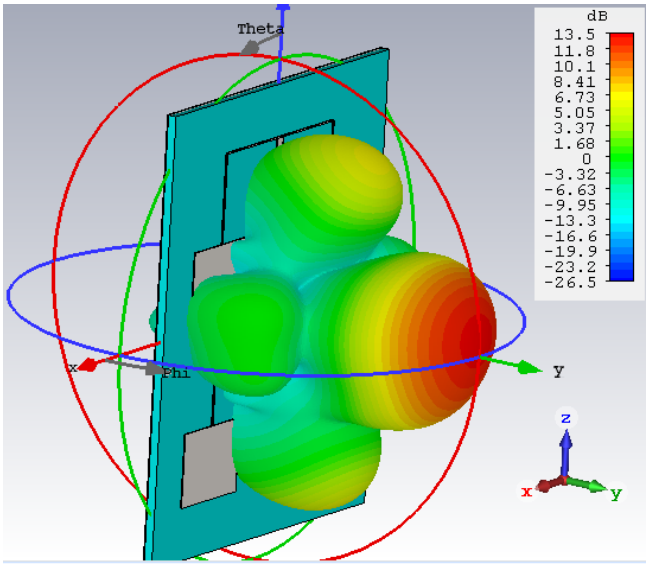

Figure 4.25 The 2-by-2 rectangular microstrip patch array farfield at 5.9 GHz.

According to the project specifications [Gonç15] regarding BBRS and the physical limitations of the AZUR metro itself, a well-confined region is established, which has to be taken into account when the microstrip patch is placed to simulate and understand its performance. In Figure 4.26, one may see, as green, the region where it is conceivable to mount the BBRS antenna. In fact, in this particular project, four on-board antennas are used, two at the front and another two at the back, providing not only redundancy to the system but also horizontal spatial diversity. The use of diversity merges uncorrelated signal replicas through multipath, improving the link budget results and overcoming several fast fading problems. Therefore, instead of having the complete available volume displayed in Figure 4.26, one has divided it into two smaller volumes with the same depth (200 mm) and height (150 mm) but half the width (225 mm).

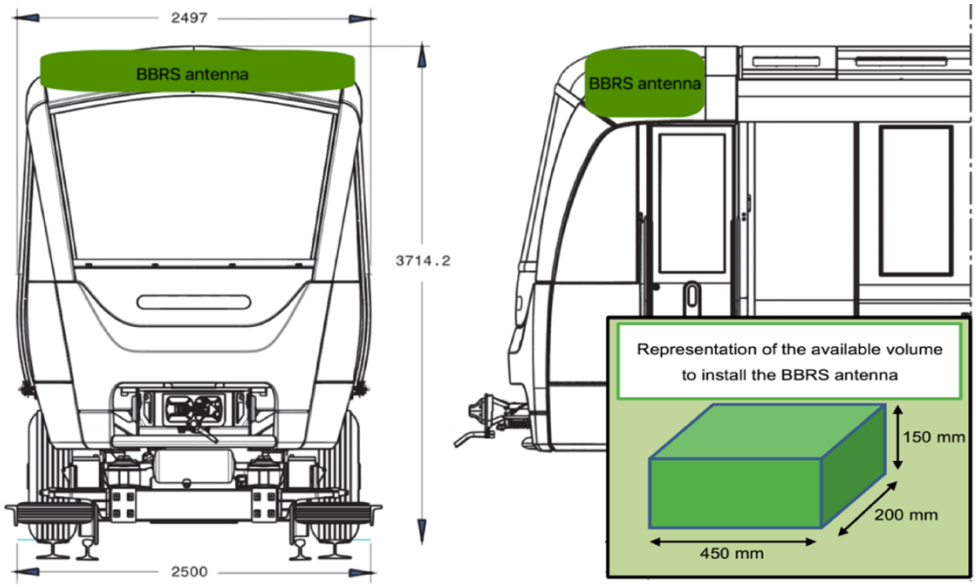

(a) Front view. (b) Side view.

Figure 4.26 Metro sketch showing the antenna installation region (adapted from [stmo17]).

Firstly, one performed a study concerning the depth and height available to install the antenna. Then, after acknowledging the optimal position to mount this particular terminal, the analysis addresses the real scenario, installing two microstrip patches separated with more than 1 m (≈20 λ) and considering a minimum distance of 0.5 m between each antenna and their respective extremity.

Figure 4.27 clarifies the six different simulations that were carried out, where one varied three different depths at which the antenna is from the front of the train (0 mm, 100 mm and 200 mm), and for the maximum and minimum achievable heights (Position 1 and 2), recognising the 100 mm of antenna's height and the available space of 150 mm.

Simulations were performed according to the model shown in Figure 4.27, but without the presence of any glass material type. Glass is a material that has a lower attenuation, and it does not have influence in the pursuit of the ideal antenna's installation position, reducing the time of each simulation approximately to 2 hours. One also addressed a concern regarding the influence of the glass material presence on the antenna's efficiency, increasing the S_{11} parameter above the acceptable - 10 dBi value. This would involve extra time changing the several settings of the rectangular microstrip patch array, to

adapt, again, the antenna, and it would not bring new information that would improve results regarding the primary purpose of this work.

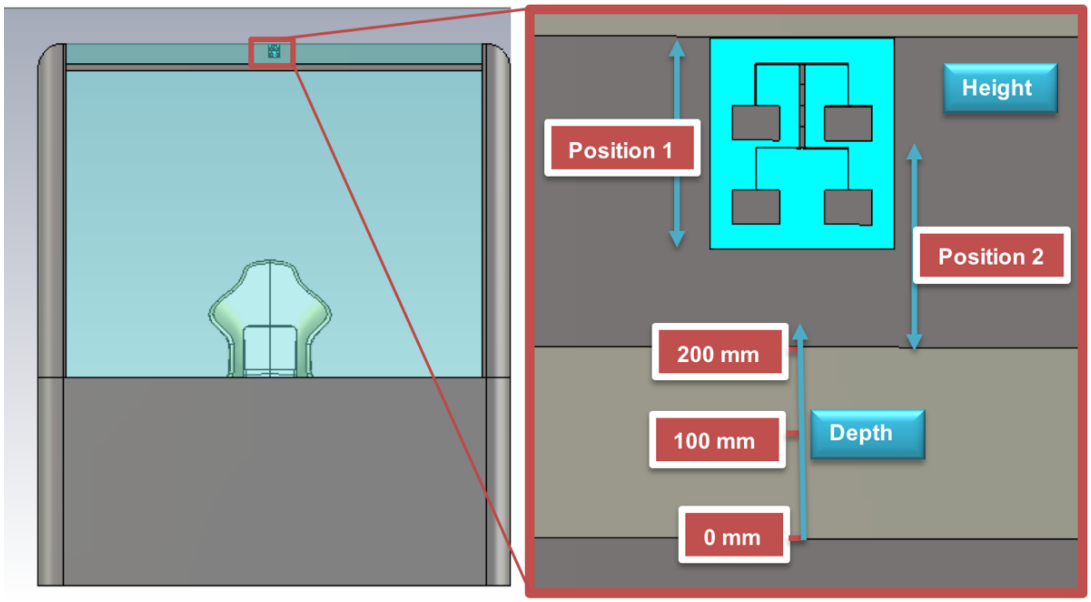

(a) Metro front view. (b) Zoom on the possible position of the antenna.

Figure 4.27 Physical parameters variation regarding the BBRS antenna.

Before beginning a detailed analysis of the simulation results, the surrounding environment must be understood so that one knows the optimal location to achieve. For this particular scenario, the on-track antennas are placed in the tunnel's ceiling. Therefore, the vertical distance between the terminal is minimal, around 1 m or 2 m, and the horizontal distance has a maximum of 1 km. Through a simple trigonometric logic, this means an irrelevant elevation smaller than 1º regarding the on-board and the on-track antennas, which translates to this work's perspective as an elevation of $\theta \approx 90º$. However, there are always additional factors that can influence elevation or horizontal direction between the terminals, such as, the ground height variations or path curvatures. Since railways are not allowed to have severe curves due to safety issues, the α_{3dB} of 40º is more than enough to have a suitable continuous gain between 14 dBi and 11 dBi. For ground variations, a margin of $\pm$ 5º is satisfactory, which is contained on the HPWB of 35º.

Since the available volume is relatively small, the performances of the different simulations do not deviate too much from each other, Figure 4.28. To enable the analysis of the gain, in polar coordinates, all angles within negative values (losses) were not considered, focusing the attention on what really matters: a high gain for $\theta \in [80º; 95º]$. One also preserved the secondary lobes values, even if they do not have a significant influence in the main topic of this work, since their presence may help to understand the antenna's performance behaviour according to the surrounding environment.

Concerning the results of Figure 4.28, the locations to mount the microstrip patch array, at both heights ("Position 1" and "Position 2"), show a clear main lobe at the expected θ elevation ($\approx$ 90º). However, there are some deviations to be considered. For "Position 1", the reference performance is very similar to the "0 mm" case, and when the biggest depth conceivable, 200 mm, is introduced, the radiation

pattern reveals some distortion regarding the main lobe that is not desirable due to its unpredictable behaviour. For “Position 2”, one sees a variation for the elevation when the antenna’s installation depth increases.

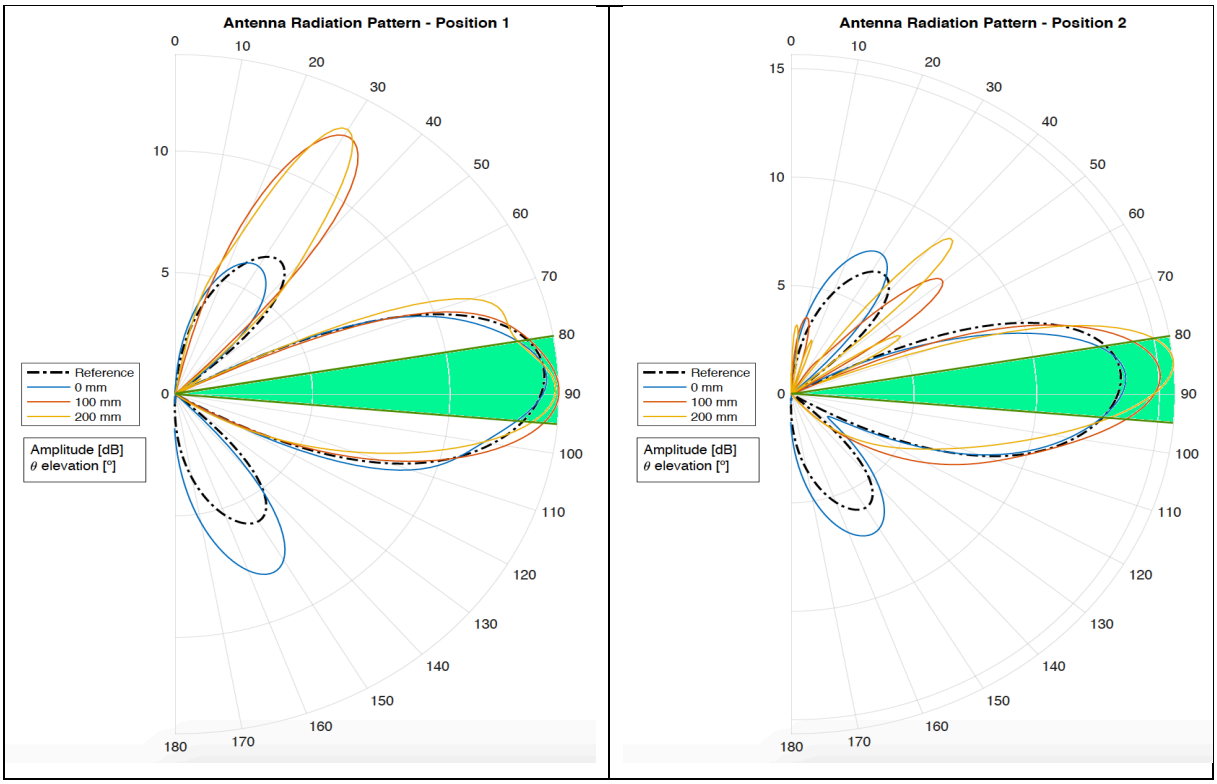

(a) Maximum height position available. (b) Minimum height position available.

Figure 4.28 Polar view of BBRS antenna with the depth and height variation.

One presents the most important results of each simulation in Table 4.5 and Table 4.6. As expected, the subway structure has an impact in the elevation gain direction. The reference value is 86º, which is almost the same as the “0 mm” case with θ = 87º. For “Position 1”, when one introduces 100 mm or 200 mm into the subway structure, this value converges to a more desirable performance (θ = 89º). For “Position 2”, the behaviour is slightly different. As sees in Table 4.6, the θ angle tends to decrease, which means an increase on the main love elevation due to the antenna being quite close to the PEC structure below. On the one hand, this behaviour must be avoided since the microstrip patch array starts to diverge from the best case scenario; on the another hand, one observes improvements for the gain due to the reflections in the structure of the metro.

Table 4.5 BBRS antenna performance for “Position 1”.

	Gain [dBi]	θ direction [º]	α_{3dB} [º]	S_{11} [dB]
Reference	13.5	86	32.8	-13.9
0 mm	13.5	87	31.8	-25.7
100 mm	14.0	89	31.3	-19.5
200 mm	13.9	89	32.4	-19.6

Table 4.6 BBRS antenna performance for “Position 2”.

	Gain [dBi]	θ direction [º]	α_{3dB} [º]	S_{11} [dB]
Reference	13.5	86	32.8	-13.9
0 mm	13.7	86	28.2	-24.3
100 mm	15.1	85	24.8	-13.9
200 mm	15.6	84	20.1	-13.8

In conclusion, one sees that, according to the available boundaries to mount the antennas, no critical results are exceeding the threshold values that are acceptable for the gains of these on-board terminals. This means that all analysed positions do not have problems regarding the connection between terminals due to low gain provided by on-board antennas. However, some future complications may be avoided if one takes these results into consideration.

In “Position 2”, there is a clear compromise between the elevation direction of the main lobe and its gain. Comparing with the other case, “Position 1”, the gain only has an improvement around 1 dB. If this enhancement is not critical, the best decision is the “Position 1” case, where it has the optimal elevation direction with a proper gain and without significant interferences from the subway structure.

The last stage is to analyse what happens to antennas’ performance when one uses spatial diversity. For that, one added a new port with an identical 2-by-2 rectangular microstrip patch array, and the two terminals were spaced by greatest length possible, 2 m, which is, proximally, 40 λ. This means the signals received from each antenna are uncorrelated and improvements of spatial diversity will be reached. Nevertheless, this maximum distance between on-board terminals brings others physical parameters to be aware of. For this particular scenario, the critical concern is the lateral limits of the subway. Figure 4.29 presents a sight of what happens in this case. As it might be easily understandable, the main concern is not the elevation direction (θ), already analysed in the last study, but the main lobe horizontal direction (φ), which might suffer some distortion or deviation for the lobe direction due to the reflections on the lateral PEC structure.

In order to understand the effects of the metro’s structure when it approaches the lateral physical limits, the data obtained in the CST simulation was imported to MABLAB. Having as reference the optimal case of the antenna position regarding its depth and height (“Position 1” with 100 mm of depth), one compared with the extreme allowed case when the system has diversity, and that is at 0.5 m from the lateral metro structure. Besides the expected differences on the behaviour of the secondary lobes, in Figure 4.30 one addresses the azimuth plane (horizontal view with θ = 90), where it is possible to observe the main lobes’ performance. For the BBRS antenna working frequency of 5.9 GHz, a distance of 0.5 m means, approximately, 10λ, hence the differences in their performance are not substantial. On the one hand, the reference has a maximum gain of 14 dBi with its direction at φ = 90º, a α_{3dB} of 30.8º and a L_{SLL} of -11 dB. On the other hand, when the antenna is shifted to the left, it has a maximum gain

of 13.9 dBi, also, at φ = 90º, a α_{3dB} of 31.8º and a L_{SLL} of -11.5 dB. Since that these results are very similar, an exhaustive analysis does not provide extra knowledge, however it is always a good practise to support the performance with exact methods, and with that purpose one calculated the associated RMSE between the curves of Figure 4.30, which is 0.12 dBi. With these results, one concludes that there is no problem to mount these antennas at the maximum distance allowed from the metro's lateral structure (0.5 m) in order to benefit from the spatial diversity implemented in this system.

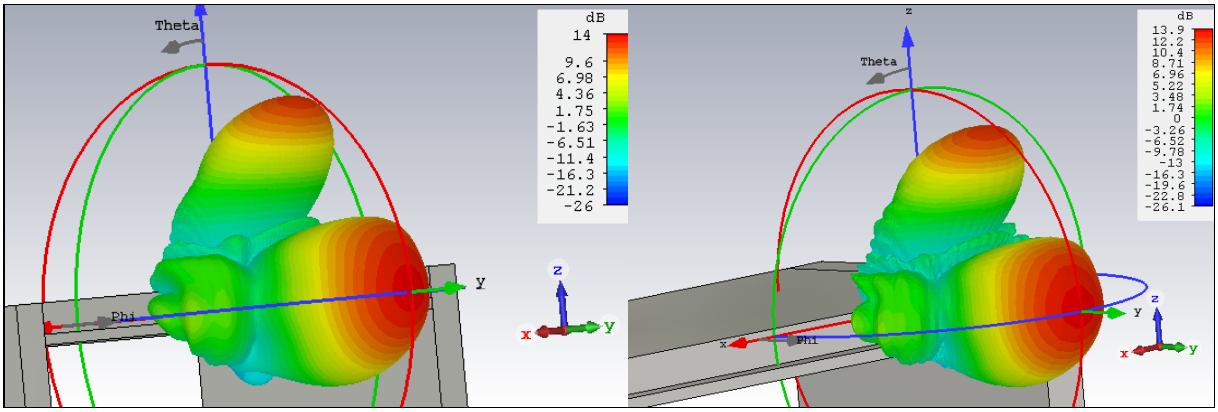

(a) Farfield at "Position 1" and 100 mm of depth.

(b) Farfield shifting the BBRS antenna to the left.

Figure 4.29 BBRS antenna 3D farfield performance at different positions.

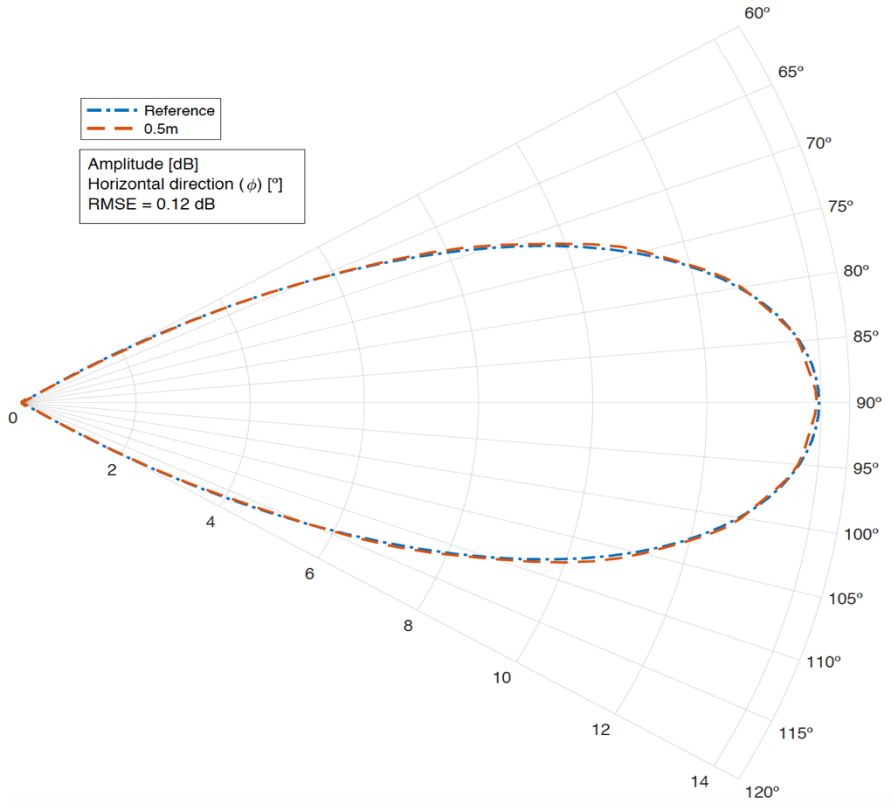

Figure 4.30 The main lobe for θ=90° with the antenna in the middle and 0.5 m from train side.

Chapter 5

Conclusions

This chapter draws the final conclusions of the thesis. It is summarised all the work developed, main conclusions and aspects that may be developed in future works.

The main purpose of this thesis was to evaluate the influence of the surrounding railways' environments in the performance of the antennas for mobile communications systems in trains that are in usage nowadays, and for the ones that are seen as the future of railway communication systems that are already implemented in some contemporary networks. To achieve this objective, a general model was developed to respect all the physical restrictions of the scenarios and several simulations were executed with the support an EM software tool, CST, evaluating the impact of different structures present on the rooftop of trains. The outcome from these simulations allows to perform a thorough analysis about the effect of curve rooftops or pure obstructions due to air-conditioning units, as well as the presence of the boundaries of the train structures in a subway environment with directional antennas.

This thesis starts with Chapter 1, where one presents a brief explanation of the mobile communication evolution until these days, and the respective context of their growth on the railways' settings, followed by an indication of the available railway market to explore new opportunities. Finally, the motivations to perform this work are clarified, along with the thesis' organisation and a short explanation of its contents.

Chapter 2 begins by introducing an overview of railway communications, identifying their most critical characteristics, which are undoubtedly related to safety issues through the ATP system, more precisely, ETCS. Additionally to that, one also mentions the rigorous requirements for railway communications based on EIRENE's system specifications, and the different types of railway scenarios, such as, the train-to-infrastructure link that is the main focus of this work. Afterwards, a theoretical background on the three railway communication systems under study (GSM-R, LTE-R and BBRS) is presented, explaining each network architecture, radio interface and the services that they are able to offer. Then, a description of the main parameters of mobile communications are explained, with special attention to the antennas parameters that are the ones to be analysed in the thesis. The last section of this chapter is the state of the art, presenting works already performed and theirs results, which will help to achieve the goals proposed by this thesis, regarding the positions of antennas on trains.

Chapter 3 contains an overview of the developed model, describing the input and output parameters to be considered for model assessment. The model depends on two different types of input parameters, the antennas settings and the surrounding scenario. The firsts ones change according to the particular system under study, adjusting the antennas' dimensions to the working frequencies. The second one concerns antennas' position and distance between them and the surrounding structures, which may have impact on their performance. To implement these parameters, one used Antenna Magus to design the antennas and the CST tool to simulate the scenarios under study, analysing the antennas' performance through their radiation pattern, α_{3dB}, reflection coefficient, among other parameters. Moreover, a theoretical approach is presented regarding the environment where the antennas are mounted, a flat metallic ground, where one describes the image theory and its implications on using vertical and horizontal dipoles. An explanation of how CST works is also presented, mentioning the main solvers and the most important features to be aware of. Then, one addresses the most frequent railway environments, regarding trains' carriages (roof train curvature, longitudinal strengthening bars, sunken roofs, HVAC units and pantographs), explaining the main problems for each specific physical characteristics.

The last section concerns antennas to use for the simulations in this work. Before implementing the antennas on particular cases of interest, one explains that the solver used in CST, the Time Domain Solver, and the settings applied to the meshcells properties. One also shows that all the three monopoles are well matched with the reflection coefficient below -10 dB, and the gains are near to the expected theoretical gain of a monopole working above an infinite ground plane, 5.16 dBi. Since there are three distinctive systems that are studied, one provides the specific physical dimensions of each monopole regarding their particular working frequency. The wavelength of GSM-R, LTE-R and BBRS are 333.1 mm, 115.3 mm and 50.81 mm, respectively.

Since simulations may last several hours, the next step taken was to understand how far does it make sense to analyse the surrounding environment, in order to minimise its simulation time without having an unsatisfactory accuracy of results. To accomplish this analysis, one used the monopole of GSM-R, for 900 MHz, and as a reference performance, one considered the results from the theoretical outcomes with a conducting wall to play the role of an infinite plane. Five simulations were made varying the squared ground area where the monopole is mounted. The areas under analysis are controlled by the wavelength associated to its working frequency (900 MHz), so that it is possible to relate to the areas of the others systems under evaluation. Thus, the monopole was simulated for 1.5 λ x 1.5 λ, and 5λ x 5 λ, 15λ x 15 λ, 25λ x 25 λ, 40λ x 40 λ. For geometrical reasons, it is only necessary to study two horizontal perspectives (φ = 0º and φ = 45º). The analysis is done through the evaluation of the behaviour of gains, α_{3dB}, L_{SLL}, number of meshcells and their simulation times. One provides the relation between the absolute error of each case, and also shows theirs surface current behaviour, which are presented in Annex B. The decision taken to have a good compromise between simulation time and problem accuracy was a ground area of 15λ x 15λ, which takes 1 hours and 36 seconds to run, and has an average error of 1.19 dB for φ = 0º and 1.68 dB for φ = 45º.

Chapter 4 begins with a description of the reference scenario considered in this thesis, mentioning the on-track and on-board settings, as well as, the standard dimensions of the train model used on CST simulations. Furthermore, one shows crucial perspectives (elevation and azimuth plane) to take into account the link between the on-board and on-track antennas, to accomplish an accurate analysis of their performance in specific circumstances.

Thereafter, a study towards the understanding of how antennas' performance change when the ground where the monopoles are implemented changes from a flat surface to a curved one. Firstly, one created from scratch a 3D model of a curve surface to replicate a curve rooftop of a standard train with a width of 3.5 m, a length of 4 m and a height of 0.6 m. For each system under study, one considered as the reference performance the flat ground cases with an area of 15λ x 15λ, and one examined two critical horizontal perspectives: φ = 0º and φ = 90º. For 900 MHz and 2.6 GHz, there is a compromise between the gains and the α_{3dB} where it is present the curvature. Comparing the results of the flat and curve grounds, what happens is a gain deterioration in favour of a higher α_{3dB} angle. In other words, the strong linear omnidirectional characteristics of the flat ground case are lost, and a main lobe with less gain but with a larger α_{3dB} for elevation viewpoint is reached. For the LTE-R case, the same compromise

happens although with less impact. Besides that, with φ = 90º, the elevation angle, θ, goes from 73º (reference) to 65º, which, considering the scenario description, means an increment of 8º, and this is not desirable. Hence, for the 900 MHz and the 2.6 GHz, it is expected a disparity between the expected characteristics provided by the antennas' manufactures and their real performance with less gain but with higher α_{3dB}, more distinct for the lateral perspective (φ = 0º), and it depends on who is planning the antennas installation and what it is required for the system to regulate this compromise. For the 5.9 GHz case, although these differences are less pronounced, they still exist. Similarly to the LTE-R case, the more problematic issue is the elevation angle for φ = 90º, which goes from 74º (reference) to 65º. Despite that, the distance between BSs are smaller, then the LTE-R situation and the angles of interests are closer to the simulation values. This means that for the last case, BBRS, there are no critical complications to implement the monopole on a ground with this type of characteristics.

In the last section, one implemented the antennas in a realistic environment regarding a standard train carriage and examined the effects on the antennas' performance due to the presence of obstacles such as HVAC units for GSM-R and LTE-R. After that, one also executed a study regarding a particular case of a metro using the BBRS antennas with spatial diversity.

Regarding GSM-R, one ran 15 different simulations changing the antenna distance from the obstacle (for 0.5 m, 1 m, 1.5 m, 2 m, 2.5 m, 3 m and 3.5 m) and the HVAC unit height (for 25 cm and 45 cm). Besides these cases, one also simulated a specific situation where the train does not have any obstacle at the train rooftop to have the reference performance scenario. Results were evaluated for three horizontal directions: φ = 0º (right side of the train which have the same results of the left side, φ = 180º), φ = 90º (where the obstacle was fixed hence it is the most important view) and φ = 270º (opposite direction to the obstacle). For each azimuth direction two aspects were analysed: the main lobe gain and elevation angle (θ). For φ = 0º, the main lobe gain starts to be close from the reference value for a distance of 2 m from the HVAC unit for both HVAC's heights and its elevation performance does not have critical variations compared with the reference results. For φ = 90º, the main lobe results steadies at 1.5 m from the obstacles for both cases with losses near to -2 dB. The elevation direction also suffers from the obstacles presence, and starts to have acceptable results at 1.5 m for the HVAC unit with 25 cm, and 2 m for the obstruction with a height of 45 cm. For φ = 270º, the overall results are higher than the reference value of 6.52 dB, due to the occurrence of reflection in the obstacle surface, which does not happen for the reference simulation where the antenna is simulated on the rooftop train without any kind of obstacle. The only exceptions are the simulations at 0.5 m and 1 m from the HVAC unit with 25 cm of height, which present lower gains due to constructive and destructive phenomena for the exact direction of φ = 270º. Subsequently, it is not advised to implement the antenna closer than 1 m from the HVAC unit with 25 cm of height, while for the other case there is no major problem. Summarising the results obtained considering the three directions, and taking into account the fact the obstruction direction outcome (φ = 90º) has more weight, one recommends a safety distance of 1.5 m between the terminal and the obstacle with 25 cm of height, and a 2 m distance for a structure with 45 cm of height. Even thought, complying with these distances to mount the terminals, it will be possible to have losses around -4 dB.

For LTE-R, a similar analysis was performed taking into account the same azimuth directions (φ = 0º, φ = 90º and φ = 270º). One has done 11 different simulations varying the distance between the antenna and the obstacle (for 0.5 m, 1 m, 1.5 m, 2 m and 2.5 m) and for the exact same HVAC unit height used in the GSM-R case (25 cm and 45 cm). Additionally to these cases, one also created a simulation using this LTE-R antenna without obstacles to obtain the reference values in this situation. For φ = 0º, the results due to the presence of the HVAC units do not have great influence on the main lobe performance or on its elevation angle. Even though the obtained gains are closest to the reference for the HVAC unit with 25 cm, the outcome for the obstruction with 45 cm of height never reaches values with a difference of more than 1 dB. Moreover, elevation angles variations are minimal, having just more 3º than the reference value, therefore for LTE-R there are no major problems with the presence of these types of obstacles. For φ = 90º, the main lobe gains are always bellow the reference of 6.63 dBi, revealing the fact that the presence of the obstacles have a negative contribution for the on-board antennas' signal, as expected. Simulations show that in critical situations when antennas are at a distance of 0.5 m from obstacles, losses may reach differences of - 4.94 dB for the obstacle with 25 cm of height, since the reference value is 6.63 dBi, and a difference of -8.07 dB for the HVAC unit with a height of 45 cm. One reaches a saturation level concerning the minimal losses of -1.5 dB at 1 m from the HVAC units, for the structure with 25 cm of height, and 1.5 m for the obstacle with an height of 45 cm. For the main lobe elevation angle, one concludes that for the HVAC with 25 cm of height results are close to the reference of 73º at distances of 1.5 m or more, and for HVAC with 45 cm it is needed to reach a space between the terminal and the obstacle of 2 m. For φ=270º, simulations show that main lobe gains are always above the reference of 6.63 dBi, due to the advantage of having an extra area where the EM waves may be reflected the signal, which is the HVAC unit that is present on φ=90º. As expected, the maximum gain is obtained for HVAC with 45 cm of height, since it has a bigger area where the signal may be reflected, reaching 11.5 dBi. For the smaller HVAC unit performances has lower values compared with the other case, but the behaviour is very similar. When the distance starts to increase, gains decline and tend to 8 dBi, in both cases. Considering all simulations made for this system, for the main love gain and elevation, it is recommended to install the LTE- R antenna at a safety distance of 1 m from the HVAC unit with 25 cm of height or an obstruction with similar characteristics, and for obstacles with an height 45 cm, it is advised to mount the terminal with 1.5 m of distance from the obstruction due to results of the main lobe elevation performance.

For BBRS, another approach was taken. The study was based on a particular metro project for a subway scenario, which is distinctive from the situation under analysis for GSM-R and LTE- R. First of all, one designed an antenna similar to the Sencity® Spot-S WiFi used in the project, choosing a 2-by-2 rectangular microstrip patch array designed to work at 5.9 GHz. The terminal is mounted on the metro's front with some restrictions regarding the available space to install the antenna. Then, one performed an analysis with the terminal positioned in the middle of the train, regarding the train's width, only changing the maximum and minimum position of the antenna height ("Position 1" and "Position 2"), and varying the depth where the antenna is installed (0 mm, 100 mm and 200 mm). Since there are no obstacles and the distances between simulation are relatively small, the differences are not critical, with minor variations regarding the main lobe gain and its elevation. Even it performance differences are

small, the best position possible is “Position 1” with a depth of 100 mm, which provides a gain of 14 dBi with an elevation of 89º. The next step was to analyse if there are complications when spatial diversity is used, since it implies a lateral swift of the terminal under analysis to apply more antennas. With this goal, one simulated the critical case regarding the train’s physical restrictions. The minimum distance allowed between the antenna and the train’s lateral side is of 0.5 m, and simulation results show that for this restriction the main lobe performance is almost equal to the reference case, which was considered as the terminal at the middle of the train’s width with the best performance (“Position 1” with 100 mm of depth). The RMSE between the two main lobe is 0.33 dB for the azimuth perspective, proving that the main lobe direction is not problematic and the spatial diversity can be implemented without future complications concerning the physical train limitations to mount the antennas.

This work may be complemented in several other perspectives that will provide additional value to what was study with the purpose of improving the railway communications system, more precisely, the on-board antennas implemented on trains. First, the same problem presented in this work may be studied using other frequencies, and consequently for other communication systems, such as TETRA, which is typically used by government agencies and emergency services. This particular system may be worth studying, since some of the standardised working frequencies are much lower than the 900 MHz analysed for GSM-R. Secondly, it would be very interesting to scrutinise the effects on the on-board terminals due to the presence of the pantograph, not only for the physical obstructions that may occur but also due to possible interferences when energy is transferred from the catenary to the pantograph itself. Finally, it would be quite stimulating from the academic viewpoint to perform measurements of what was done in this thesis to understand if results are in agreement with conclusions.

Annex A

Theoretical Performance

This annex presents the meshcells view used in CST, as well as the S_{11} performance and the gain patterns for 2D and 3D views regarding the monopoles frequencies of the three different systems analysis (GSM- R, LTE-R and BBRS). The simulations consider the ground as a conducting wall to have results similar to an infinite ground plane.

A.1 GSM-R (900 MHz)

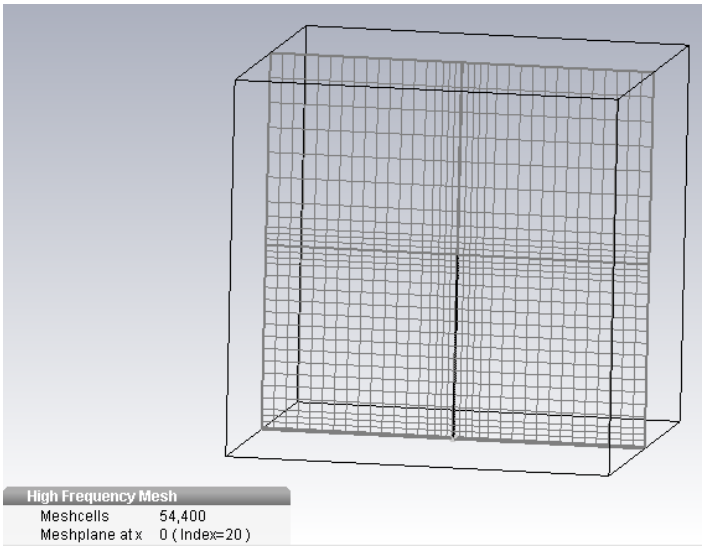

Figure A.1 Mesh view of a λ/4 monopole working at 900 MHz.

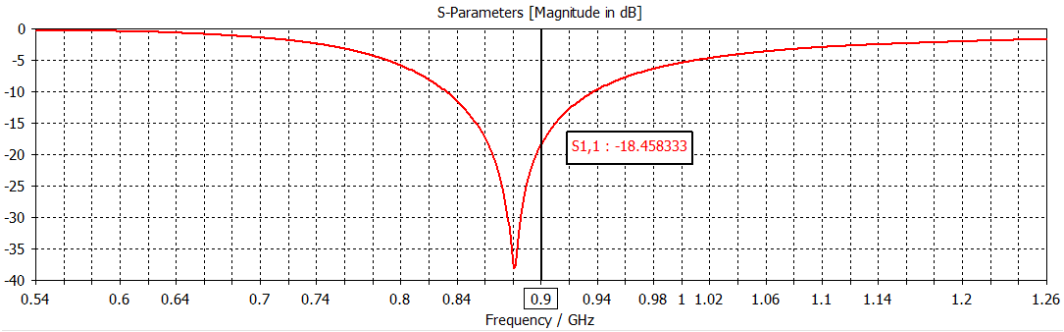

Figure A.2 S_{11} parameter of the theoretical λ/4 monopole at 900 MHz.

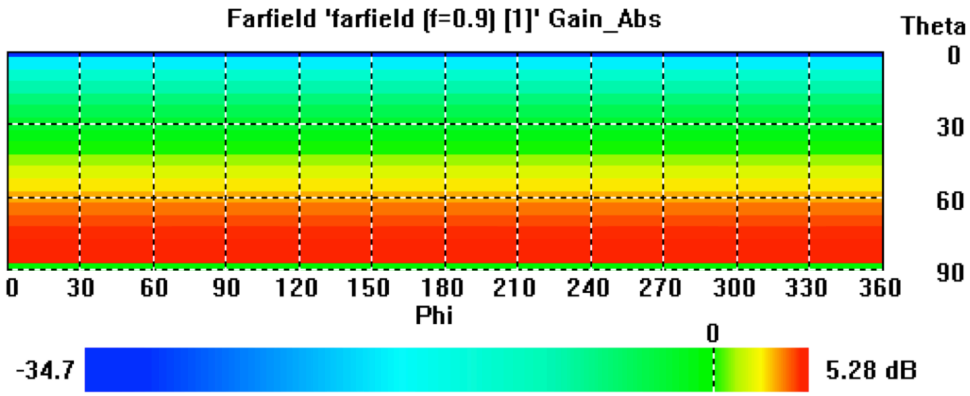

Figure A.3 The theoretical 2D performance for the λ/4 monopole at 900 MHz.

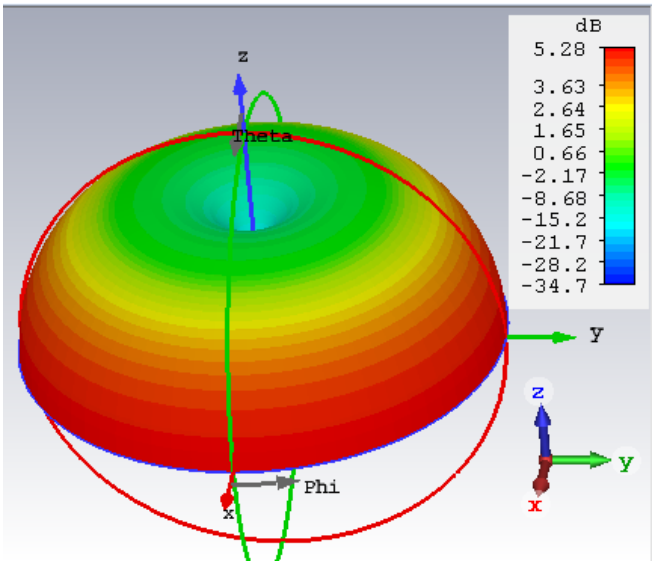

Figure A.4 The theoretical 3D performance for the λ/4 monopole at 900 MHz.

A.2 LTE-R (2.6 GHz)

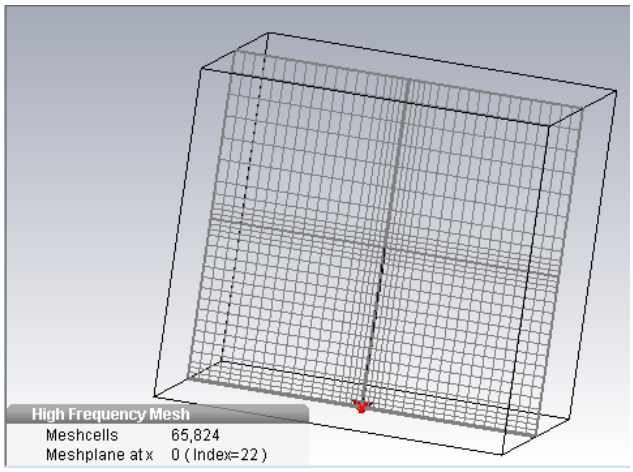

Figure A.5 Mesh view of a λ/4 monopole working at 2.6 GHz

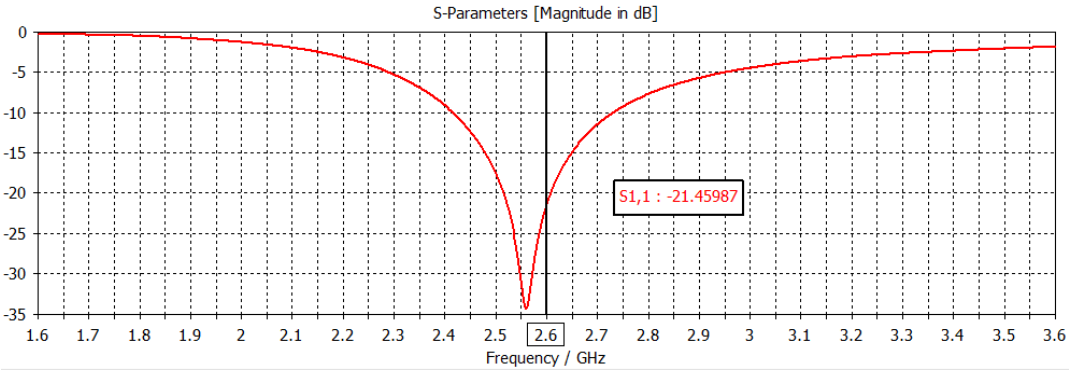

Figure A.6 S_{11} parameter of the theoretical λ/4 monopole at 2.6 GHz.

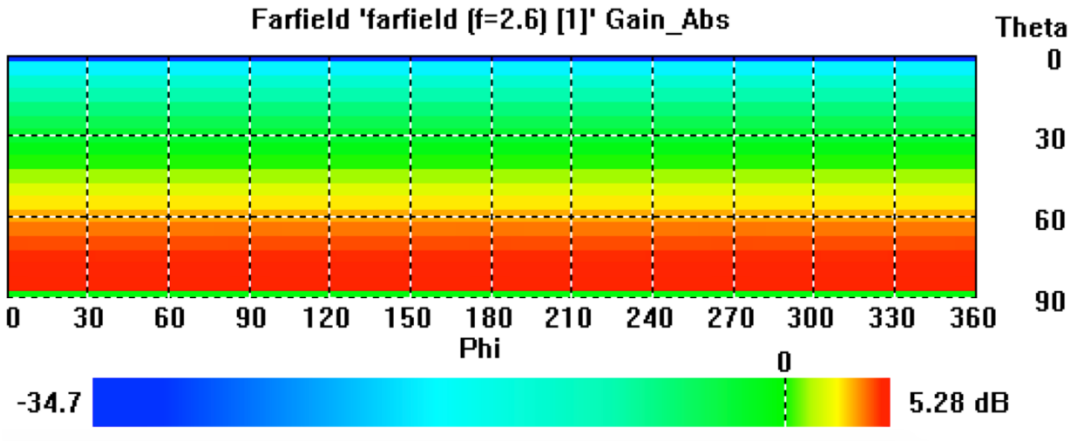

Figure A.7 The theoretical 2D performance for the λ/4 monopole at 2.6 GHz

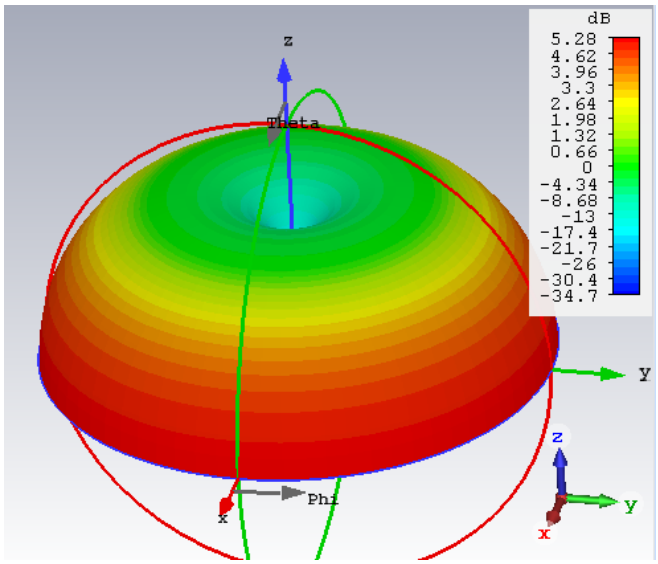

Figure A.8 The theoretical 3D performance for the λ/4 monopole at 2.6 GHz

A.3 BBRS (5.9 GHz)

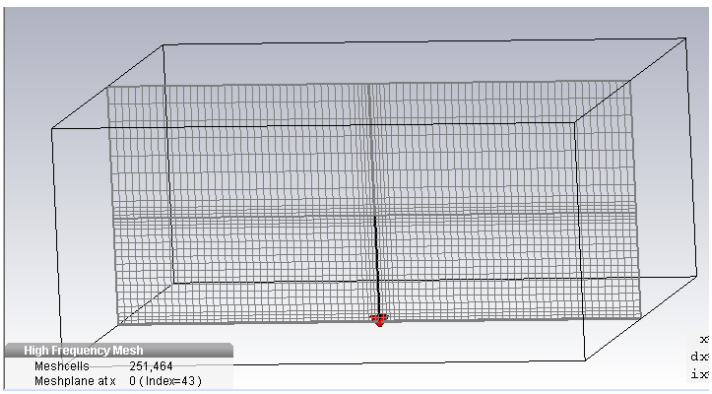

Figure A.9 Mesh view of a λ/4 monopole working at 5.9 GHz.

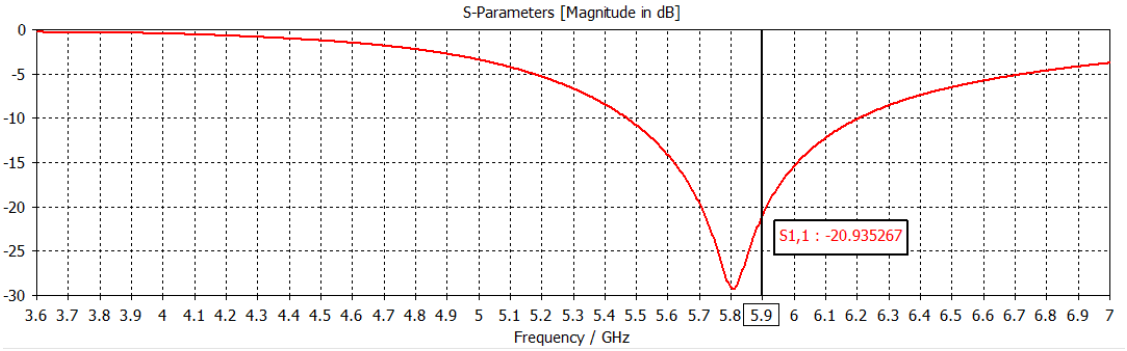

Figure A.10 S_{11} parameter of the theoretical λ/4 monopole at 5.9 GHz.

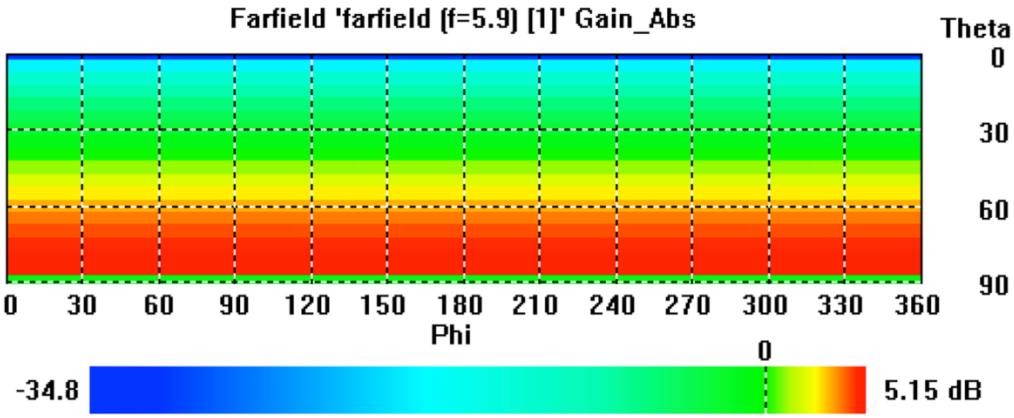

Figure A.11 The theoretical 2D performance for the λ/4 monopole at 5.9 GHz.

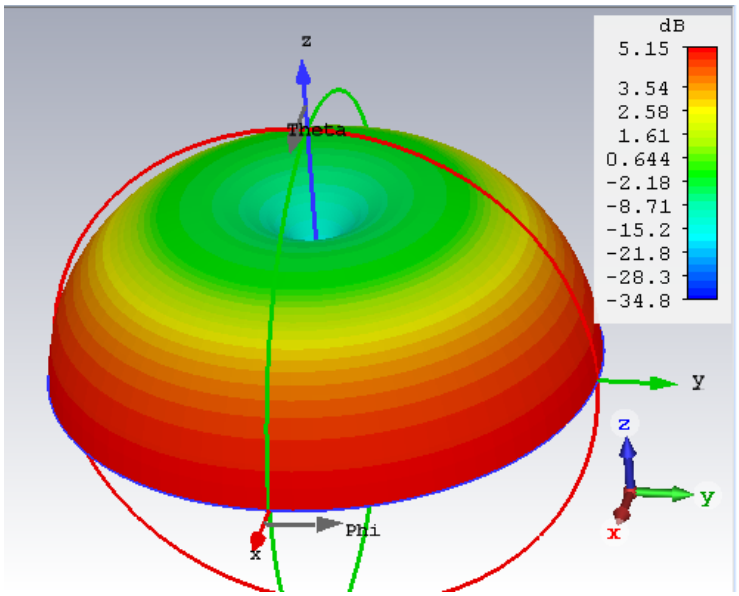

Figure A.12 The theoretical 3D performance for the λ/4 monopole at 5.9 GHz.

Annex B

Study of Antennas' Boundaries

Study of Antennas' Boundaries

This annex presents the performance of monopoles when the ground area changes, displaying different perspectives such as the 2D and 3D performances and the surface current.

.

B.1 The 2D performance with a ground area variation

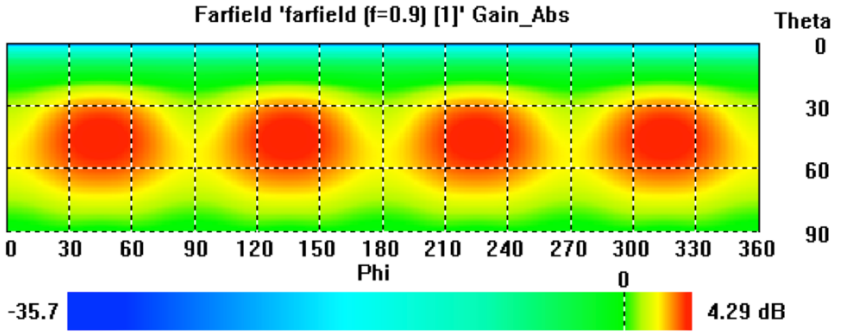

Figure B.1. The 2D farfield view for a squared plane of 1.5λ x 1.5λ at 900 MHz.

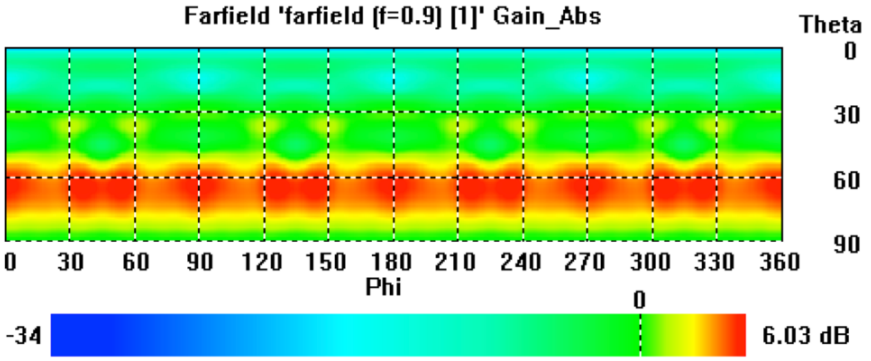

Figure B.2. The 2D farfield view for a squared plane of 5λ x 5λ at 900 MHz.

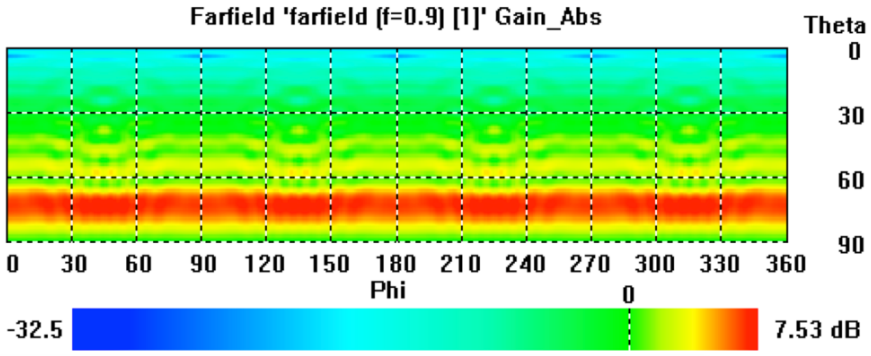

Figure B.3. The 2D farfield view for a squared plane of 15λ x 15λ at 900 MHz.

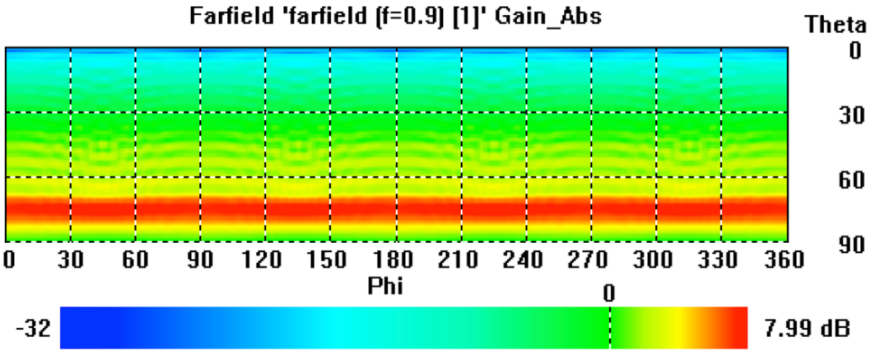

Figure B.4. The 2D farfield view for a squared plane of 25λ x 25λ at 900 MHz.

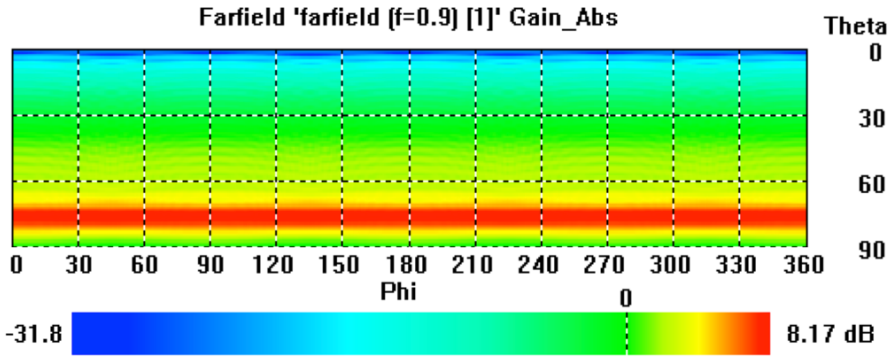

Figure B.5. The 2D farfield view for a squared plane of 40λ x 40λ at 900 MHz.

B.2 The 3D performance with a ground area variation

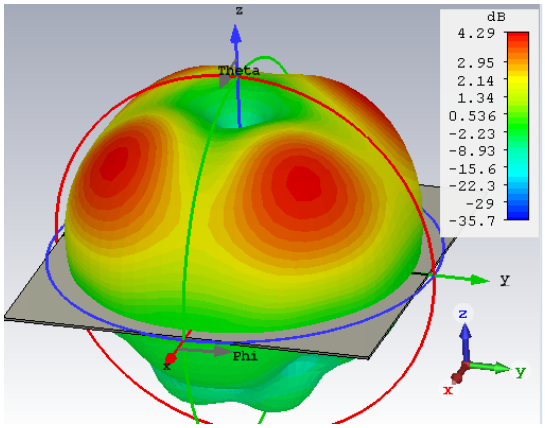

(a) Squared plane of 1.5λ x 1.5λ

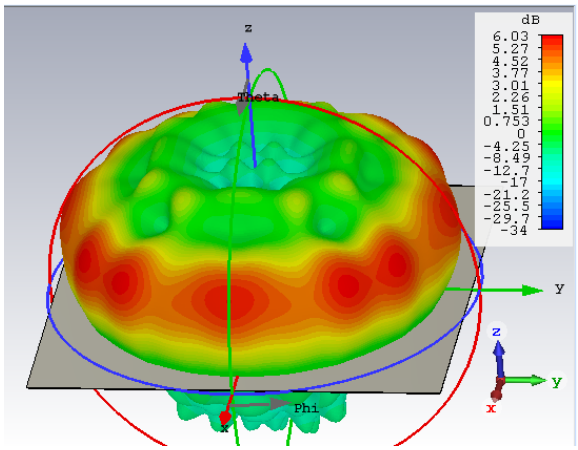

(b) Squared plane of 5λ x 5λ

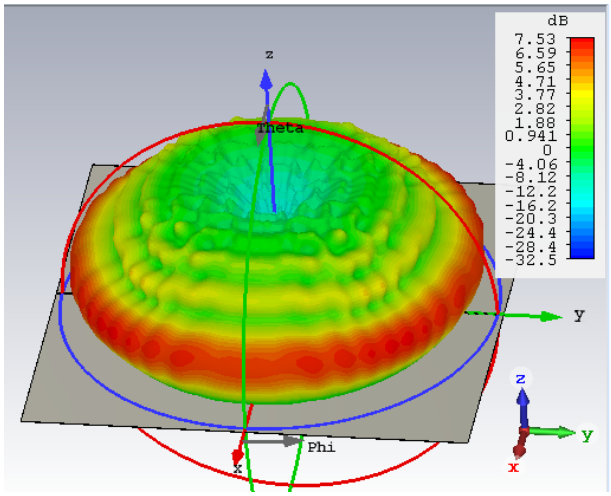

(c) Squared plane of 15λ x 15λ

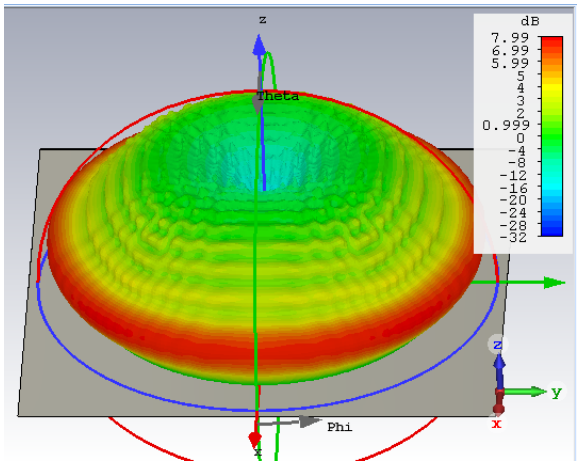

(d) Squared plane of 25λ x 25λ

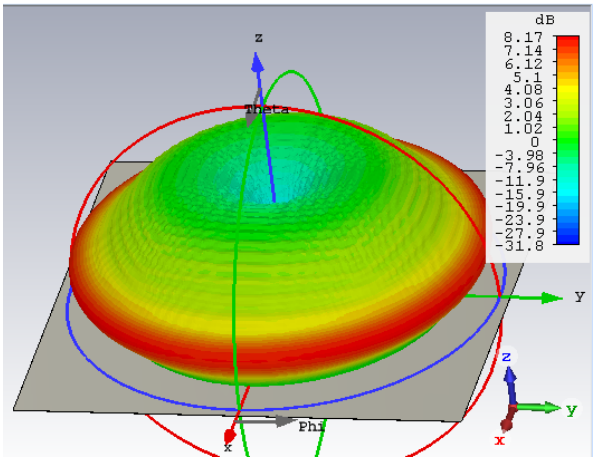

(e) Squared plane of 40λ x 40λ

Figure B.6 The 3D farfield view for grounds with different dimension at 900 MHz.

B.3 The surface current with a ground area variation

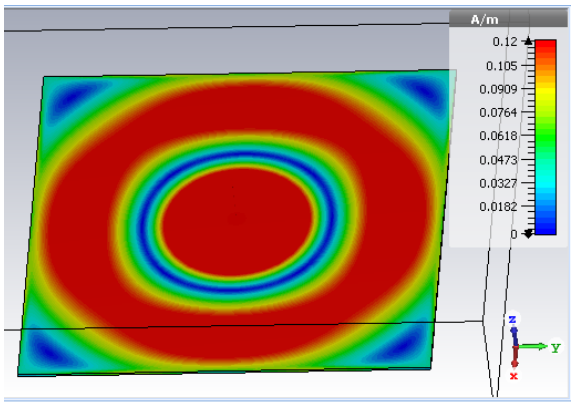

(a) Squared plane of 1.5λ x 1.5λ

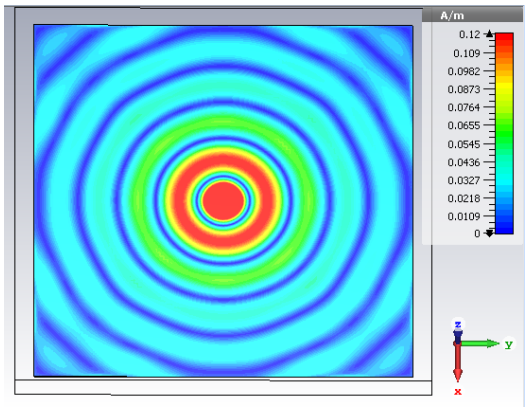

(b) Squared plane of 5λ x 5λ

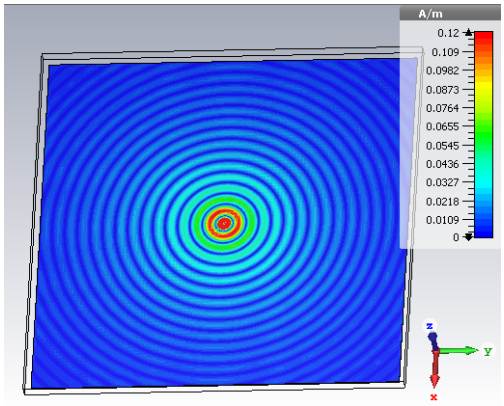

(c) Squared plane of 15λ x 15λ

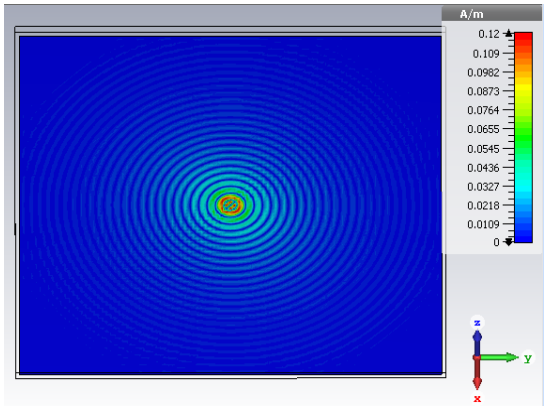

(d) Squared plane of 25λ x 25λ

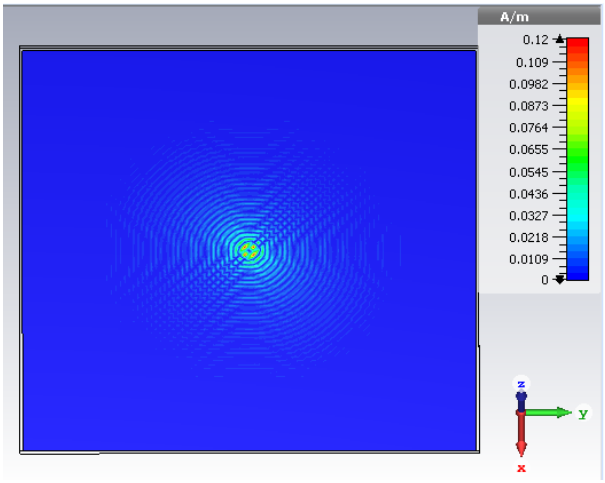

(e) Squared plane of 40λ x 40λ

Figure B.7 The surface current for grounds with different dimension at 900 MHz.

Annex C

Curve Ground Performance

Curve Ground Performance

This annex provides an overview regarding the monopoles behaviour performance when they are installed above a ground with curve characteristics, for each system under study (GSM-R, LTE-R and BBRS).

C.1 GSM-R (900 MHz)

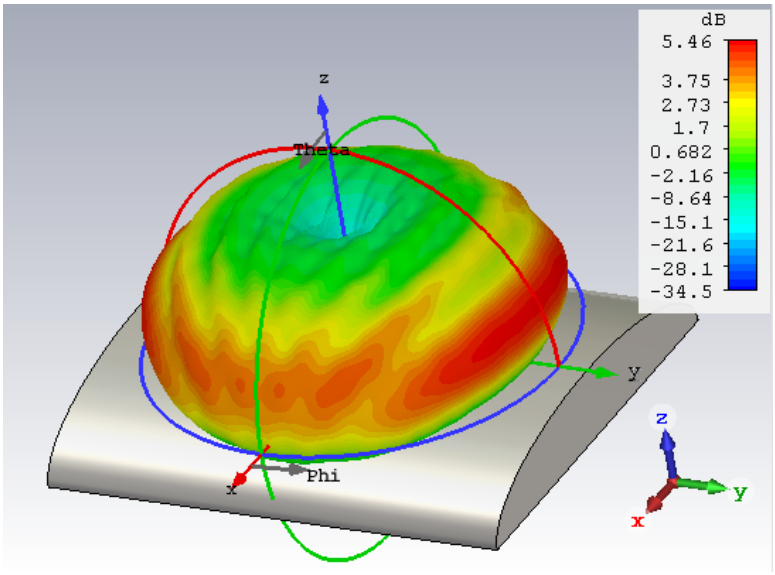

Figure C.1 The farfield performance under a curved ground for the λ/4 monopole at 900 MHz.

C.2 LTE-R (2.6 GHz)

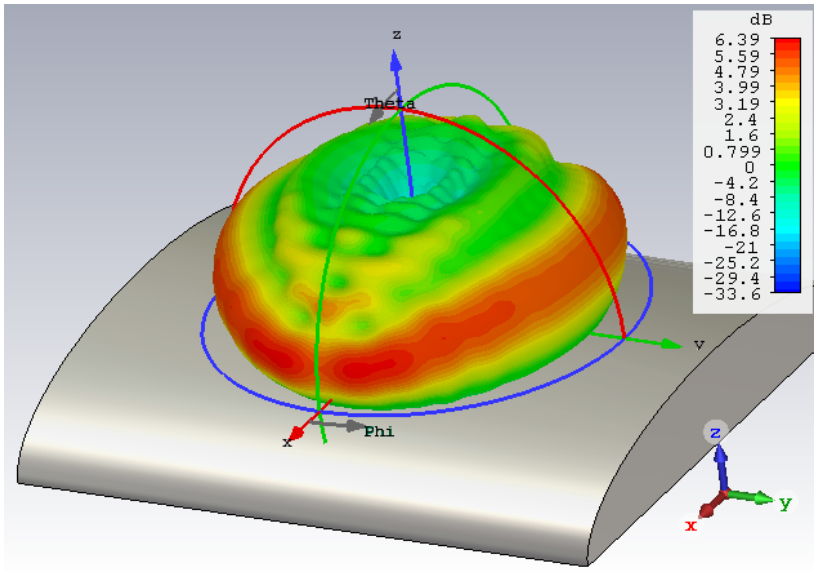

Figure C.2 The farfield performance under a curved ground for the λ/4 monopole at 2.6 GHz.

C.3 BBRS (5.9 GHz)

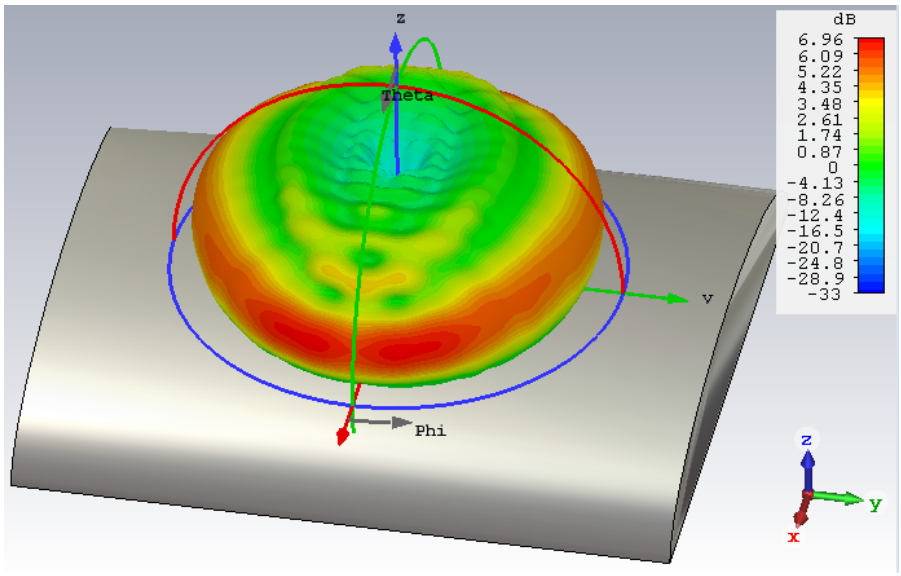

Figure C.3 The farfield performance under a curved ground for the λ/4 monopole at 5.9 GHz.

Annex D

Antennas' Specifications

This annex includes antennas that are used in railways projects with specific characteristics for each system under study (GSM-R, LTE,R and BBRS), presenting the specifications and the gain patterns for the vertical and horizontal planes.

D.1 GSM-R antenna

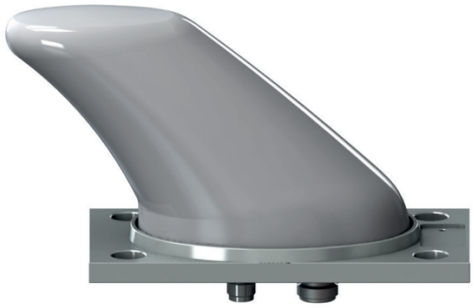

Figure D.1 BGLI antenna (extracted from [Polo16]).

Table D.1. Antenna specifications (extracted from [Polo16]).

Frequency band [MHz]	876-960
Polarisation	Vertical
Characteristic impedance [Ω]	50
VSWR (on a metallic plane 60x60 cm)	<1,7:1
Gain (over λ/4 monopole) [dB]	0
Dimensions (Height x Width x Depth) [mm]	98 x 80 x 145

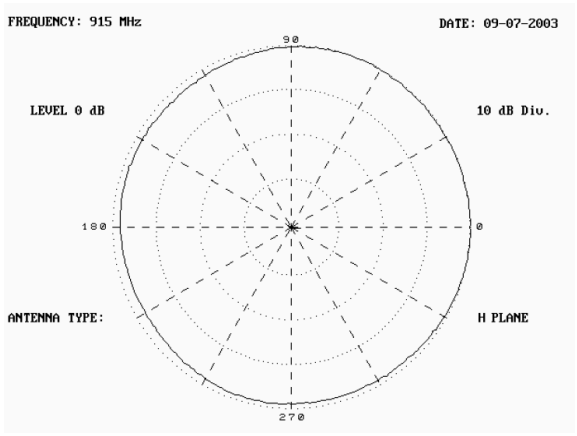

(a) Horizontal plane.

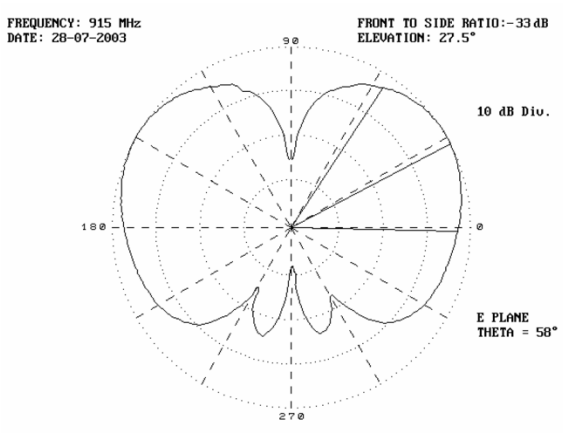

(b) Vertical plane.

Figure D.2 Radiation pattern at 915 MHz (extracted from [BGLI10]).

D.2 LTE-R antenna

Figure D.3 Sencity Rail Antenna (extracted from [Hube17]).

Table D.2. Antenna specifications (extracted from [Hube17]).

Frequency band (4) [MHz]	2700 - 3300
VSWR	1.5
Gain [dBi]	6.5
Nominal impedance [Ω]	50.0
Polarisation	Vertical
Dimensions (Height x Width x Depth) [mm]	154 x 100 x 256

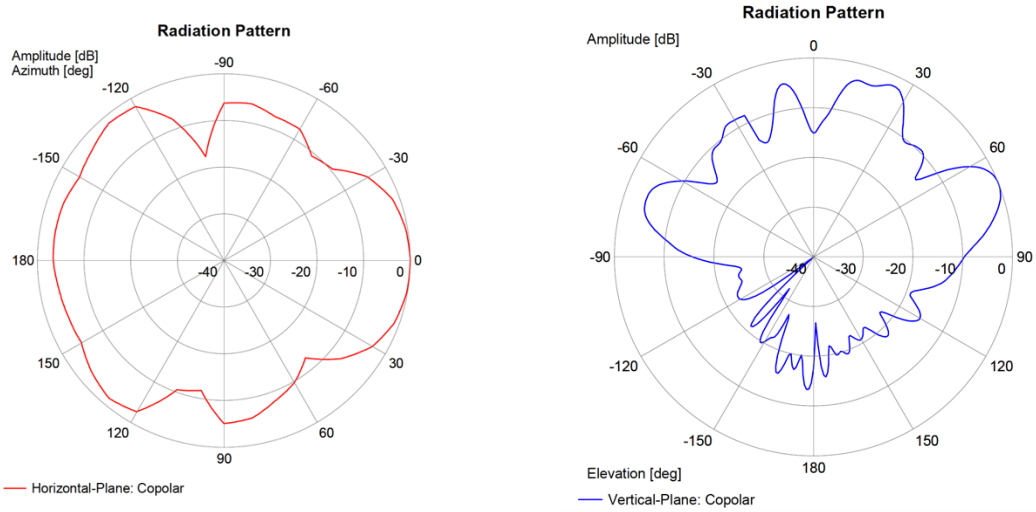

(a) Horizontal plane. (b) Vertical plane.

Figure D.4 Radiation pattern at 2.6 GHz (extracted from [Hube17]).

D.3 BBRS antenna

Figure D.5 Sencity Spot- S WiFi Antenna (extracted from [Hube09b]).

Table D.3. Antenna specifications (extracted from [Hube09b]).

Frequency band [MHz]	5150 - 5970
VSWR	1.5
Gain [dBi]	14.0
3 dB beamwidth (h) [º]	40.0
3 dB beamwidth (v) [º]	35.0
Nominal impedance [Ω]	50.0
Polarisation	Vertical
Dimensions (Height x Width x Depth) [mm]	101 x 80 x 35

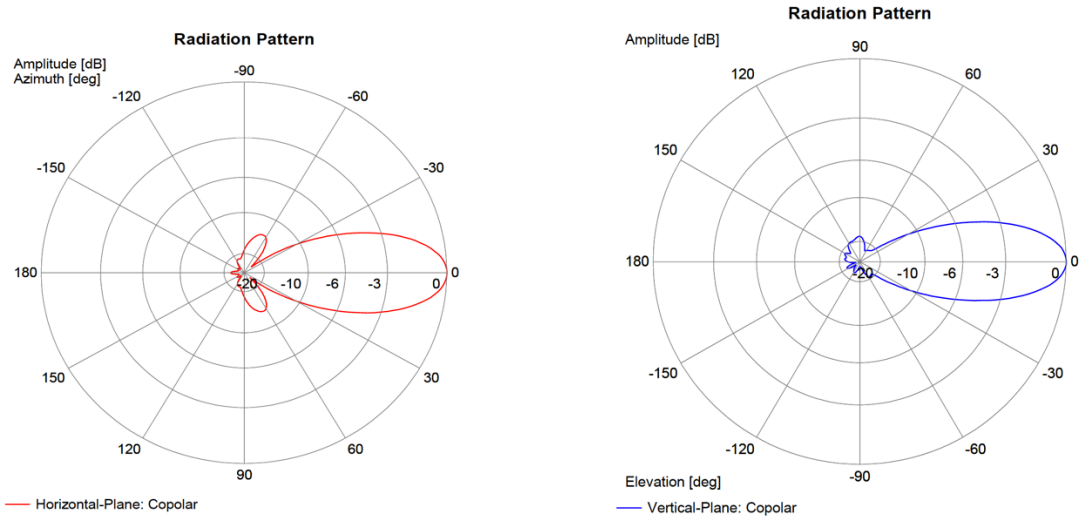

(a) Horizontal plane. (b) Vertical plane.

Figure D.6 Radiation pattern at 5.9 GHz (extracted from [Hube09b]).

Annex E

Realistic Approach

This annex demonstrates the performance results obtained in CST regarding the detailed scenarios of section 4.3.

E.1 GSM-R (900 MHz)

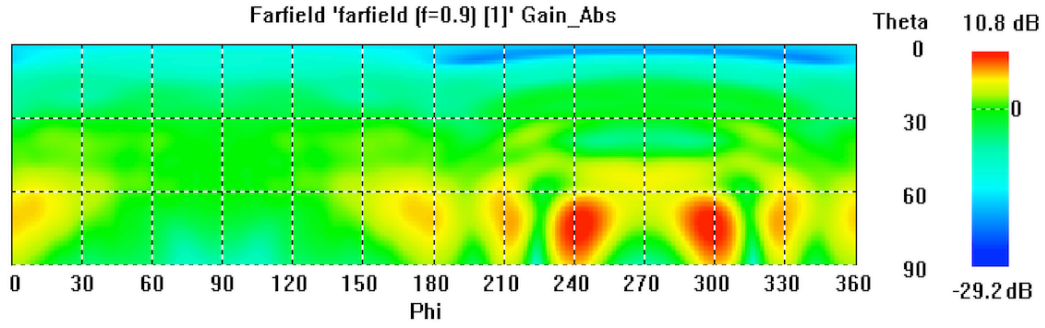

Figure E.1. Farfield for a distance of 0.5 m from a 25 cm height HVAC unit at 900 MHz.

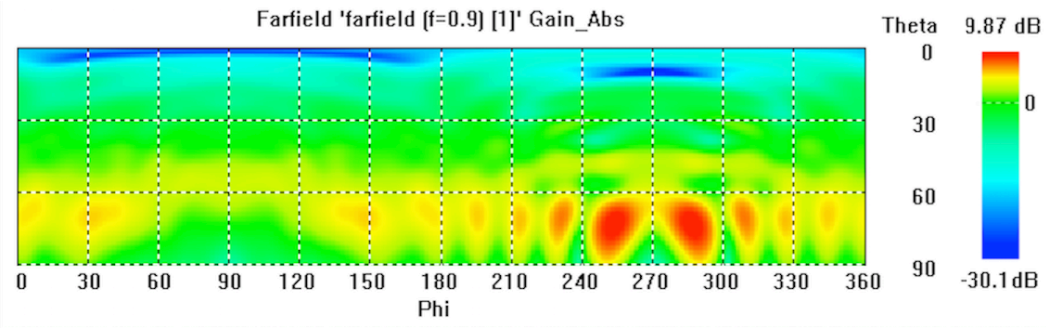

Figure E.2. Farfield for a distance of 1 m from a 25 cm height HVAC unit at 900 MHz.

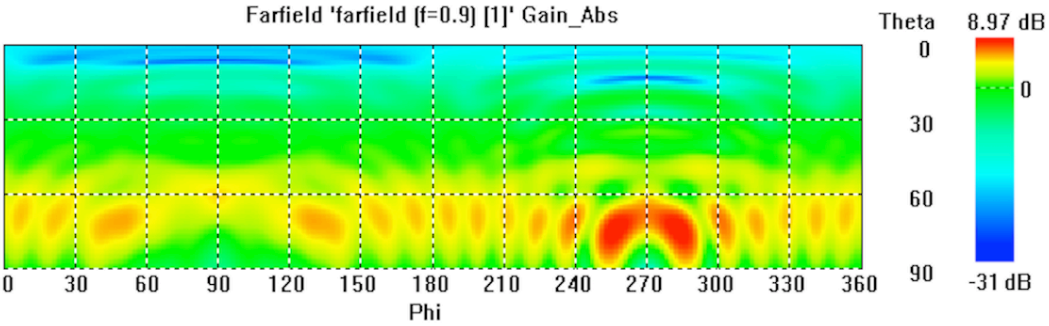

Figure E.3. Farfield for a distance of 1.5 m from a 25 cm height HVAC unit at 900 MHz.

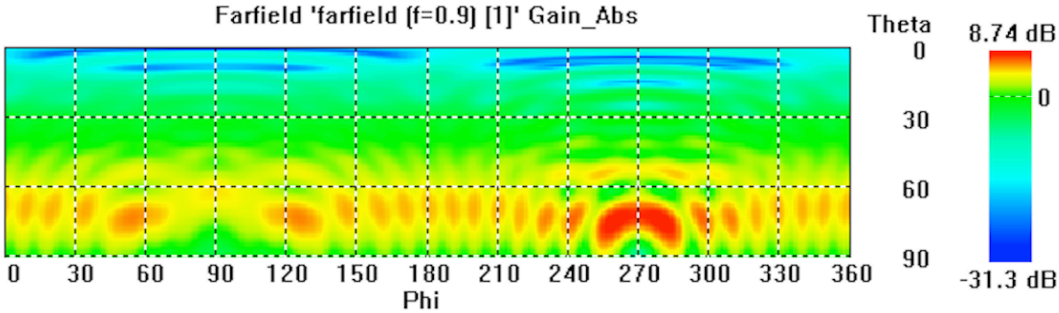

Figure E.4. Farfield for a distance of 2 m from a 25 cm height HVAC unit at 900 MHz.

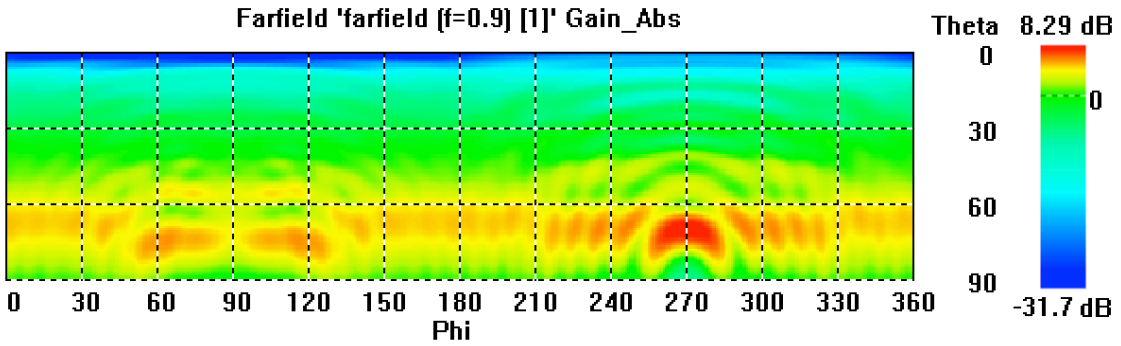

Figure E.5. Farfield for a distance of 2.5 m from a 25 cm height HVAC unit at 900 MHz.

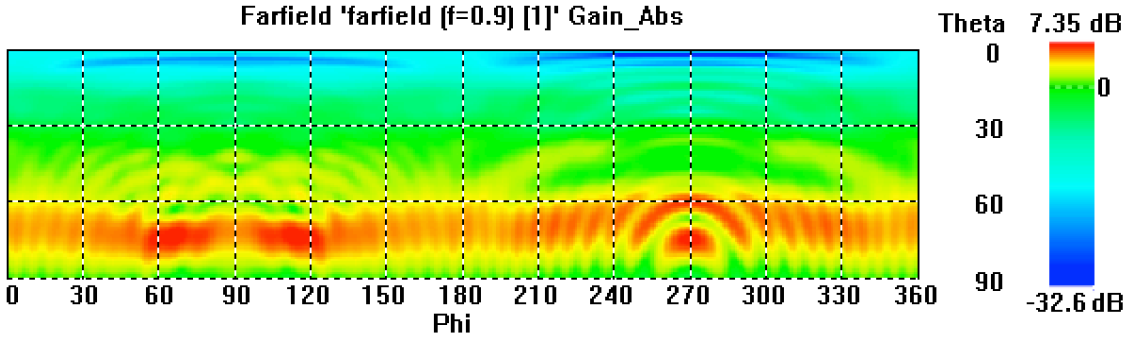

Figure E.6. Farfield for a distance of 3 m from a 25 cm height HVAC unit at 900 MHz.

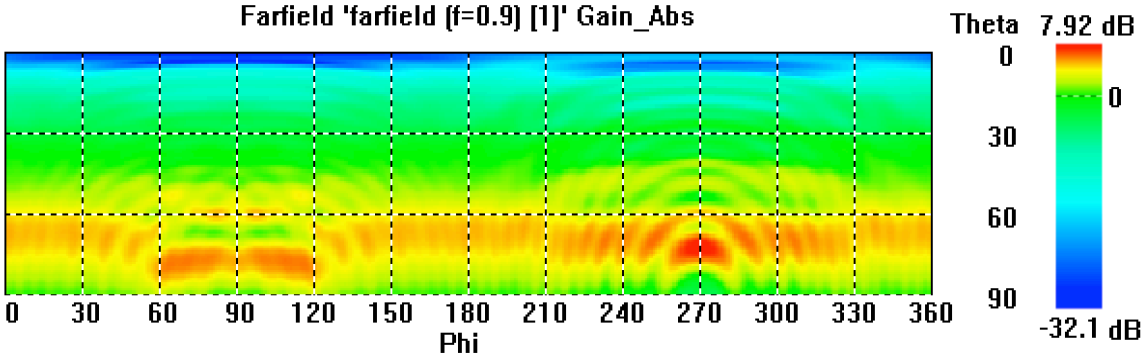

Figure E.7. Farfield for a distance of 3.5 m from a 25 cm height HVAC unit at 900 MHz.

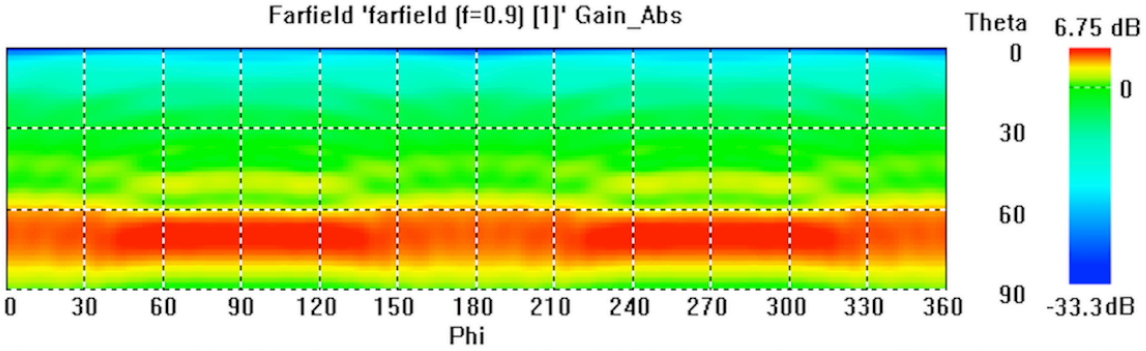

Figure E.8. Farfield performance for a rooftop without obstructions at 900 MHz.

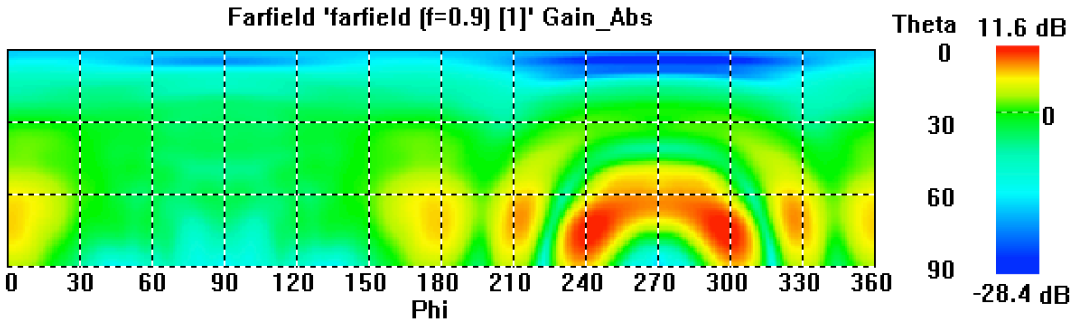

Figure E.9. Farfield for a distance of 0.5 m from a 45 cm height HVAC unit at 900 MHz.

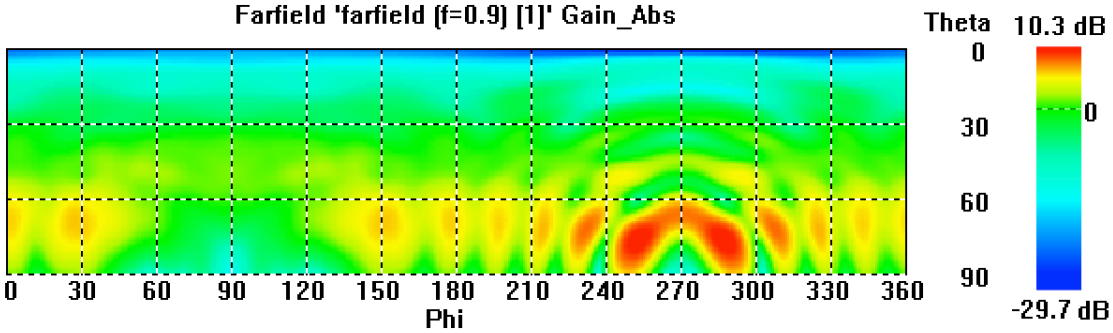

Figure E.10. Farfield for a distance of 1 m from a 45 cm height HVAC unit at 900 MHz.

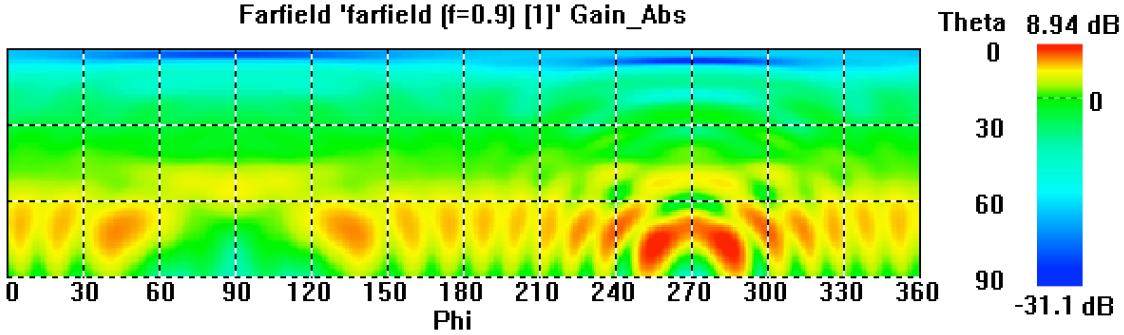

Figure E.11. Farfield for a distance of 1.5 m from a 45 cm height HVAC unit at 900 MHz.

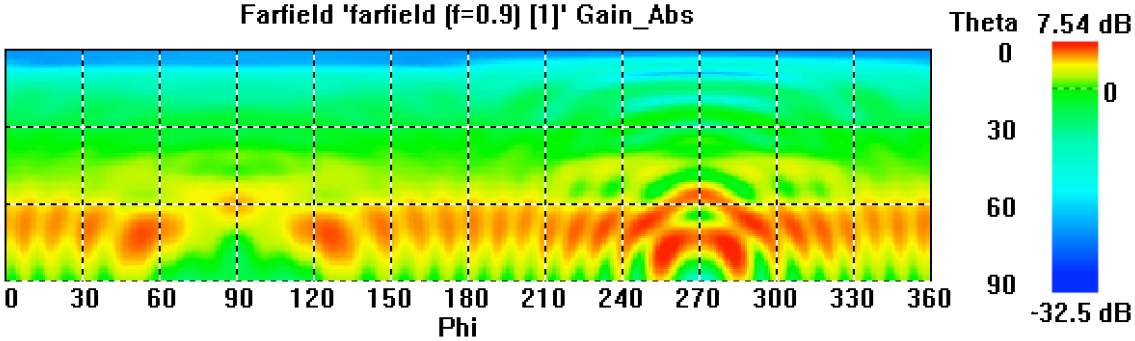

Figure E.12. Farfield for a distance of 2 m from a 45 cm height HVAC unit at 900 MHz.

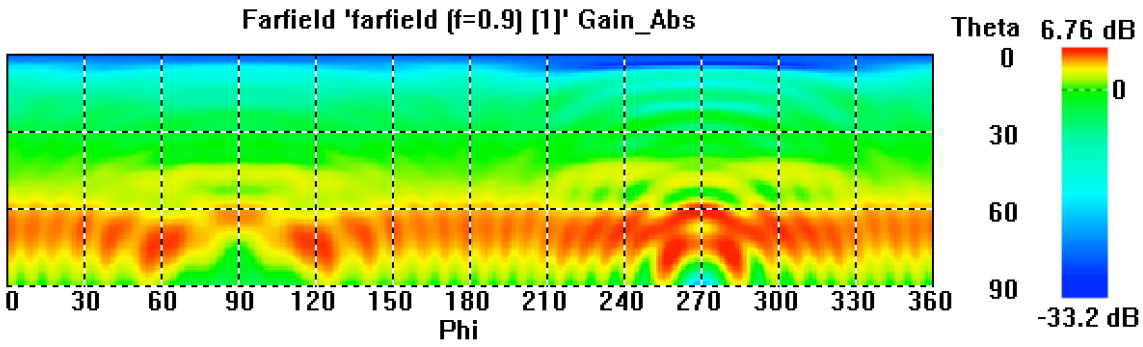

Figure E.13. Farfield for a distance of 2.5 m from a 45 cm height HVAC unit at 900 MHz.

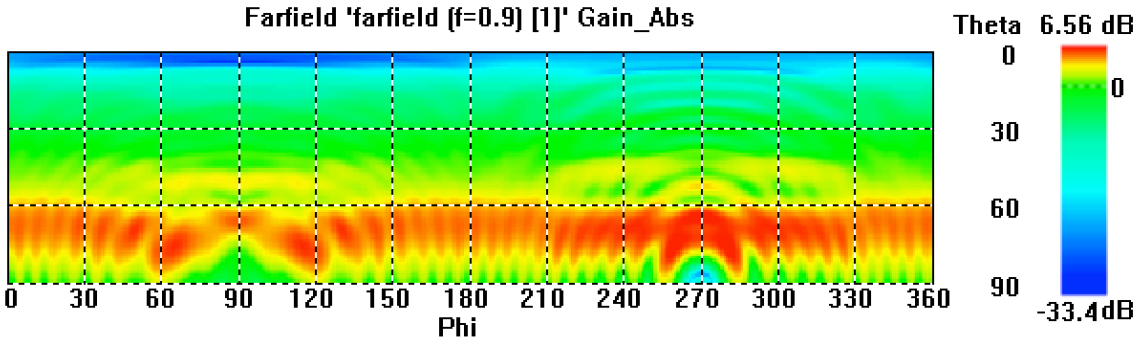

Figure E.14. Farfield for a distance of 3 m from a 45 cm height HVAC unit at 900 MHz.

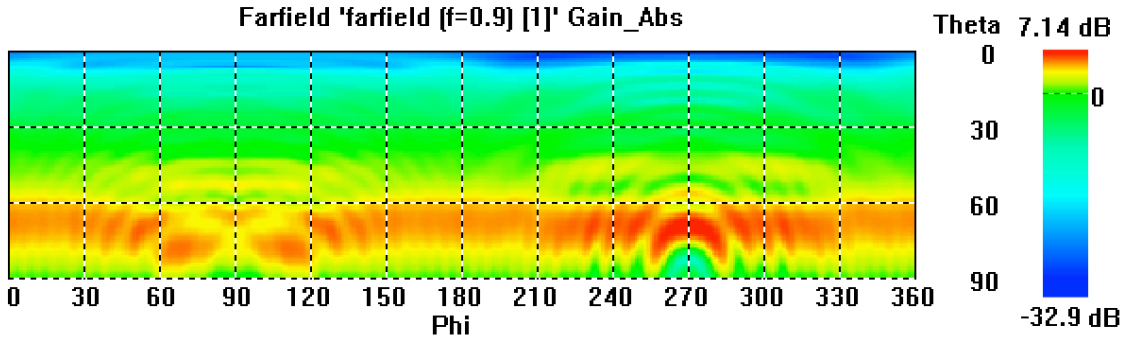

Figure E.15. Farfield for a distance of 3.5 m from a 45 cm height HVAC unit at 900 MHz.

E.2 LTE-R (2.6 GHz)

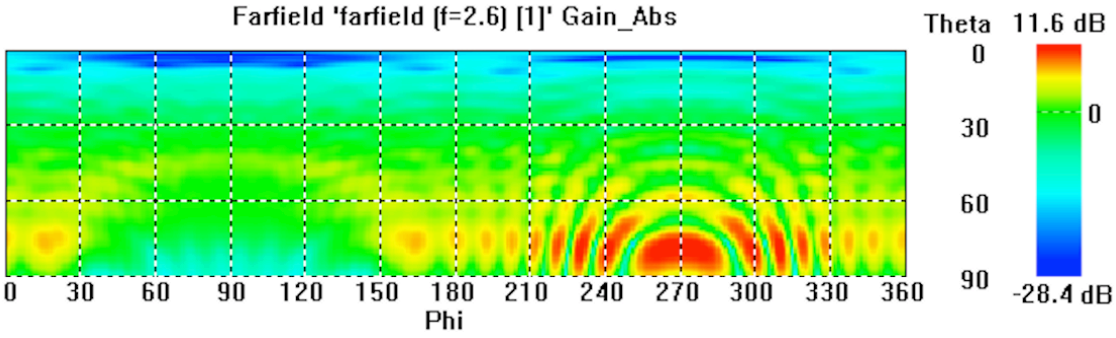

Figure E.16. Farfield for a distance of 0.5 m from a 25 cm height HVAC unit at 2.6 GHz.

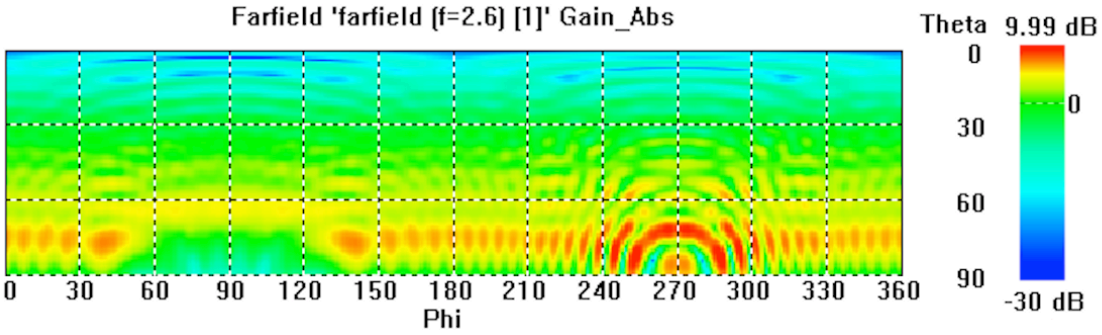

Figure E.17. Farfield for a distance of 1 m from a 25 cm height HVAC unit at 2.6 GHz.

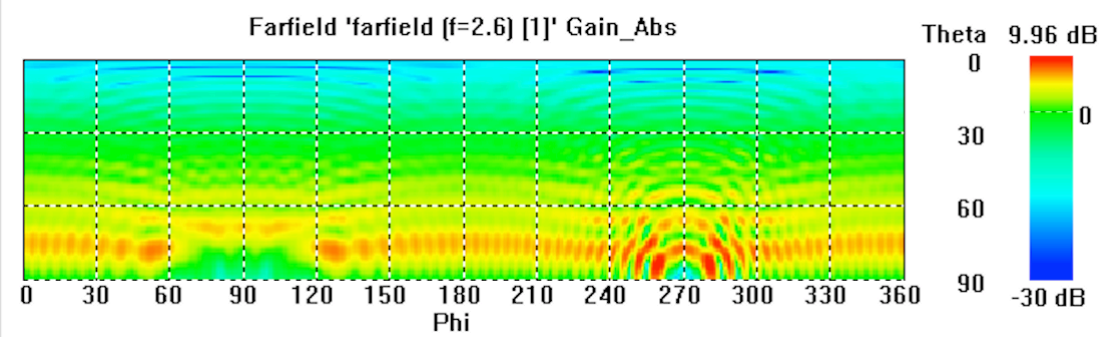

Figure E.18. Farfield for a distance of 1.5 m from a 25 cm height HVAC unit at 2.6 GHz.

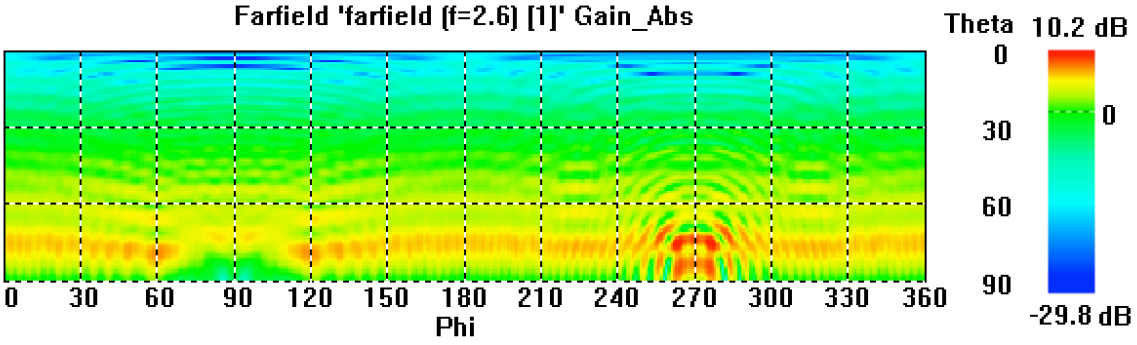

Figure E.19. Farfield for a distance of 2 m from a 25 cm height HVAC unit at 2.6 GHz.

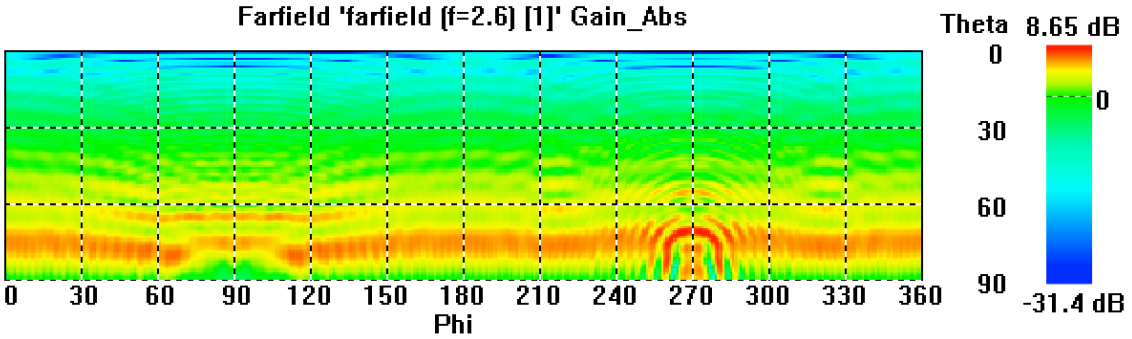

Figure E.20. Farfield for a distance of 2.5 m from a 25 cm height HVAC unit at 2.6 GHz.

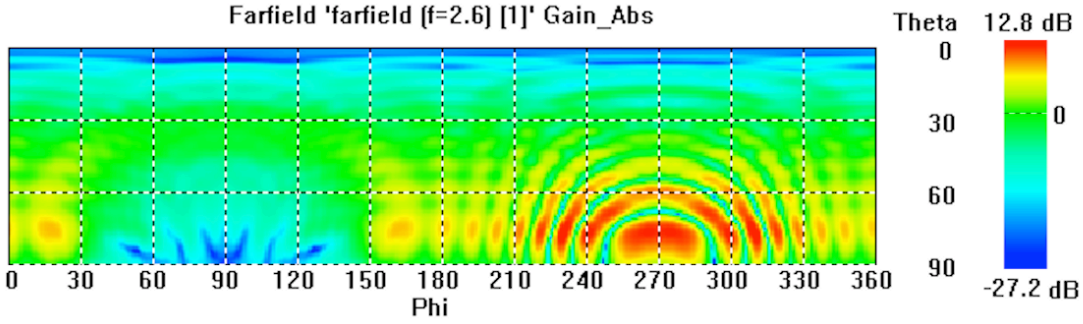

Figure E.21. Farfield for a distance of 0.5 m from a 45 cm height HVAC unit at 2.6 GHz.

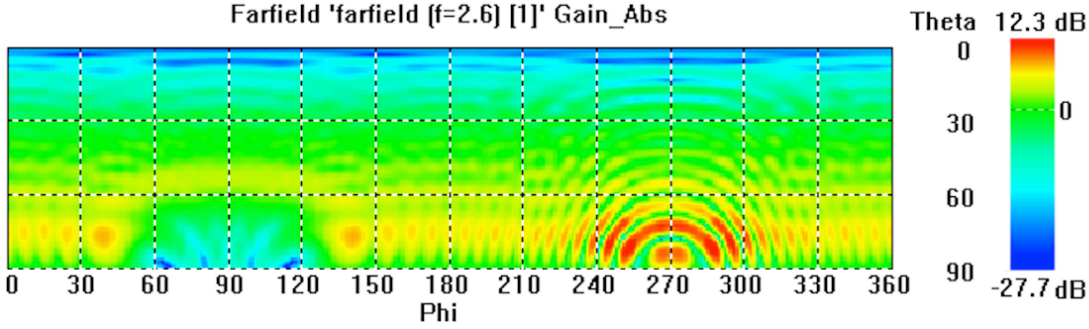

Figure E.22. Farfield for a distance of 1 m from a 45 cm height HVAC unit at 2.6 GHz.

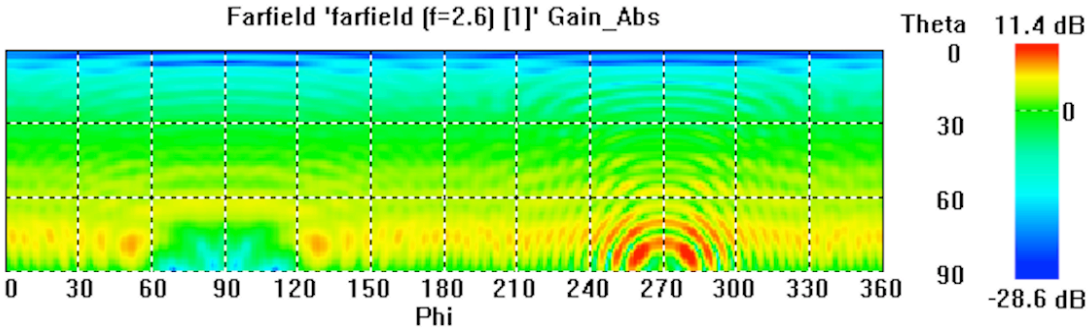

Figure E.23. Farfield for a distance of 1.5 m from a 45 cm height HVAC unit at 2.6 GHz.

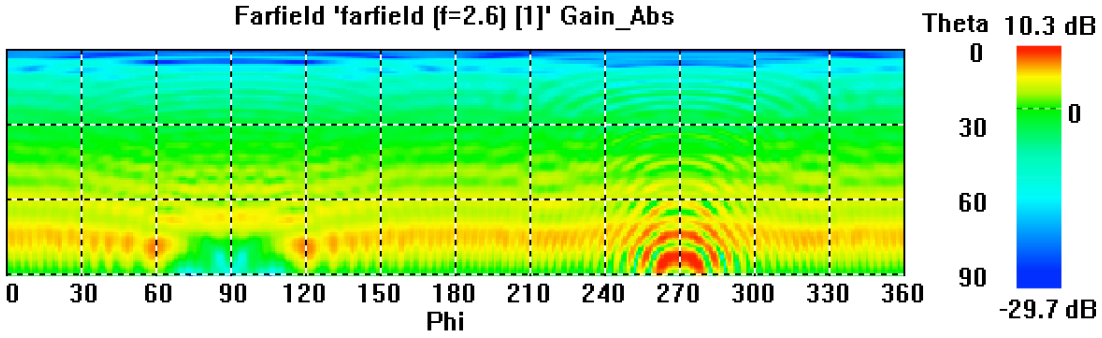

Figure E.24. Farfield for a distance of 2 m from a 45 cm height HVAC unit at 2.6 GHz.

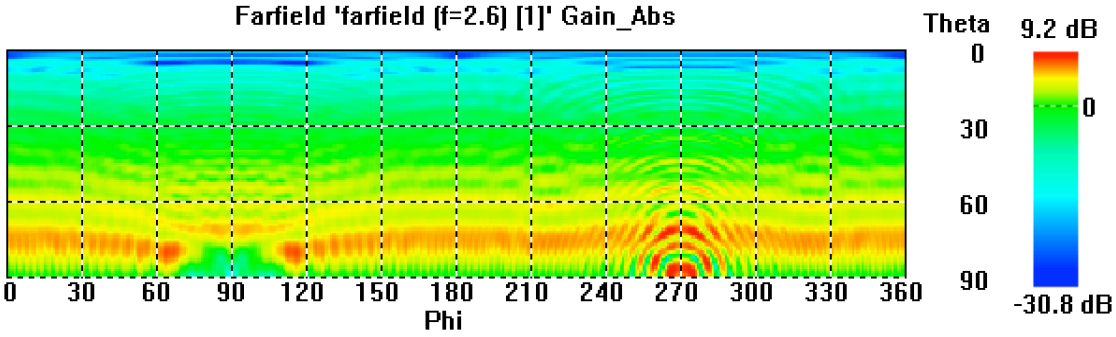

Figure E.25. Farfield for a distance of 2.5 m from a 45 cm height HVAC unit at 2.6 GHz.

E.3 BBRS (5.9 GHz)

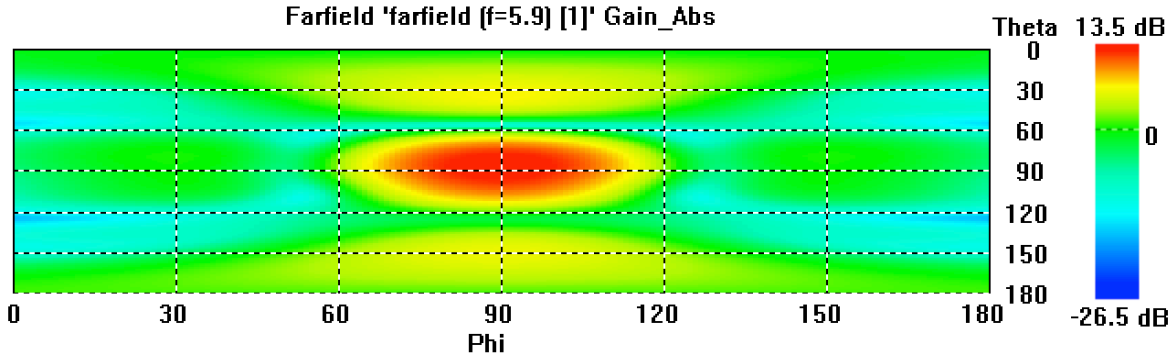

Figure E.26. Farfield for BBRS antenna without subway structure (reference).

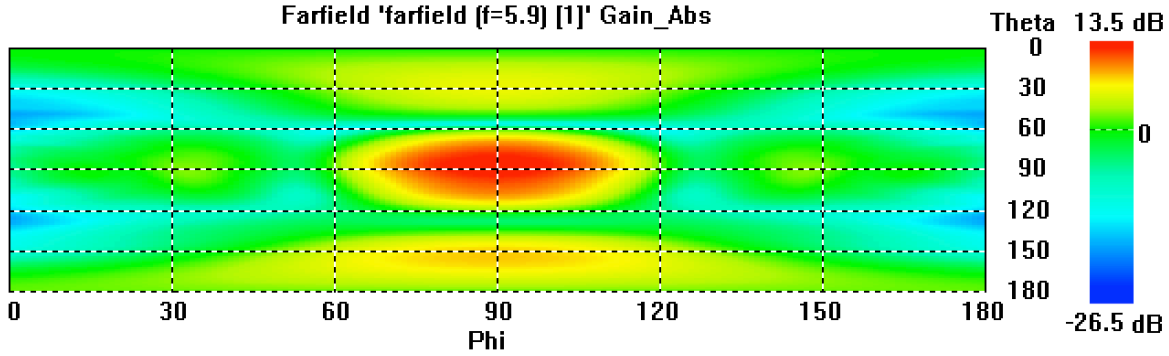

Figure E.27. Farfield for BBRS antenna at position 1 and 0 mm of depth.

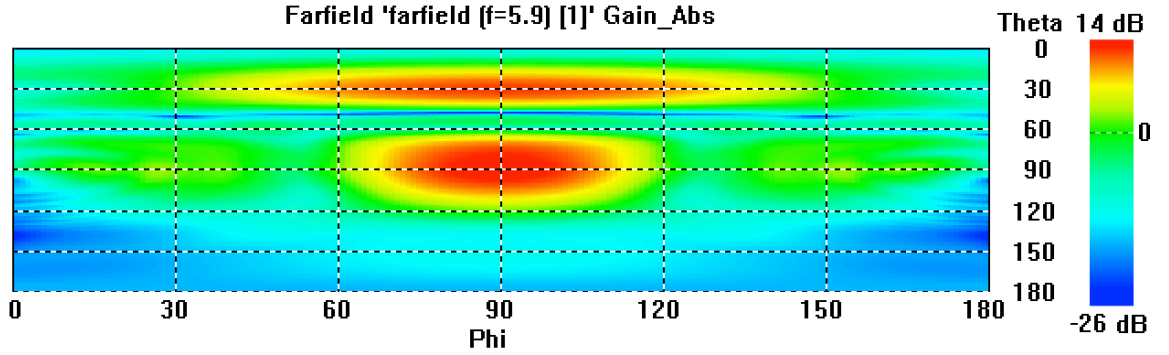

Figure E.28. Farfield for BBRS antenna at position 1 and 100 mm of depth.

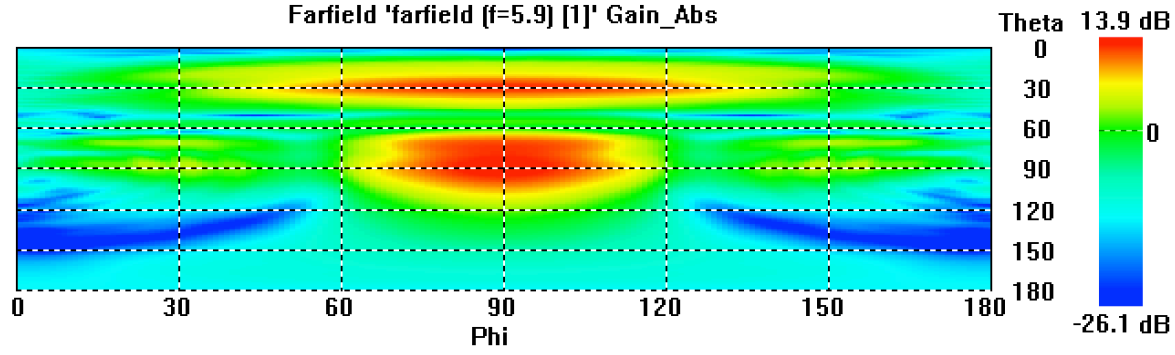

Figure E.29. Farfield for BBRS antenna at position 1 and 200 mm of depth.

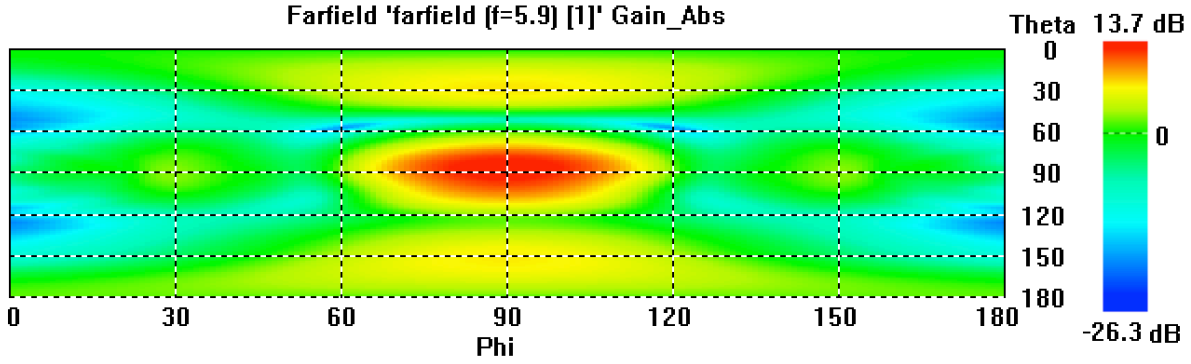

Figure E.30. Farfield for BBRS antenna at position 2 and 0 mm of depth.

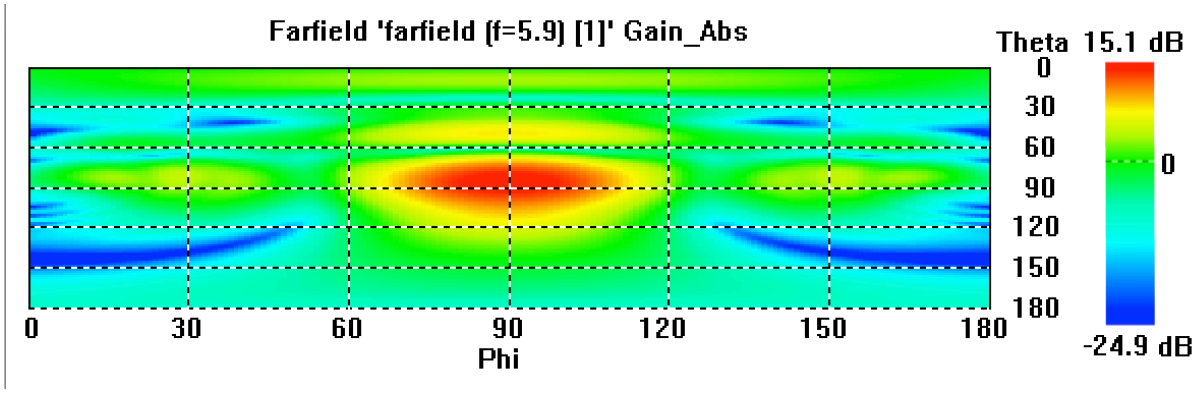

Figure E.31. Farfield for BBRS antenna at position 1 and 100 mm of depth.

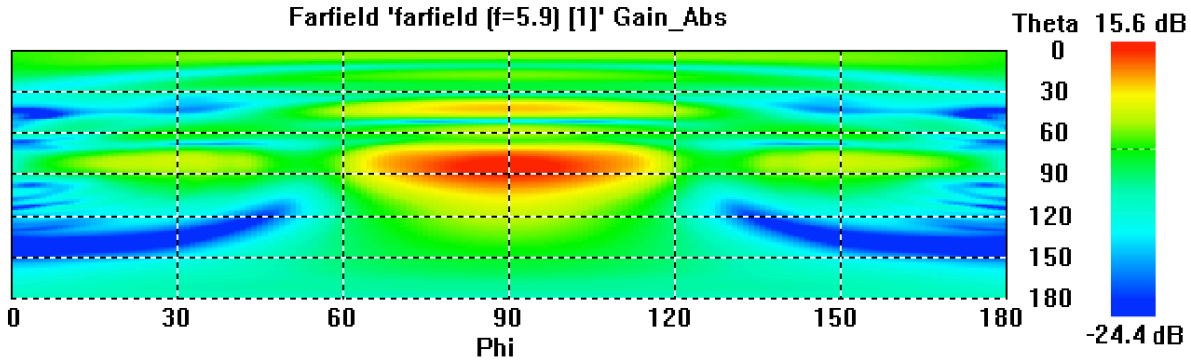

Figure E.32. Farfield for BBRS antenna at position 2 and 200 mm of depth.

References

[3GPP05] 3GPP, *Technical Specification Group GSM/EDGE Radio Access Network; Radio transmission and reception*, Report ETSI TS 05.05, V8.20.0, Release 1999, Nov. 2005. [Online] Available in:(https://portal.3gpp.org/desktopmodules/Specifications/SpecificationDetails.aspx?specificationId=258). [Accessed in Dec. 2017].

[3GPP17] 3GPP, *Evolved Universal Terrestrial Radio Access (E-UTRA); User Equipment (UE) radio transmission and reception*, Report ETSI TS 36.101, V14.3.0, Release 14, Apr. 2017. [Online] Available in:(http://www.etsi.org/deliver/etsi_ts/136100_136199/136101/14.03.00_60/ts_136101v140300p.pdf). [Accessed in Mar. 2018].

[ACKZ14] B. Ai, X. Cheng, T. Kürner, Z. Zhong, K. Guan, R. He, L. Xiong, D. W. Matolak, D. G. Michelson and C. Briso-Rodriguez, "Challenges Toward Wireless Communications for High-Speed Railways", *IEEE Transactions on Intelligent Transportation Systems*, Vol.15, No.5, Oct. 2014, pp. 2143 - 2158. [Online] Available in: (http://ieeexplore.ieee.org/document/6808529/). [Accessed in Mar. 2018].

[AGRK15] B. Ai, K. Guan, M. Rupp, T. Kürner, X. Cheng, X. Yin, Q. Wang, G. Ma, Y. Li, L. Xiong and J. Ding, "Future Railway Services-Oriented Mobile Communication Network", *IEEE Communications Magazine*, Vol.53, No. 10, Oct. 2015, pp. 78-85. [Online] Available in: (http://ieeexplore.ieee.org/document/7295467/). [Accessed in Jan. 2018].

[Ali16] S. Ali, *Passenger Train*, 3D Train Model created with SolidWorks CAD, ITM University, Gwalior, India, 2016. [Online] Available in: (https://grabcad.com/library/passenger-train-1) [Accessed in Jan. 2018].

[AntM17] Antenna Magus 2017 Help, Help document 2017.

[ANTO18] ANTONICS – ICP GmbH, *Antenna consulting and RF-simulation*, Berlin, Germany. [Online] Available in: (https://www.antonics.com/fileadmin/antonics/img/Bilder/Downloads/RF-Simulation_Support_V06.pdf) [Accessed in Feb. 2018].

[Bala16] C. A. Balanis, *Antenna Theory: Analysis and Design*, Fourth Edition, John Wiley & Sons, Hoboken, New Jersey, USA, Feb. 2016.

[BBRS17] Broad Band Radio System (BBRS), Thales Portugal, July 2017.

[BeBe12] A. Berttout and E. Bernard, "Next Generation of Railways and Metros Wireless Communication Systems", *Alcatel-Lucent*, Institute of Railway Signal Engineers (IRSE), 2012. [Online] Available in: (http://www.irse.org/knowledge/publicdocuments/3.10%20Bertout%20-

%20Next%20generation%20of%20railways%20and%20metros%20wireless%20communications.pdf). [Accessed in Dec. 2017].

[BFML10] G. Baldini, I.N. Fovino, M. Masera, M. Luise, V. Pellegrini, E. Bagagli, G. Rubino, R. Malangone, M. Stefano and F. Senesi, “An early warning system for detecting GSM-R wireless interference in the high-speed railway infrastructure”, *International Journal of Critical Infrastructure Protection* , Vol.3, No.3, Dec. 2010, pp.140 - 156. [Online] Available in: (https://www.sciencedirect.com/science/article/pii/S1874548210000430) [Accessed in Nov. 2017].

[BGLI10] *DualBand Antenna Technical document BGLI*, λεα LEANTENNE, Technical department, DSF-07 Rev. 1, Valeggio sul Mincio, Verona, Italy, 2010.

[Cisc16] Cisco, “Mobility Management Entity Overview”, in MME Administration Guide, StarOS Release 21, Oct. 2016. [Online] Available in: (https://www.cisco.com/c/en/us/td/docs/wireless/asr_5000/21/MME/b_21_MME_Admin.pdf?dtid=osscdc000283).[Accessed in Jan. 2018].

[CMAF13] J. Calle-Sánchez, M. Molina-García, J. I. Alonso, and A. Fernández-Durán, “Long Term Evolution in High Speed Railway Environments: Feasibility and Challenges”, *Bell Labs Technical Journal*, Vol.18, No.2, Sep. 2013, pp.237-253. [Online] Available in: (http://ieeexplore.ieee.org/document/6772145/). [Accessed in Dec. 2017].

[Corr17] L. M. Correia, *Mobile Communication Systems*, Lecture Notes, Instituto Superior Técnico, Lisbon, Portugal, 2017.

[CST18] CST – Computer Simulation Technology. Online] Available in: (https://www.cst.com/). [Accessed in Jan. 2018].

[CSTH17] CST STUDIO SUITE® 2017 Help, Help documentation 2017.

[Dan08] M. Dan, *GSM-R SIAFI 2008*, Infrastructure Dept., UIC, Paris, France, Apr. 2008. [Online] Available in: (https://uic.org/cdrom/2008/05_SIAFI08_source/docs/april/3_mercredi/6_GSM-R.pdf). [Accessed in Nov. 2017].

[DFHR13] V. Deniau, H. Fridhi, M. Heddebaut, J. Rioult, I. Adin and J. Rodriguez, “Analysis and modelling of the EM interference produced above a train associated to the contact between the catenary and the pantograph”, in *Proc. of 2013 International Symposium on Electromagnetic Compatibility (EMC EUROPE)*, Brugge, Belgium, Sep. 2013. [Online] Available in: (https://hal.archives-ouvertes.fr/hal-00911695/document). [Accessed in Feb. 2018].

[ECCa18] Electronic Communications Committee (ECC), *Practical Mechanism to Improve the Compatibility Between GSM-R and Public Mobile Networks and Guidance on Practical Coordination*, ECC within the European Conference of Postal and Telecommunications Administrations (CEPT), ECC Report 162, Montegrotto Terme, Italy, May 2011. [Online]

Available in: (https://www.ecodocdb.dk/download/1ac09063-352f/ECCREP162.DOC) [Accessed in Mar. 2018].

[EngM18] Engineering Master – Engineering blog, *What is Pantograph? How they are used in Electric Rail Engines?* [Online] Available in: (https://engineeringmaster.in/2017/04/23/what-is-pantograph-how-they-are-used-in-electric-rail-engines/) [Accessed in Feb. 2018].

[FrFC17] P. Fraga-Lamas, T.M. Fernández-Caramés and L. Castedo, "Towards the Internet of Smart Trains: A Review on Industrial IoT-Connected Railways", *Sensors*, Vol.17, No.6, June. 2017, pp.1457(1-44). [Online] Available in: (http://www.mdpi.com/1424-8220/17/6/1457/pdf). [Accessed in Dec. 2017].

[FRGC15] P. Fraga-Lamas, J. Rodríguez-Piñeiro, J. A. García-Naya and L. Castedo, "Unleashing the Potential of LTE for Next Generation Railway Communications", *Communications Technologies for Vehicles*, in *Proc. of 8th International Workshop on Communication Technologies for Vehicles (Nets4Cars / Nets4Trains / Nets4Aircraft)*, vol.9066, pp. 153-164, Sousse, Tunisia, May 2015. [Online] Available in: (https://link.springer.com/chapter/10.1007%2F978-3-319-17765-6_14). [Accessed in Dec. 2017].

[GeRK12] C. Gessner, A. Roessler, and M. Kottkamp, UMTS Long Term Evolution (LTE) – Technology Introduction, Rohde & Schwarz, Note 1MA111, July 2012 [Online]. Available in:(https://cdn.rohde- schwarz.com/pws/dl_downloads/dl_application/application_notes/1ma111/1MA111_4E_LTE_technology_introduction.pdf) [Accessed in Mar. 2018]

[Gonç13a] J. Gonçalves, *Detailed Design Plan – BMRC Project*, 2S-&TDM-THAL-GEN-COM-DOC-0020-A03, Thales Portugal, Lisbon, Apr. 2013.

[Gonç15] J. Gonçalves, *Conception Finale – Spécification du SRLB Partie I – Description Technique du Système*, 3BF 70088 0041 DSAKE – A11, Thales, Lisbon, Portugal, Mar. 2015.

[GSMR15a] GSM-R Operations Group, EIRENE – System Requirements Specification Version 16.0.0, UIC, Paris, France, 2015. [Online] Available in: (https://uic.org/IMG/pdf/srs-16.0.0_uic_951-0.0.2_final.pdf) [Accessed in Dec. 2017].

[GSMR15b] GSM-R Operations Group, EIRENE – Functional Requirements Specification Version 8.0.0, UIC, Paris, France, 2015. [Online] Available in: (https://uic.org/IMG/pdf/frs-8.0.0_uic_950_0.0.2_final.pdf) [Accessed in Dec. 2017].

[HAWG16] R. He, B. Ai, G. Wang, K. Guan, Z. Zhong, A. F. Molisch, C. Briso-Rodriguez and C. P. Oestges, "High-speed railways communications: From GSM-R to LTE-R", *IEEE Vehicular Technology Magazine*, Vol. 11, No. 3, Sep.2016, pp.49-58. [Online] Available in: (http://ieeexplore.ieee.org/document/7553613/). [Accessed in Jan. 2018].

[HoTo11] H. Holma and A. Toskala, LTE for UMTS: Evolution to LTE Advanced (2nd edition), John Wiley & Sons Ltd, Chichester, UK, 2011.

[Hube09b] Huber+Suhner, *Sencity® Spot- S WiFi Antenna*, 1356.17.0077, SPA 5600/40/14/0/V 2, June 2009 [Online]. Available in:(https://ecatalog.hubersuhner.com/?fcode=m_cs_catdeta

il&m_cs_gv_itmguid=051MaWqK7jUmaeRPR4RBV0&m_cs_gv_with_navi=X) [Accessed in Apr. 2018].

[Hube17] Huber+Suhner, *Sencity Rail Antenna*, 1399.17.0094, SWA 0459/360/4/25/V, Feb. 2017. [Online]. Available in: (https://ecatalog.hubersuhner.com/product/ecatalog/Radio-frequency/Antennas-Accessories/Antennas/1399-17-0094) [Accessed in Apr. 2018].

[IEEE13] IEEE Standards Board, *IEEE Standard for Definitions of Terms for Antennas*, IEEE Std 145-2013 (Revision of IEEE Std 145-1993), New York, USA, Dec. 2013. [Online] Available in:(https://ieeexplore.ieee.org/stamp/stamp.jsp?tp=&arnumber=6758443). [Accessed in Nov. 2017].

[IRSt18] International Railway Statistics, *High Speed Traffic in the world*, Internal Report, UIC, Nov. 2017 [Online]. Available in: (https://uic.org/IMG/pdf/high_speed_passenger-km_20171130_.pdf) [Accessed in Feb. 2018].

[IvRS12] G. Ivo, S. Rodrigues, P. Silva, *Definitive Design Plan – Technical Specification – Video Transfer System*, Thales, THAL-DFD-ALL-VTS-TES-00371-A06, Lisbon, Portugal, Aug. 2012.

[KSTW98] B. Krietenstein, R. Schuhmann, P. Thoma, and T. Weiland, "The Perfect Boundary Approximation technique facing the big challenge of high precision field computation", in *Proc. of LINAC98 - 19th International Linear Accelerator Conference*, Chicago, USA, Aug. 1998. [Online] Available in: (https://accelconf.web.cern.ch/accelconf/l98/PAPERS/TH4041.PDF). [Accessed in Feb. 2018].

[Kunz18] A. Kunze, *It's not just self-driving cars. Trains could soon be autonomous too*, World Economic Forum, June 2017. [Online]. Available in: (https://www.weforum.org/agenda/2017/06/digitization-can-mean-a-bright-future-for-rail-travel-heres-how/) [Accessed Feb. 2018].

[LXFZ16] Y. Lu, K. Xiong, P. Fan, Y. Zhang and Z. Zhong, "Deploying multiple antennas on High-speed Trains: Equidistant Strategy vs Fixed-Interval Strategy", in *Proc. of 2016 IEEE 84th Vehicular Technology Conference (VTC-Fall)*, Monreal, Canada, Sept. 2016. [Online] Available in: (https://arxiv.org/pdf/1511.07564.pdf)[Accessed in Dec. 2018].

[Macn10] T. M. Macnamara, *Introduction to antenna placement and installation*, John Wiley & Sons Ltd, Chichester, UK, 2010.

[Mana16] L. Manara, *Investigating Antenna Placement on Autonomous Mining Vehicle*, M.Sc. Thesis, KTH Royal Institute of Technology – School of Information and Communication Technology, Stockholm, Sweden, 2016. [Online] Available in: (http://www.diva-portal.org/smash/get/diva2:1086761/FULLTEXT01.pdf) [Accessed in Feb. 2018].

[Maso13] S. H. Masood, *Performance comparison of IEEE 802.11g and IEEE 802.11n in the presence of interference from 802.15.4 networks*, Department of Electrical Engineering,

McGill University, Montreal, Quebec, Canada, Aug. 2013. [Online] Available in: (https://arxiv.org/pdf/1308.0678v1.pdf) [Accessed in Dec. 2017].

[Mend10] L. Mendonça, *Detailed Design Plan – Technical Specification Broad Band Radio System*, MMMP-SL-THA-MSN-GEN-DSP-D-00437-A05, Thales, Mar. 2010.

[More17] A. Moreira, *Antennas*, Lecture Notes, Instituto Superior Técnico, Lisbon, Portugal, 2017.

[Pals13] V. A. F. Pals, *Analysis of influence on antenna radiation patterns by conducting environments for the development of vehicle antennas*, MS.c Thesis, Technische Universität München, München, Germany, 2013.[Online]. Available in: (https://riunet.upv.es/bitstream/handle/10251/33007/FuertesPals_VicenteAlejandro_MasterERASMUS.pdf;jsessionid=CDA7DC7555FEB6FBD7F6578E6C4454CF?sequence=1) [Accessed in Jan. 2018].

[Palu13] M. Palumbo, "Railway Signalling since the birth to ERTMS", *railwaysignalling.eu*, Italy, Nov. 2013. [Online] Available in: (http://www.railwaysignalling.eu/wp-content/uploads/2014/06/Railway_Signalling_since_birth_to_ERTMS.pdf) [Accessed in Dec. 2017]

[Polo16] Polomarconi, *Dual Band GSM-R – GPS Antenna*, Ver. 04, June 2016. [Online]. Available in: (https://www.polomarconi.it/wp-content/uploads/datasheet/BGLI.pdf). [Accessed in Mar. 2018].

[PRRB11] R. Parameswar, P. H. Rao, K. P. Ray and N. Balakrishnan, "Analysis of distributed conformal antennas on a moving platform", in *Proc. of 2011* IEEE *Applied Electromagnetics Conference (AEMC)*, Kolkata, India, Dec. 2011.[Online] Available in: (http://ieeexplore.ieee.org/document/6256843/). [Accessed in Jan. 2018].

[PuTa09] L. Pushparatnam, T. Taylor, "Overview of GSM-R", in UIC, *GSM-R Implementation and Procurement Guide*, UIC, Paris, France, 2009. [Online] Available in: (https://uic.org/IMG/pdf/2009gsm-r_guide.pdf). [Accessed in Dec. 2017].

[PuWa09] S. Pu and J. Wang, "Research on the Receiving and Radiating Characteristics of Antennas on High-Speed Train using Integrative Modeling Technique", in *Proc. of 11th Asia Pacific Microwave Conference (APMC),* pp. 1072-1075, Singapore, Dec. 2009. [Online] Available in: (https://www.researchgate.net/publication/224100598_Research_on_the_receiving_and_radiating_characteristics_of_antennas_on_high-speed_train_using_integrative_modeling_technique). [Accessed in Dec. 2017].

[Reed18] Marc Reed, "Licensed vs. Unlicensed Spectrum for Utility Communications" [Online]. Available in: (http://www.utilityproducts.com/articles/print/volume-7/issue-7/product-focus/amr_ami/licensed-vs__unlicensed.html) [Accessed Mar. 2018].

[SAUH14] M. K. Sarkar, G.M. F. Ahmed, A.T.M. J. Uddin, M.H. Hena, M. A. Rahman and R. Kabiraj, "Wireless cellular network for high speed (up to 500 km/h) vehicles", *IOSR Journal of Electronics and Communication Engineering*, Vol.9, Issue 1, Jan. 2014, pp.1-9.[Online]

Available in:(https://pdfs.semanticscholar.org/8ffd/77a407197382f074b3b1af95fde221f45c4b.pdf). [Accessed in Nov. 2017].

[SCIV18] SCI Verkehr, *Rail Transport Markets – Global Markets Trends 2016-2025*, MultiClient Study, Hamburg, Germany, Mar. 2017. [Online]. Available in:(https://www.sci.de/fileadmin/user_upload/Flyer_Rail_Transport_Markets_eng.pdf) [Accessed in Feb. 2018].

[Stat18] Statista Inc., *Annual average accessible railway market from 2013 to 2021, by segment (in billion euros)*, Hamburg, Germany, May 2017. [Online]. Available in:(https://www.statista.com/statistics/201760/worldwide-market-share-of-leading-global-rail-equipment-manufacturers/) [Accessed in Feb. 2018].

[stmo17] stm – Société de transport de Montréal, "New AZUR metro cars", Technical characteristics, Apr. 2017. [Online] Available in: (http://www.stm.info/sites/default/files/feuillet_azur-web_ang.pdf) [Accessed in Apr. 2018].

[Thal17] Thales Group – A French company dedicated in services for aerospace, space, ground transportation, defence and security. [Online] Available in:(https://www.thalesgroup.com/en/european-train-control-system-etcs), [Accessed in Oct. 2017].

[UIC17] UIC – The worldwide Railway Organisation, [Online] Available: (https://uic.org/) , [Accessed in Dec. 2017].

[Viss12] H. J. Visser, *Antenna Theory and Applications*, John Wiley & Sons, Chichester, UK, 2012.

[WaZG12] J. Wang, H. Zhu and N.J. Gomes, "Distributed Antennas Systems for Mobile Communications in High Speed Trains", *IEEE Journal on Selected Areas in Communications*, Vol.30, No. 4, May 2012, pp. 675-683. [Online] Available in: (http://ieeexplore.ieee.org/document/6180090/) [Accessed in Nov. 2017].

[Wiki18a] Wikipedia – An online free-content encyclopaedia, *Passenger rail transport in China*. [Online] Available in: (https://en.wikipedia.org/wiki/Passenger_rail_transport_in_China#/media/File:Yichang-arrival-of-the-Hankou-train-4774.jpg) [Accessed in Feb. 2018].

[Wiki18b] Wikipedia – An online free-content encyclopaedia, *British Rail Class 59*. [Online] Available in:(https://en.wikipedia.org/wiki/British_Rail_Class_59) [Accessed in Feb. 2018].

[Wiki18c] Wikipedia – An online free-content encyclopaedia, *Dome car*. [Online] Available in: (https://en.wikipedia.org/wiki/Dome_car#/media/File:InlandLakesDome.jpg) [Accessed in Feb. 2018].

[Will09] D.J.S. Williams, *Train Roof Antenna Positioning Issue Study*, Rail Safety and Standards Board (RSSB) Research Project T739, Siemens Mobility, London, UK, July 2009. [Online] Available in: (https://www.rssb.co.uk/research-development-and-innovation/research-reports-catalogue/pb009801) [Accessed in Feb. 2018].

[XZAZ16] S. Xu, G. Zhu, B. Ai and Z. Zhong, "A Survey on High-Speed Railway Communications: A Radio Resource Management Perspective", *State Key Laboratory of Rail Traffic Control*

and safety, Beijing, China, Mar. 2016. [Online] Available in: (https://arxiv.org/pdf/1603.05368.pdf) [Accessed in Dec. 2017].

[ZAZW17] Z. Zhong, B. Ai, G. Zhu, H. Wu, L. Xiong, F. Wang, L. Lei, J. Ding, K. Guan and R. He, *Dedicated Mobile Communications for High-speed Railway*, Beijing Jiaotong University Press, Beijing, China, 2017.

[ZRFG17] L. Zhang, J. Rodríguez-Piñero, J. R. O. Fernández, José A. Gracía-Naya, D. W. Matolak, C. Briso and L. Castedo, "Propagation modelling for outdoor-to-indoor and indoor-to-indoor wireless links in high-speed train", *Journal of International Measurement Confederation*, Vol.110, Nov. 2017, pp. 43- 52. [Online] Available in: (https://www.sciencedirect.com/science/article/pii/S0263224117304001) [Accessed in Nov. 2017].